END
8-87
DTIC

DTIC FILE COPY ②

REPORT DOCUMENTATION PAGE

1a. REPORT SECURITY CLASSIFICATION UNCLASSIFIED	1b. RESTRICTIVE MARKINGS

SECURITY CLASSIFICATION AUTHORITY	3. DISTRIBUTION / AVAILABILITY OF REPORT
	Approved for public release; distribution unlimited

DTIC ELECTE JUL 0 7 1987 D

AD-A181 928

5. MONITORING ORGANIZATION REPORT NUMBER(S)

AFOSR-TR- 87-0851

6a. NAME OF PERFORMING ORGANIZATION Cornell University	6b. OFFICE SYMBOL (If applicable)	7a. NAME OF MONITORING ORGANIZATION AFOSR/NE
6c. ADDRESS (City, State, and ZIP Code) Ithaca, NY 14853		7b. ADDRESS (City, State, and ZIP Code) Bldg 410 Bolling AFB, DC 20332-6448

8a. NAME OF FUNDING / SPONSORING ORGANIZATION AFOSR	8b. OFFICE SYMBOL (If applicable) NE	9. PROCUREMENT INSTRUMENT IDENTIFICATION NUMBER AFOSR-85-0175

8c. ADDRESS (City, State, and ZIP Code) Bldg 410 Bolling AFB, DC 20332-6448	10. SOURCE OF FUNDING NUMBERS			
	PROGRAM ELEMENT NO. 61102F	PROJECT NO. 2306	TASK NO. B2	WORK UNIT ACCESSION NO.

11. TITLE (Include Security Classification)
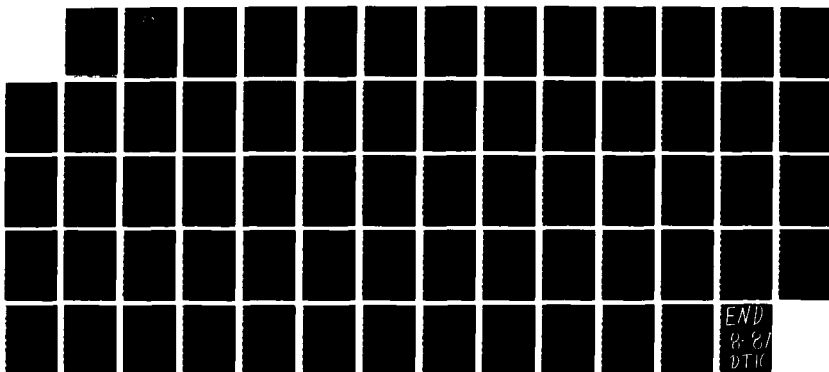
EXPERIMENTAL STUDY OF ELECTRONIC STATES AT INTERFACES

12. PERSONAL AUTHOR(S)
A J Sievers

13a. TYPE OF REPORT Final	13b. TIME COVERED FROM 85/06/01 TO 86/08/31	14. DATE OF REPORT (Year, Month, Day)	15. PAGE COUNT 64

16. SUPPLEMENTARY NOTATION

17. COSATI CODES			18 SUBJECT TERMS (Continue on reverse if necessary and identify by block number)
FIELD	GROUP	SUB-GROUP	

19. ABSTRACT (Continue on reverse if necessary and identify by block number)

The goal of this research program has been explore and understand the interaction of electromagnetic radiation with the low lying excitation spectra in condensed matter and on clean metal surfaces. Both coherent optical, infrared, and far infrared techniques have been required to probe the dynamics of these many body systems both in and out of thermal equilibrium. The formation of persistent spectral holes is one new aspect of solid state spectroscopy. Another is the discovery of large far infrared nonlinearities in high mobility two dimensional electron gas semiconducting systems.

20. DISTRIBUTION / AVAILABILITY OF ABSTRACT ☐ UNCLASSIFIED/UNLIMITED ☑ SAME AS RPT ☐ DTIC USERS	21. ABSTRACT SECURITY CLASSIFICATION UNCLASSIFIED
22a. NAME OF RESPONSIBLE INDIVIDUAL KEVIN J MALLOY CAPT USAF	22b. TELEPHONE (Include Area Code) 202-767-4931 22c. OFFICE SYMBOL NE

DD FORM 1473, 84 MAR 83 APR edition may be used until exhausted. All other editions are obsolete.

FINAL TECHNICAL REPORT

June 1, 1985 - August 31, 1986

Experimental Study of Electronic States at Interfaces

Submitted to :

AFOSR/NE
Att: Capt. K. Malloy

Submitted by:

Cornell University
Ithaca, NY 14853

Principal Investigator

A. J. Sievers
Professor of
Physics
Lab. of Atomic and
Solid State Physics

Accesion For	
NTIS CRA&I	☑
DTIC TAB	☐
Unannounced	☐
Justification	
By	
Distribution /	
Availability Codes	
Dist	Avail and / or Special
A-1	

Table of Contents

I. Abstract

The goal of this research program has been to explore and understand the interaction of electromagnetic radiation with the low lying excitation spectra in condensed matter and on clean metal surfaces. Both coherent and incoherent optical, infrared, and far infrared techniques have been required to probe the dynamics of these many body systems both in and out of thermal equilibrium. The formation of persistent spectral holes is one new aspect of solid state spectroscopy. Another is the discovery of large far infrared nonlinearities in high mobility two dimensional electron gas semiconducting systems.

II. Objectives

Novel high resolution electromagnetic wave techniques have been used in the optical, infrared and far infrared spectral regions to explore the electronic states at metal/dielectric interfaces. Because infrared surface plasmons on metal surfaces propagate for many wavelengths, a measurement of the transmission of these surface excitations has proven to be a sensitive probe of the surface itself. Both broadband and single frequency generation techniques have been developed. Reconstructed surfaces as well as surfaces covered with a chemisorbed atomic monolayer or a thin dielectric or molecular film have been investigated with these new methods.

Persistent IR spectral holes provide a new high resolution technique with which to explore the properties of defects in solids. The inhomogeneously broadened absorption lines associated with the electronic states in semiconductors are in general not coincident with the frequencies of ir-line tunable gas laser; consequently, the high power techniques of incoherent saturation and transient hole burning cannot be applied to identify the dominant relaxation process in most electronic-defect-lattice combinations. With low power tunable diodes two techniques are potentially available: electronic fluorescence, which gives the excited state lifetime; and persistent hole burning which not only provides a high resolution probe of the defect but also identifies the excited state dephasing time of the electronic state.

Measurements have been made on the far infrared nonlinear properties of high mobility 2-DEG samples. One goal has been to drive the collective 2-DEG electronic mode far from equilibrium with high intensity radiation tuned to the natural quantum transition frequencies. Large changes are observed. Very little other work has been carried out on the nonlinear high frequency properties of 2-DEG systems and it represents an exciting area for future studies.

III. Accomplishments

A. Introduction

This program started with the application of three different IR techniques to probe the electronic and vibrational properties of deep level defects in semiconductors, namely, fourier transform, diode laser, and saturation spectroscopy. The overall theme of this program has been to investigate the stability and dynamics of specific lattice-defect systems by probing the energy level spectra using these modern high resolution spectroscopic techniques. Although the spectra for most of the deep-level defects in Si were investigated initially in the 1960's[1], the motivation for our work came from a number of studies in the 1970's and early 1980's on related solid state systems which showed that persistent spectroscopic changes could often be induced in defect systems [2-6]. The persistent effect is usually characterized by a very small quantum efficiency, i.e., it takes $\sim 10^6$ transitions before the defect becomes trapped in another state which is not resonant with the laser frequency; on the other hand, because of the high brightness of the cw probe and the integrating nature of the effect, appreciable conversion can be observed on minute time scales. Dynamical mechanisms which produce this optical effect continue to be identified for an ever increasing number of inorganic and organic crystals and glasses [7-9]. Persistent IR spectral hole burning also has been observed for molecular defects in noble gas and alkali halide crystals where no electronic excitation is involved and only vibrational degrees of freedom are photoexcited with infrared radiation [10].

With complex defects a variety of inequivalent defect orientations may provide the necessary low temperature traps preventing the return of the defect-lattice system to the equilibrium ground state but there is now concrete evidence that even a point defect in an ionic crystal can have more than one low energy elastic configuration available to it [11,12]. Perhaps some of the diverse results found in the persistent hole experiments with other kinds of solids are a consequence of these little understood low lying elastic states which also would inhibit a direct return to the ground state configuration.

For covalently bonded crystals only one observation of persistent spectral hole burning in diamond had been reported [12]. The zero phonon lines of four different defect centers all showed this effect indicating that the phenomenon was a rather general one for this host. Silicon is one of the best controlled hosts for defect-lattice work hence it provides an interesting medium in which to study the stability and dynamics of defect-lattice system. Since persistent IR spectral holes (PIRSH's) provide a new way of probing these states it is important to determine the conditions on PIRSH production in the SI host. In a

general sense, one expects that three requirements must be met. First, there must be several ground state configurations of the total system, and the IR absorption energies from these ground states must differ by more than the laser linewidth. Second, there must exist an IR pumping pathway that connects these nearly degenerate "ground" state configurations. Finally, the relaxation among the "ground" states must be slower than the excited state lifetime. If all of these conditions are met then persistent spectral holes may result.

We have succeeded in observing persistent spectral holes for a few Si-defect systems but unlike diamond most combinations do not show long time hole burning effects. To understand the differences between these two hosts it has been necessary to fabricate a large number of defect systems. Fourier transform IR spectroscopy has not only provided the first high resolution data on many of these centers but also operated as a broad band probe beam in a new class of pump-probe experiments on defect centers. By combining IR laser and broad band techniques, we made a number of discoveries including the first observation of motional tunneling at deep level electronic defects in elemental semiconductors.

B. IR Saturation Measurements on Deep Levels

Although high power saturation studies of shallow levels in semiconductors show that impurity lifetimes in the range from 1 ns to 1μs can be obtained at low temperatures [14-17], before our work no similar measurements on deep levels had been reported. The main reason for this lack of data has been that high power tunable lasers are not available in the IR region so that even a simple saturation measurement requires that the absorption spectrum of the defect-lattice system accidentally be coincidence with the fixed frequencies available from a gas laser (such as CO_2). We have found two absorption lines which satisfy this requirement: one is the $1s(A_1) \rightarrow 1s(T_1)$ transition of the Se donor in AlSb[18] and the other is the $1s(A_1) \rightarrow 1s(T_1)$ transition of H:S donor in Si. We review now the important findings[19] for the Se donor in AlSb.

At low temperature the 5.6 cm^{-1} wide $1s(A_1) \rightarrow 1s(T_1)$ transition is straddled by two CO_2 laser lines. The line breadth can be interpreted in one of two ways: either the line is homogeneously broadened and the low temperature linewidth is a measure of the intrinsic multiphonon decay lifetime or the line is inhomogeneously broadened due to crystal strains so the low temperature width obtained from linear spectroscopy provides no intrinsic information about the lifetime. For the former case the laser intensity where saturation should commence can be estimated since both the absorption cross section and the linewidth are known. The calculated number, 3.7 MW/cm^2, represents the

5

maximum possible value for this system. The saturation parameter must be smaller in the case of inhomogeneous broadening since the excited state lifetime is necessarily longer. An experimental measurement permits one to distinguish between these two possibilities. We find that the $1s(T_1)$ lifetime is very short between 1 and 5 ps which is about three orders of magnitude smaller than found for shallow levels in three-five compounds. This result shows for the first time that the increase in the electron-phonon coupling constant for these localized states more than balances against the highly forbidden multiphonon decay required to relax them.

Similar results have been obtained for the H:S donor in Si.

C. Tunneling at Deep Level Acceptor Complexes in Si

Some unusual properties of hydrogen or lithium-related shallow centers in Ge, which have been identified by FIR photo-electric spectroscopy, were originally ascribed to the dynamic tunneling of the light atom among its equivalent sites in the lattice[20-22]. Recently it has been shown that all of these acceptor centers with the possible exclusion of the $Cu-H_2$ do not behave as tunneling centers[23]. For the donors other models exist[24] to explain their unusual stress dependent IR spectra and measurements are in progress to determine which model is correct[23]. The current status is that none of the shallow centers unambiguously display dynamic tunneling behavior.

With IR/FIR spectroscopy we have carried out a systematic study in Si on a series of isomorphic defects[25,26] Be-H, Be-D and Be-Li. Dynamical tunneling is observed for the acceptor complexes composed of substitutional Be plus H or D.

The acceptor A(Li, Be), an example of a non-tunneling center, produces an acceptor hydrogen series[27] around 800 cm^{-1}. Temperature dependent measurements show that the Γ_8 ground state is split into two Kramers doublets ($\Delta E \sim 11.3$ cm^{-1}) due to the symmetry lowering ($T_d \rightarrow C_{3v}$) produced by the Li^+ ion^3. The hole absorption spectra of the A(H, Be) and A(D, Be) centers are different and show three new distinguishing features. 1) When H -> D the eight transitions all display a large isotope shift of 7.8 cm^{-1} to higher frequencies. 2) A weak high frequency replica of these transitions is observed, even at the lowest temperature of 1.7 K, with a shift of 38.8 cm^{-1} for A(H, Be) and 16.2 cm^{-1} for A(D, Be). 3) With increasing temperature two additional replicas appear in sequence on the high frequency side of the main lines. The spectra for the A(D ,Be) center at a number of temperatures are shown in Fig. 2 of Ref. () . I R spectra for A(H ,Be) show quite similar temperature dependences but the spectral changes occur at somewhat higher temperatures.

These high resolution temperature dependent measurements of the

infrared and far infrared spectra associated with the acceptor complexes Be-H and Be-D in Si provide a direct identification of motional tunneling at electronic defects in semiconductors. The large isotope shift of 7.8 cm^{-1} in the IR demonstrates that the dynamical properties of hydrogen play an important role in the determination of the electronic energies. The observation of two sets of optical transitions from the ground to the excited states with different tunneling configurations provides the first direct determination of the tunneling parameter. At least three levels of the ground state manifold have been identified for A(H,Be) and A(D,Be) from the temperature dependent studies of IR and FIR spectra which should be compared to the theoretical predictions of five manifolds with dynamic tunneling and two without. Our discovery[28] that large isotope effects can be observed for deep level tunneling centers in Si (density $\sim 10^{16}$ cm^{-3}) opens up the experimental possibilities so that now a variety of spectroscopic tools can be employed to probe the dynamical behavior of these unusual electronic defects.

D. Nonlinear Properties of Cyclotron Resonance in a Two Dimensional Electron Gas

Although the d.c. electric field dependence of the nonlinear mobility of electrons in a two dimensional electron gas (2-DEG) structure has been well characterized because of applications to fast field effect transistors[29,30], information on the nonlinear mm wave response of these high mobility systems was lacking until the work initiated by Schlesinger and Sievers[31]. The inital measurements were made while one of us (AJS) was on sabbatic leave at the high intensity near mm wave laboratory of Dr. F. Keilmann at the Max Plank Institute in Stuttgart. This opportunity was used both to learn about new high power techniques in this frequency region and to initiate an investigation into the nonlinear mm wave properties of semiconductor interfaces which support a 2-DEG. Our preliminary measurements on the far infrared intensity dependence of the magneto-transmissivity of a 2-DEG at a GaAs/($Al_{0.3}Ga_{0.7}$)As interface has been described in Ref. (31). The data demonstrate that high intensity cyclotron resonance provides a new method for identifying and studying specific hot electron effects in these systems.

7

IV. References

1. R. K. Watts, _Point Defects in Crystals_, John Wiley and Son's, New York, (1977).

2. A. A. Gorokhovskii, R. K. Kaarli and L. A. Rebane, JETP lett. **20**, 216 (1974).

3. B. M. Kharlamov, R. I. Personov and L. A. Bykovskaya, Opt. Commun. **12**, 191 (1974).

4. L. A. Rebane, A. A. Gorokhovskii and J. V. Kikas, Appl. Phys. B **29**, 235 (1982).

5. J. Friedrich and D. Haarer, Angew. Chem. **23**, 113 (1984).

6. G. J. Small, in _Spectroscopy and Excitation Dynamics of Condensed Molecular Systems_, edited by V. M. Agranovitch and R. M. Hochstrasser, pp. 515-554, North Holland, Amsterdam (1983).

7. W. E. Moerner, Jour. of Molecular Electronics **1**, 55 (1985).

8. A. Winnacker, R. M. Shelby and R. M. Macfarlane, Opt. Lett. **10**, 350 (1985).

9. H. W. H. Lee, M. Gehrtz, E. E. Marinero and W. E. Moerner, Chem. Phys. Lett. **118**, 611 (1985).

10. A. J. Sievers and W. E. Moerner, in _Persistent Spectral Hole-Burning: Science and Applications_, Topics in Current Physics, W. E. Moerner, Editor (Springer-Verlag Publishing Co., New York, 1987) Chapter 6.

11. S. B. Hearon and A. J. Sievers, Phys. Rev. B **30**, 4853 (1984).

12. F. Bridges, M. Reece, and M. Morgan, Rad. Effects **73**, 31 (1983).

13. R. T. Harley, M. J. Henderson, and R. M. Macfarlane, J. Phys. C: Solid State Phys. L233, (1984).

14. T. Murotani and Y. Nisida, J. Phys. Soc. Japan **32**, 986 (1972).

15. E. Gornik, t. Y. Chang, T. J. Bridges, V. T. Nguyen, I. D. McGee and W. Muller, Phys. Rev. Lett. **40**, 1151 (1978).

16. K. Muro, N. Yutani and S. Narita, J. Phys. Soc. Japan **49**, Suppl. A 593 (1980).

17. G. R. Allan, A. Black, C. R. Pidgeon, E. Gornik, W. Seidenbusch and P. Cotter, Phys. Rev. B **31**, 3560 (1985).

18. B. T. Ahlburn and A. K. Ramdas, Phys. Rev. **167**, 717 (1986).

19. R. E. Peale, K. Muro, J. T. McWhirter and A. J. Sievers, Solid State Commun. **60**, 753-755 (1986).

20. E. E. Haller, Phys. Rev. Letters, **40** 584, (1978).

21. E. E. Haller, B. Joos, and L. M. Falicov, Phys. Rev. B **21**, 4729 (1980).

22. E. E. Haller, Festkorperprobleme **26**, 203 (1986).

23. J. Kahn, R. E. McMurray, E. E. Haller and L. M. Falicov, Bull. Amer. Phys. Soc. **32**, 841 (1987); and J. Kahn, private communication.

24. J. Broeckx, P. Clauws, and J. Vennik, J. Phys. C: Solid State Physics **13**, L141 (1980).

25. R. K. Crouch, J. B. Robertson and T. E. Cilimer, Phys. Rev. B **5** , 3111 (1972).

26. R. K. Crouch, J. B. Robertson, H. T. Morgan, T. E. Gilmer and R. K. Frank, J. Phys. Chem. Solids **35**, 833 (1974).

27. A. Onton, P. Fisher, and A. K. Ramdas, Physical Review **163**, 686 (1967).

28. K. Muro and A. J. Sievers, Phys. Rev. Lett. **57**, 897 (1986).

29. J. Shah, A. Pinczuk, H. L. Stormer, A. C. Gossard, and W. Wiegmann, Appl. Phys. Lett. **44**, 322 (1984) and references therein.

30. J. Shah, A. Pinczuk, H. L. Stormer, A. C. Gossard, and W. Wiegmann, Appl. Phys. Lett. **42**, 55 (1983).

31. G. A. Rodriguez, R. M. Hart, A. J. Sievers, F. Keilmann, Z. Schlesinger, S. Wright, and W. I. Wang, Applied Physics Letters **49**, 458-460 (1986).

V. AFOSR Publications (1985-1986)

.

Possibility of observing quantum size effects in the electromagnetic absorption spectrum of small metal particles

R. P. Devaty

Department of Physics and Astronomy, University of Pittsburgh, Pittsburgh, Pennsylvania 15260

A. J. Sievers

Laboratory of Atomic and Solid State Physics and Materials Science Center, Cornell University, Ithaca, New York 14853

(Received 31 January 1985)

The possibility of observing quantum size effects in very small metal particles by absorption spectroscopy is reexamined. According to the Gor'kov-Eliashberg theory, nonquadratic frequency dependence of the absorption coefficient persists at sufficiently low frequencies even when there is a size distribution.

Early experimental studies of the absorption of far-infrared radiation by very small metal particles[1,2] were motivated in part by the possibility of observing quantum size effects (QSE's) predicted by the theory of Gor'kov and Eliashberg[3] (GE). According to GE, the signature of QSE's is the presence of oscillations superimposed on the quadratic frequency dependence of the absorption coefficient. No evidence for QSE's in the far infrared has been observed. The negative results are consistent with the corrected[4-6] GE theory if experimentally realizable particle-size distributions are taken into account. The oscillations are washed out by "destructive interference."

The purpose of this note is to reexamine the possibility of observing QSE's by far-infrared or microwave spectroscopy. The GE theory is emphasized over other models[7] due to the richness of phenomena it predicts. In particular, nonquadratic frequency dependence in the low-frequency absorption coefficient, which remains even if there is a size distribution, is pointed out for the first time.

Gor'kov and Eliashberg calculated the frequency-dependent electric susceptibility of a small metal particle by linear response theory. Their result is

$$\chi(\omega) = \chi_0 + QF(\omega) , \tag{1}$$

where $\chi_0 = \Lambda k_F x^2 / 20\pi^2 a_B$ is the static susceptibility and

$$Q = \frac{139}{1200\pi^2} \frac{\Lambda}{k_F a_B} . \tag{2}$$

Here x is the particle diameter, k_F is the Fermi wave vector, $\Lambda = m^*/m$ is the specific-heat effective-mass ratio, and a_B is the Bohr radius. $F(\omega) \equiv F_1 + iF_2$ is the dimensionless integral,

$$F(\omega) \equiv 2(\hbar\omega)^2 D(E_F) \int_{-\infty}^{\infty} \frac{R(E)dE}{E^2 - (\hbar\omega + i0^+)^2} , \tag{3}$$

where $D(E_F)$ is the density of electron states at the Fermi energy and $R(E)$ is a two-level correlation function. Specifically, $R(E_1 - E_2)dE_1 dE_2$ is the probability that an energy level of the particle is within each of the intervals $(E_1, E_1 + dE_1)$ and $(E_2, E_2 + dE_2)$, regardless of the posi-

tions of any other levels. GE borrowed the function $R(E)$ from the statistical theory of levels,[8] which was developed by Wigner,[9] Dyson and Mehta,[10] and others for application to highly excited atomic nuclei. In this model, the levels of the particle are treated statistically by means of an ensemble average over all possible Hamiltonians consistent with general symmetries (e.g., time-reversal invariance, rotational invariance, etc.). There are three cases and hence three distinct ensembles, called orthogonal, symplectic, and unitary after the groups of transformations under which the ensembles are invariant. The model takes into account correlations between levels due to level repulsion. The expressions for $F(\omega)$ in GE are incorrect, but the integrals were recently reevaluated.[6] The corrected results predict oscillations of the far-infrared absorption coefficient, largest for the symplectic ensemble, superimposed on the quadratic background predicted for electric dipole absorption by Drude metal particles.

In the far infrared, both the electric dipole and magnetic dipole terms of the Mie series[11] make important contributions to the absorption coefficient of a dilute, spatially random collection of small $(x < 100 \text{ Å})$ metal particles embedded in a transparent host.[7] Both the GE model and quantum-box models[7] predict a quartic frequency dependence for the magnetic dipole absorption for frequencies sufficiently greater than the Kubo[12] gap

$$\delta = 12\pi\hbar^2/m^* k_F x^3 ,$$

in contrast to the quadratic frequency dependence obtained for particles of Drude metal. Dyson's three ensembles become identical for $\hbar\omega \gg \delta$ if the oscillatory parts are neglected. Let $\hat{\epsilon} \equiv \epsilon_1 + i\epsilon_2$ and $\hat{\mu} \equiv \mu_1 + i\mu_2$ be the complex dielectric function and magnetic permeability of a particle and let the corresponding quantities for the host be unity. If the volume fraction of metal, f, in the composite satisfies $f \ll 1$ and $\epsilon_2 \ll \epsilon_1$, $\mu_1 \simeq 1$, $\mu_2 \ll 1$, and $4\pi\chi_0 \gg 1$, the low-frequency absorption coefficient in the GE model is

$$\alpha = 18\pi f\tilde{\nu} \left[\frac{\epsilon_2}{(4\pi\chi_0)^2} + \frac{\mu_2}{9} \right] \tag{4}$$

where $\tilde{v} = \omega/2\pi c$ is the frequency in wave numbers. The two terms represent electric and magnetic dipole absorption, respectively. Note that the GE model requires[3] that $\omega \ll 2v_F/x$, where v_F is the Fermi velocity. In the far infrared

$$\hat{\mu} \simeq 1 + \frac{\pi^2}{10}(x\tilde{v})^2\hat{\epsilon} \tag{5}$$

for small spheres.[13] Thus, for the GE model[14] under the specified conditions,

$$\frac{\alpha}{f} = \frac{139\pi^3}{2}\frac{a_B}{\lambda_c k_F^2 x}\tilde{v}^2 + \frac{139\pi^3}{4500}\frac{\Lambda^2 x^5}{a_B \lambda_c}\tilde{v}^4, \tag{6}$$

where $\lambda_c = \hbar/mc$ is the Compton wavelength of the electron. The GE model predicts the same frequency and size dependence for the electric dipole term, but higher powers of $\tilde{v}$ and x for the magnetic dipole term, compared with the Drude model. Quantum-box models[7] lead to the frequency and size dependence given by Eq. (6), but to slightly different values for the coefficients.

As an example, consider Au particles[15,16] with $k_F = 1.21 \times 10^8$ cm^{-1} and $\Lambda = 1.1$. Equation (6) for the GE model predicts

$$\frac{\alpha}{f} = 2.02 \times 10^{-3}\frac{\tilde{v}^2}{x} + 5.68 \times 10^{-22}x^5\tilde{v}^4. \tag{7}$$

For particles of Drude Au

$$\frac{\alpha}{f} = 1.59 \times 10^{-3}\frac{\tilde{v}^2}{x} + 2.21 \times 10^{-11}x^3\tilde{v}^2. \tag{8}$$

In Eqs. (7) and (8), α and $\tilde{v}$ are in cm^{-1} and x is in Å. The electric dipole terms are comparable in magnitude. To observe the quartic frequency dependence of the magnetic dipole term predicted by the GE model, while satisfying the assumptions of the model, the Au particles should be a few hundred angstroms in diameter.

A quartic frequency dependence of the absorption coefficient in the far infrared can be interpreted as a quantum size effect. However, the magnetic dipole term was obtained by substitution without justification of the dielectric function into the classical expression rather than by explicit quantum-mechanical calculation.[17]

If the GE model in fact describes the behavior of small metal particles, there is a quantum size effect at very low frequencies ($\tilde{v} \ll \tilde{\delta}$) due to level repulsion that does not arise in the box model. For $f \ll 1$, the electric dipole absorption coefficient for uniformly distributed particles of one size is

$$\frac{\alpha}{f} = \begin{cases} \frac{\pi^3}{3}C\tilde{v}^3/\tilde{\delta}^2 & \text{(orthogonal ensemble)} \\ \frac{32}{135}\pi^5 C\tilde{v}^6/\tilde{\delta}^5 & \text{(symplectic ensemble)} \\ \frac{2\pi^3}{3}C\tilde{v}^4/\tilde{\delta}^3 & \text{(unitary ensemble)}, \end{cases} \tag{9}$$

where

$$C = \frac{417}{50}\frac{\Lambda}{k_F a_B}\frac{1}{(3+4\pi X_0)^2} \tag{10}$$

and $\tilde{\delta}$ is the Kubo gap in wave numbers. Note that each ensemble has a different exponent for the frequency dependence and that the predictions for all three ensembles differ from the Drude model.

This effect is present even when there is a size distribution. Let the subscript i denote the components of a discrete size distribution. For $f \ll 1$ and $4\pi X_{0i} \gg 3$ (to make the integrals easy to evaluate),

$$\alpha \simeq \frac{9}{8\pi}\tilde{v}\sum_i f_i\epsilon_{2i}/X_{0i} = \frac{417}{2}\pi^2\frac{a_B}{\Lambda k_F^3}\tilde{v}\sum_i f_i F_{2i}/x_i^4 \tag{11}$$

with $\sum_i f_i = f$, x_i the diameter of particles of type i, and F_{2i} the result of integration over one of Dyson's ensembles.[6] For convenience, replace the sum by an integral over the log-normal distribution, i.e.,

$$\sum_i f_i \to f\frac{\exp[-\frac{9}{2}(\ln^2\sigma)]}{(2\pi)^{1/2}\ln\sigma}\int_{-\infty}^{\infty} dy \exp\left[\frac{-y^2}{2(\ln^2\sigma)}+3y\right], \tag{12}$$

where $y = \ln(x/\bar{x})$, and $\bar{x}$ and σ determine the mean size and width. The log-normal distribution often provides a good fit to measured histograms.[18] After integration, for $\tilde{v} \ll \tilde{\delta}$ (here $\tilde{\delta}$ is the Kubo gap, in wave numbers, for a particle of diameter $\bar{x}$), the reduced absorption coefficient, $A(z) \equiv \alpha\bar{x}k_F^2/f\tilde{v}^2$, which would be constant for low-frequency electric dipole absorption by well-separated particles of Drude metal, is

$$A(z) = \begin{cases} \pi Bz \exp[8(\ln^2\sigma)z] & \text{(orthogonal)} \\ \frac{4}{45}Bz^4\exp[-\frac{187}{2}(\ln^2\sigma)] & \text{(symplectic)} \\ Bz^2\exp[\frac{35}{2}(\ln^2\sigma)] & \text{(unitary)}, \end{cases} \tag{13}$$

where $B \equiv (139\pi^3/24)(a_B/\lambda_c)$ and $z \equiv 2\pi\tilde{v}/\tilde{\delta} = 2\pi\hbar\omega/\delta$.

In the Mie theory, which applies to the dilute limit, the electric dipole absorption coefficient is

$$\alpha = 18\pi\tilde{v}\epsilon_0^{2/3}\sum_j \frac{f_j\epsilon_{2j}}{(2\epsilon_0+\epsilon_{1j})^2+\epsilon_{2j}^2}, \tag{14}$$

where ϵ_0 is the dielectric constant of the supporting host and

$$\hat{\epsilon}_j \equiv \epsilon_{1j} + i\epsilon_{2j} = 1 + 4\pi[X_{0j} + QF_j(\omega)].$$

Figures 1 through 3 show log-log plots of the low-frequency absorption coefficient obtained from Eq. (14) for small Au particles in the GE model when the oscillations due to discrete levels are washed out by a log-normal size distribution. Although the calculations were done specifically for Au particles of 20-Å mean diameter, the plots in dimensionless units are essentially "universal" and should apply to particles of any metal with reasonable mean diameter. The reduced absorption at low frequencies should appear as a gap in a linear plot. Figure 4 shows the far-infrared absorption coefficient predicted for the three ensembles as well as for the Drude model for $\bar{x} = 20$ Å Au particles. According to this plot there is a change in absorption due to discrete levels for a log-normal distribution with $\sigma = 1.2$ in the far infrared. The three ensembles show distinct non-Drude power law
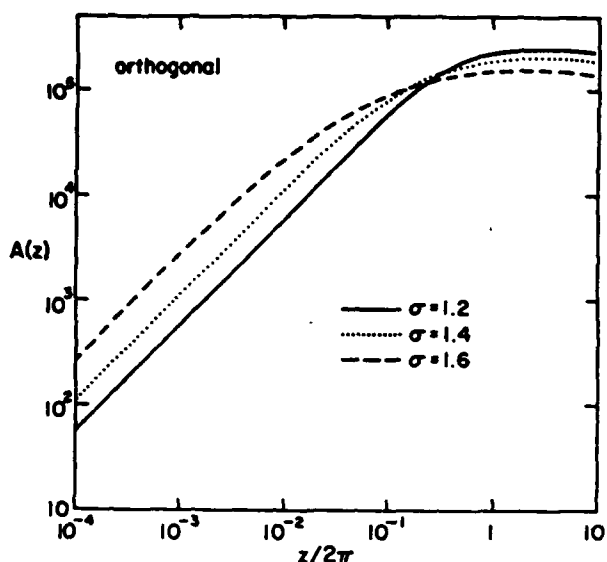
FIG. 1. Reduced Mie electric dipole absorption coefficient vs reduced frequency predicted by the Gor'kov-Eliashberg model for polydisperse Au particles with $k_F = 1.21 \times 10^8$ cm^{-1} and $\Lambda = 1.1$ for the orthogonal ensemble. The supporting dielectric is vacuum ($\epsilon_0 = 1.0$). The log-normal size distribution is used, with $\bar{x} = 20$ Å.

FIG. 3. Reduced Mie electric dipole absorption coefficient vs reduced frequency predicted by the Gor'kov-Eliashberg model for polydisperse Au particles with $k_F = 1.21 \times 10^8$ cm^{-1} and $\Lambda = 1.1$ for the unitary ensemble. The supporting dielectric is vacuum ($\epsilon_0 = 1.0$). The log-normal size distribution is used, with $\bar{x} = 20$ Å.
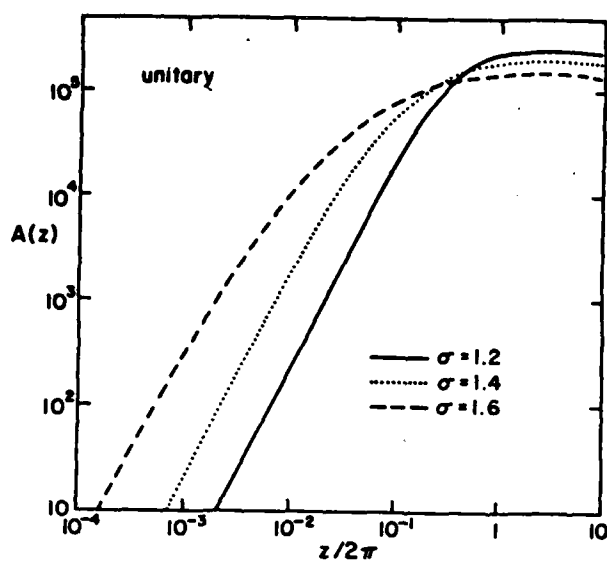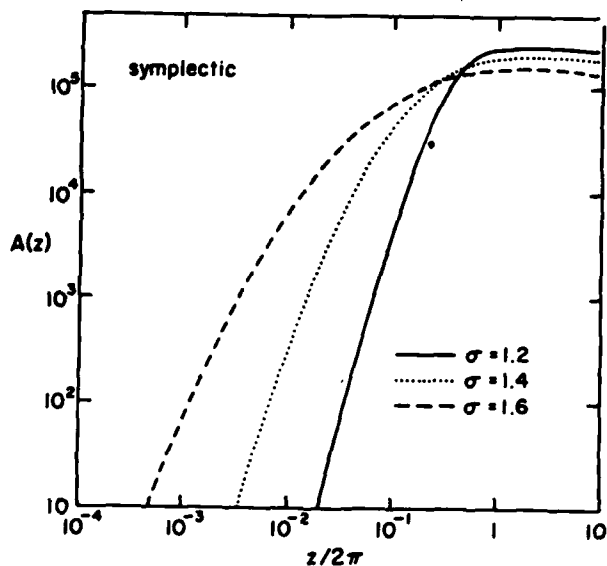

FIG. 2. Reduced Mie electric dipole absorption coefficient vs reduced frequency predicted by the Gor'kov-Eliashberg model for polydisperse Au particles with $k_F = 1.21 \times 10^8$ cm^{-1} and $\Lambda = 1.1$ for the symplectic ensemble. The supporting dielectric is vacuum ($\epsilon_0 = 1.0$). The log-normal size distribution is used, with $\bar{x} = 20$ Å.
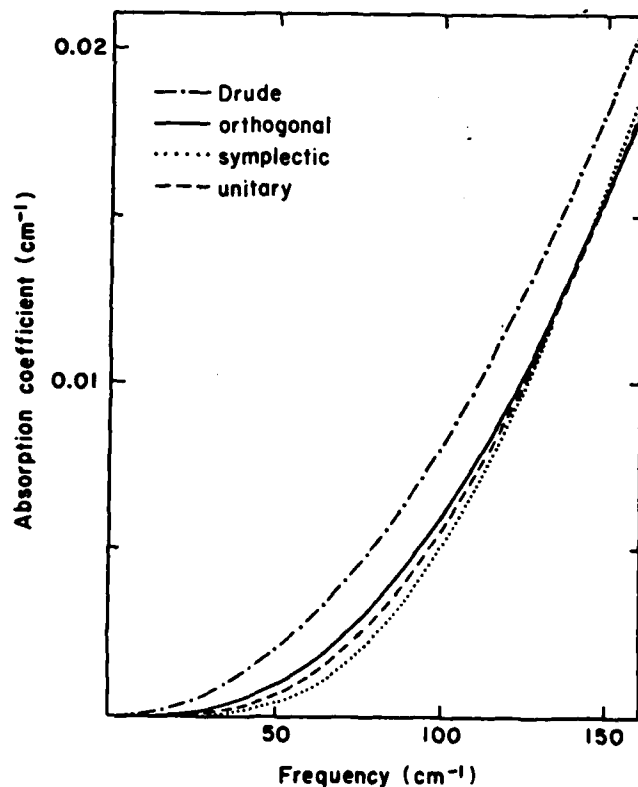

FIG. 4. Frequency dependence of the electric dipole absorption coefficient for a log-normal distribution of Au particles predicted by the GE model with $k_F = 1.21 \times 10^8$ cm^{-1}, $\Lambda = 1.1$, $f = 0.01$, $\bar{x} = 20$ Å, and $\sigma = 1.2$. Also shown is the prediction for particles of Drude Au with boundary scattering ($\tau = x/2v_F$).

13

behavior for $\tilde{v} < \tilde{\delta}$ and quadratic frequency dependence for $\tilde{v} > \tilde{\delta}$. The small discrepancies between these curves and the predictions of Eqs. (7) and (13) are due to the simplifying assumptions $(4\pi\chi_0 \gg 3, 2\epsilon_0 + \epsilon_{1j} \gg \epsilon_{2j})$ made to obtain the asymptotes analytically. The "gap" due to discrete levels (Fig. 4) is not abrupt because the low-frequency absorption follows a power law rather than an exponential, and the size distribution introduces broadening. Surprisingly, α becomes constant (not shown in the figure), rather than quadratic, in frequency according to Eq. (14) for sufficiently high frequencies $(\tilde{v}/\tilde{\delta} \gg \frac{30}{139}k_F^2 x^2)$. However, the assumptions of the GE model break down in this region, so this prediction cannot be taken seriously.

For $\bar{x} = 20$ Å and $\bar{x} = 50$ Å Au particles, $\tilde{\delta} = 218$ and 13.9 cm^{-1}, respectively, so it is advantageous to use very small particles to search for nonquadratic frequency dependence. The effect would be difficult to pin down for any $\bar{x}$, since the high power laws imply very small absorption coefficients for small $\tilde{v}$. Also, to extract the exponent from data, the baseline for α must be known accurately. Figure 4 shows that the predictions for the three ensembles are not much different in the far infrared when linear axes are used. The most convincing verification of the GE theory would be to transform one ensemble into another and observe the change in frequency dependence. For example, the symplectic ensemble $(\alpha \sim \tilde{v}^6)$ applies to a metal with strong spin-orbit coupling, but in a strong magnetic field the unitary ensemble $(\alpha \sim \tilde{v}^4)$ is appropriate. The transformation could be observed by dividing the spectra obtained for a specific sample by Fourier-transform spectroscopy (FTS) with and without an ap-

plied magnetic field. The sensitivity of the FTS technique is maximized for this measurement because no properties of the sample, including its position, are changed, except for the applied field. If additional sensitivity is required, a strong coherent source with discrete lines, such as a far-infrared laser, might be used. Samples with dilute concentrations of well-separated particles are required to avoid interactions between particles, including the enhanced far-infrared absorption[1,2,19,20] associated with clusters of particles, which might overwhelm the small effect under consideration here. A small-particle composite with well-characterized morphology that can be studied by far-infrared techniques was recently developed,[20] but a search for quantum size effects using this material would be difficult due to absorption by the host.

We conclude the following.

(1) Oscillations in the frequency dependence of the far-infrared absorption coefficient α predicted by the GE model are unobservable with presently available samples due to the width of the size distribution.[6]

(2) Quartic frequency dependence of α in the far infrared, if observed, can be interpreted as a quantum size effect.

(3) The GE model can be tested by looking for nonquadratic frequency dependence (i.e., an energy gap) in α at low frequencies for very small particles.

ACKNOWLEDGMENTS

[1]D. B. Tanner, A. J. Sievers, and R. A. Buhrman, Phys. Rev. B **11**, 1330 (1975).

[2]C. G. Granqvist, R. A. Buhrman, J. Wyns, and A. J. Sievers, Phys. Rev. Lett. **37**, 625 (1976).

[3]L. P. Gor'kov and G. M. Eliashberg, Zh. Eksp. Teor. Fiz. **48**, 1407 (1965) [Sov. Phys.—JETP **21**, 940 (1965)].

[4]S. Strassler, M. J. Rice, and P. Wyder, Phys. Rev. B **6**, 2575 (1972).

[5]A. A. Lushnikov and A. J. Simonov, Phys. Lett. **44A**, 45 (1973).

[6]R. P. Devaty and A. J. Sievers, Phys. Rev. B **22**, 2123 (1980).

[7]L. Genzel and U. Kreibig, Z. Phys. B **37**, 93 (1980).

[8]M. L. Mehta, *Random Matrices and the Statistical Theory of Energy Levels* (Academic, New York, 1967).

[9]E. P. Wigner, Ann. Math. **53**, 36 (1951); **62**, 548 (1955).

[10]F. J. Dyson, J. Math. Phys. **3**, 140, 166 (1962); M. L. Mehta and F. J. Dyson, *ibid.* **4**, 713 (1963).

[11]G. Mie, Ann. Phys. (Leipzig) **25**, 377 (1908); M. Born and E. Wolf, *Principles of Optics*, 5th ed. (Pergamon, Oxford, 1975),

pp. 633ff.

[12]R. Kubo, J. Phys. Soc. Jpn. **17**, 975 (1962).

[13]L. D. Landau and E. M. Lifshits, *Electrodynamics of Continuous Media* (Pergamon, Oxford, 1975), p. 193.

[14]C. G. Granqvist, Z. Phys. B **30**, 29 (1978).

[15]N. W. Ashcroft and N. D. Mermin, *Solid State Physics* (Holt, Rinehart, and Winston, New York, 1976), p. 38.

[16]C. Kittel, *Introduction to Solid State Physics*, 4th ed. (Wiley, New York, 1971), p. 254.

[17]D. M. Wood and N. W. Ashcroft, Phys. Rev. B **25**, 6255 (1982).

[18]C. G. Granqvist and R. A. Buhrman, J. Appl. Phys. **47**, 2200 (1976); R. A. Buhrman and C. G. Granqvist, *ibid.* **47**, 2220 (1976).

[19]G. L. Carr, R. L. Henry, N. E. Russell, J. C. Garland, and D. B. Tanner, Phys. Rev. B **24**, 777 (1981); N. E. Russell, J. C. Garland, and D. B. Tanner, *ibid.* **23**, 632 (1981).

[20]R. P. Devaty and A. J. Sievers, Phys. Rev. Lett. **52**, 1344 (1984).

Two-dimensional electron gas in $In_{0.53}Ga_{0.47}As/InP$ heterojunctions grown by atmospheric pressure metalorganic chemical-vapor deposition

L. D. Zhu,[a] P. E. Sulewski,[b] K. T. Chan, K. Muro,[c] J. M. Ballantyne, and A. J. Sievers

School of Electrical Engineering and Physics Department, Cornell University, Ithaca, New York 14853

High-quality modulation doped $In_{0.53}Ga_{0.47}As/InP$ heterostructures have been grown by atmospheric pressure metalorganic chemical-vapor deposition (MOCVD) using solid trimethylindium source. The two-dimensional nature of electrons bound in the $In_{0.53}Ga_{0.47}As/$ InP heterojunctions is proved by a Shubnikov-de Haas effect experiment. Electron Hall mobilities as high as 12000, 83000, 98000, and 92000 cm^2/V s at 300, 77, 40, and 4.2 K are obtained, respectively. The electron effective mass is measured to be $m^*_{CR} = 0.043\ m_0$ by cyclotron resonance experiments on the samples with two-dimensional electron sheet concentrations of $(3.0-3.7)\times10^{11}/cm^2$. From far-infrared impurity absorption data the ionization energy of the residual donors in the MOCVD-grown $In_{0.53}Ga_{0.47}As$ is determined to be 2.95 meV.

I. INTRODUCTION

Two-dimensional electron systems bound in semiconductor surfaces, heterojunction interfaces, or quantum wells have been attracting great attention for their unusual physical properties such as quantum hall effect,[1] and because of their promise for applications.[2] Advanced silicon MOS technology has made the electron system in this structure available for scientific investigations, which confirmed for the first time the two-dimensional nature of the electrons in the inversion layer at the surface.[3] However, it has been found that electron mobility in this structure is limited by surface roughness scattering,[4] which is difficult to eliminate. GaAlAs/GaAs heterojunction interfaces grown by molecular beam epitaxy or metalorganic chemical-vapor deposition (MOCVD) are abrupt and smooth on the monolayer scale, and mobility of the two-dimensional electron gas (2-DEG) is limited mainly by ionized impurity scattering at low temperature. Hence, modulation-doped GaAlAs/GaAs heterostructure exhibited 4 K electron mobilities as high as 2×10^6 cm^2/V s under illumination,[5] a result which stimulated intensive research on high-speed devices. The lattice-matched $In_{0.53}Ga_{0.47}As/InP$ heterostructure is another interesting materials system. For $In_{0.53}Ga_{0.47}As$, room-temperature electron mobility as high as 12000 cm^2/V s is available, and peak electron-drift velocity is higher and negative-differential mobility is larger than GaAs.[6] This makes InGaAs especially attractive for high-speed devices. Furthermore, its band gap is wide enough for device application at room temperature and its optical properties are suitable for fabricating optoelectronic devices. So far, the only reports on 2-DEG in InGaAs/InP heterostructures grown by MOCVD have come from the French group at Thomson-CSF.[7,8] They used a low-pressure MOCVD system with liquid triethylindium (TEI) as the indium source to get sharp heterointerfaces and

to avoid adduct formation. Their highest 77 K mobility is 60000 cm^2/V s[9] and reported highest 4.2 K mobility is 51000 cm^2/V s.[7] Besides, some groups are working for high-mobility InGaAs/InP structures by VPE. For example, M. Takikawa *et al.* obtained 2-DEG mobilities of 9400, 71200, and 106000 cm^2/V s at 300, 77, and 4, 2 K, respectively, by chloride transport VPE.[10]

We report here the first observation of 2-DEG formation in $In_{0.53}GA_{0.47}As/InP$ heterojunctions grown by atmospheric pressure MOCVD using more stable solid trimethylindium (TMI) as the indium source. Various experimental techniques were applied to characterize the 2-DEG at the heterointerface. Standard Hall measurements were carried out to obtain the mobility and the sheet-carrier density n, as a function of temperature. Shubnikov-de Haas experiments were also performed to determine independently the sheet density and to confirm the two-dimensional nature of the electron gas at the heterointerface. Cyclotron resonance experiments at various magnetic fields using far-infrared Fourier-transform spectroscopy determined the effective mass for the 2-DEG. Unlike laser spectroscopy, Fourier-transform spectroscopy enables one to view the entire resonance in frequency space and determine the linewidths at different fields unambiguously. In addition, far-infrared absorption spectra of the donor impurities in the MOCVD-grown $In_{0.53}Ga_{0.47}As$ resulted in the determination of the ionization energy of the residual donors.

II. EXPERIMENTS

Our measurements were carried out on two typical samples. Sample 1 is a double heterostructure (DH) grown on an iron-doped semi-insulating InP substrate. A 0.6-μm-InP buffer layer is grown on the substrate, followed by a 3.0-μm-thick $In_{0.53}Ga_{0.47}As$ epilayer and a 0.3-μm-InP cap layer. The electron concentrations of the InP epilayers are $\sim 1\times10^{16}$ cm^{-3} and the estimated electron concentration for the InGaAs is $\sim 2.7\times10^{14}$ cm^{-3}. Sample 2 is the same as sample 1 except without InP cap layer. The sample struc-

---

[a] On leave from the Institute of Semiconductors, Chinese Academy of Sciences, Beijing, China.

[b] AT&T Bell Laboratories Scholar.

[c] On leave from Department of Engineering Science, Osaka University, Osaka, Japan.

Sample 1

0.3μ InP n: 1×10^{16} cm^{-3}

3.0μ In$_{0.53}$Ga$_{0.47}$As

n: 2.7×10^{14} cm^{-3}

$- - - - - - - - -$ ← 2 DEG →

0.6μ InP n: 1×10^{16} cm^{-3}

S. I. InP Sub.

Sample 2

3.0μ In$_{0.53}$Ga$_{0.47}$As

n: 2.7×10^{14} cm^{-3}

$- - - - - - - - -$

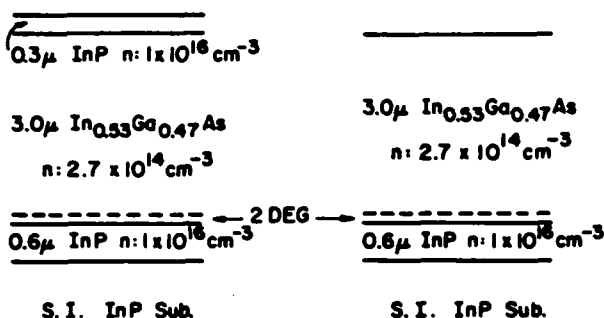0.6μ InP n: 1×10^{16} cm^{-3}

S. I. InP Sub.

FIG. 1. Schematic diagram of the sample structures and parameters.

tures are shown schematically in Fig. 1. Growth of the samples was carried out by atmospheric pressure MOCVD with a specially designed reactor configuration to enhance growth efficiency and interface sharpness.[11] TMI was used as the In source with sublimation temperature as low as 12.1 °C. Attention was paid to changing the gas flows when growing interface regions; the details of the growth procedure are described elsewhere.[12] It is worth pointing out that our samples are a little negatively mismatched, with a lattice mismatch $\Delta a/a = -0.04\%$ at room temperature for sample 1. This was done to assure exact lattice matching at the 650 °C growth temperature where excited atomic motion easily forms mismatch dislocations.

Hall measurements were carried out by standard Van der Pauw technique, using an Oxford instruments' CF204 continuous flow cryostat in the temperature range from 2.7–300 K. The sample was made clover-leaf shaped, and tin dots were alloyed at 420 °C for 2 min. to make good Ohmic contacts to the 2-DEG. Hall measurements were done with a magnetic field of 2 kG, keeping the sample in the dark.

Shubnikov-de Haas effect experiments were carried out at 1.3–1.8 K on the samples immersed in pumped liquid ^{4}He. The sample was bar-shaped with six tin Ohmic contacts on it. A constant current, perpendicular to the magnetic field, was passed through the sample, and magnetoresistance and Hall resistance were measured through the respective pairs of contacts. A superconducting magnet provided a continuously variable magnet field from 0 to 7.4 T. The angle between the sample surface normal and the magnetic field was varied from 0 to 90 °C by tilting the sample.

Cyclotron resonance experiments were made using far-infrared Fourier-transform spectroscopy. A lamellar interferometer was used in the frequency range from 5–50 cm^{-1} and a Michelson interferometer was used from 50–250 cm^{-1}. The far-infrared source was a mercury arc and the detector a germanium bolometer cooled to 0.3 K by pumped ^{3}He. Samples were held at 1.3 K by immersing them in a pumped liquid ^{4}He bath. The magnetic field supplied by a superconducting magnet was varied from 0 to 6 T. The sample transmissivity was measured as a function of frequency for given magnetic fields.

III. RESULTS AND DISCUSSION

A. Low-field transport properties

For the double heterostructure sample there are two heterojunction interfaces which may form two separated quantum-well channels. To determine the contribution of each channel to the total mobility and sheet-carrier concentration, the Hall measurement was repeated after selectively etching away the cap InP layer with HCl. Within the ~10% experimental error, the Hall mobilities and sheet-carrier concentrations were the same before and after the etching. The Hall measurement results of sample 1 are shown in Fig. 2. In the high-temperature region from 100 to 300 K the mobility decreases approximately as $T^{-1.75}$ because of two-mode LO phonon scattering. The mobility peak occurs at about 40 K. The Hall data at some important temperatures are tabulated in Table I. We believe these are the highest mobilities reported to date for 2-DEG in I$_{0.53}$Ga$_{0.47}$As/InP grown by MOCVD.

Generally, the measured Hall data are effective values when a sample has several conduction channels. At temperatures below about 7 K all carriers in the bulk material are frozen out, leaving only the 2-DEG still conducting. Because the cap layer removal did not affect the sheet-carrier concentration and mobility, the cap layer interface apparently did not form a 2-DEG; this is possibly because the surface barrier depletion layer extended to the interface, and prevented the conduction band edge from being below the Fermi energy. Hence, only the buffer-layer interface formed a quantum-well conduction channel, and this channel contains a sheet 2-DEG density of $n_s = 3.0 \times 10^{11}$/cm^2. Our repeated experiments showed that InP layers less than 2.0–2.5 μm thick grown with similar conditions on semi-insulating InP substrates were completely depleted by the surface barrier and the substrate-epilayer interface barrier. If the surface barrier of InP is ~0.25 eV and the interface barrier is ~0.6 eV,[13] then respective depletion layer widths are ~0.8 and ~1.2 μm for our doping level. This corroborates our conclusion that, for our samples, cap and buffer InP layers are completely depleted.

For a triangular well, the lowest quantum state energy is (cf. Stern[14])
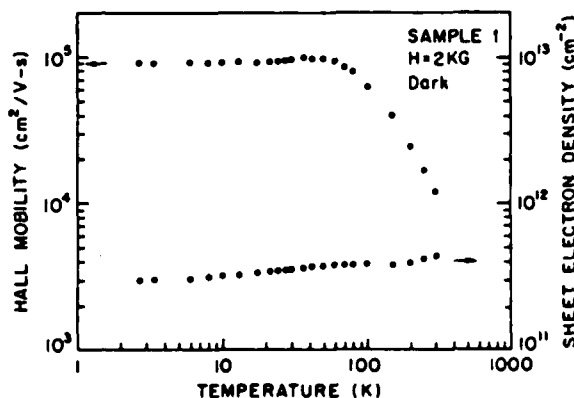

FIG. 2. Temperature dependence of the electron mobility and sheet-electron density of sample 1, In$_{0.53}$Ga$_{0.47}$As/InP double heterostructure.

3146   J. Appl. Phys., Vol. 58, No. 8, 15 October 1985

Zhu et al.   3146

16

T(K)	300	77	40	4.2
$\mu(\text{cm}^2/\text{V s})$	12000	83000	98000	92000
$n_s(\text{cm}^{-2})$	4.4×10^{11}	3.8×10^{11}	3.8×10^{11}	3.0×10^{11}

$$E_0 = \tfrac{3}{5}(33\, e^2\hbar n_s/8\epsilon_0\epsilon_r m^*_{CR}{}^{1/2})^{2/3} = 48.0 \text{ meV}. \quad (1)$$

Here we used our cyclotron resonance effective mass of the 2-DEG as $m^*_{CR} = 0.043\, m_0$, and $\epsilon_r = 14$. The Fermi-level height of 16.7 meV above E_0 is deduced by computing the occupancy of this level n_s using the density of states $D(E) = m^*_{CR}/\pi\hbar^2$, and neglecting the occupation of higher subbands. Hence, the Fermi level is only 64.7 meV above the bottom of the well. This means the interface quantum well is shallow, and most of the conduction-band discontinuity is above the Fermi level. Hence, the conduction band-edge picture of sample 1 can be drawn as shown in Fig. 3.

At high temperatures, because the dominant scattering is two-mode LO phonon scattering, the mobility of both the 2-DEG and the InGaAs bulk carriers is the same value of 1200 cm^2/V s at 300 K for the best samples.[9,12,15] We assume that at 200 K, the 2-DEG and the InGaAs bulk carriers still have the same mobility. In a two-conduction channel case the effective Hall concentration and mobility are expressed by[16]

$$n_{\text{eff}} = (n_1\mu_1 + n_2\mu_2)^2/(n_1\mu_1^2 + n_2\mu_2^2), \quad (2)$$

$$\mu_{\text{eff}} = (n_1\mu_1^2 + n_2\mu_2^2)/n_1\mu_1 + n_2\mu_2), \quad (3)$$

where the subscripts 1 and 2 denote the bulk and the 2-DEG, respectively. If $\mu_1 = \mu_2$ at 200 K, then $n_{\text{eff}} = n_1 + n_2$. From the measured Hall data we therefore get the In$_{0.53}$Ga$_{0.47}$As bulk-carrier concentration (n_b^{200}) to be $(2.7-3.0)\times10^{14}$/cm^3. If the surface depletion barrier of InGaAs is not zero, this estimation is lower than the real value. At the temperature ($\sim$40 K) of peak mobility, the donors in InGaAs are completely ionized; hence, the bulk-electron concentration is nearly the same as that at 200 K, since the sheet density of the 2-DEG is a weak function of temperature, we can take $n_1 = 0.8\times10^{11}$/cm^2, $n_2 = 3.0\times10^{11}$/cm^2, and from the measured Hall data using Eqs. (2) and (3) we get $\mu_b = 65080$ cm^2/V s, and $\mu_{2\text{-DEG}} = 103600$ cm^2/V s. Because the electrons in the 2-DEG are transferred from the InP buffer layer to the interface quantum well, the separation of the 2-DEG
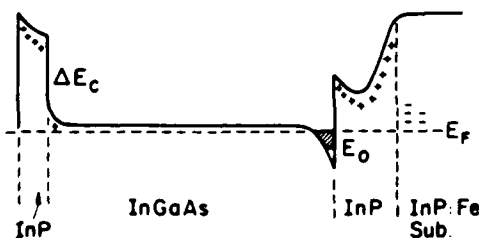
from the parent ions reduces the ionized impurity scattering. This enhances the low-temperature mobility of the 2-DEG to a value much higher than that of the carrier in bulk In$_{0.53}$Ga$_{0.47}$AS, as shown previously for AlGaAs/GaAs heterostructures.[17]

B. Shubnikov-de Haas effect measurements

The existance of a 2-DEG may be inferred from Fig. 2. Direct proof is given by Shubnikov-de Haas effect measurements shown in Fig. 4. These measurements were done on sample 2. The sheet-carrier concentration of the sample is 3.1×10^{11}/cm^2 at 4.2 K by Hall measurement. Figure 4 demonstrates pronounced Shubnikov-de Haas oscillations of magnetoresistance ρ_{xx} and shows the strong dependence on the angle θ between the magnetic field direction and the layer normal. Also shown are corresponding multistage Hall resistances ρ_{xy} for $\theta = 55°$. Figure 5 shows the reciprocal magnetic field corresponding to the ρ_{xx} oscillation maxima as a function of the Landau-level index N for $\theta = 0$ and 55°. The oscillations are periodic in B^{-1} and follow the dependence

$$\frac{1}{B} = \frac{N}{n_s}\frac{2e\cos\theta}{h}. \quad (4)$$

This proves the two dimensionality of the electron gas. From Eq. (4) and Fig. 5 the sheet density of the 2-DEG is calculat-

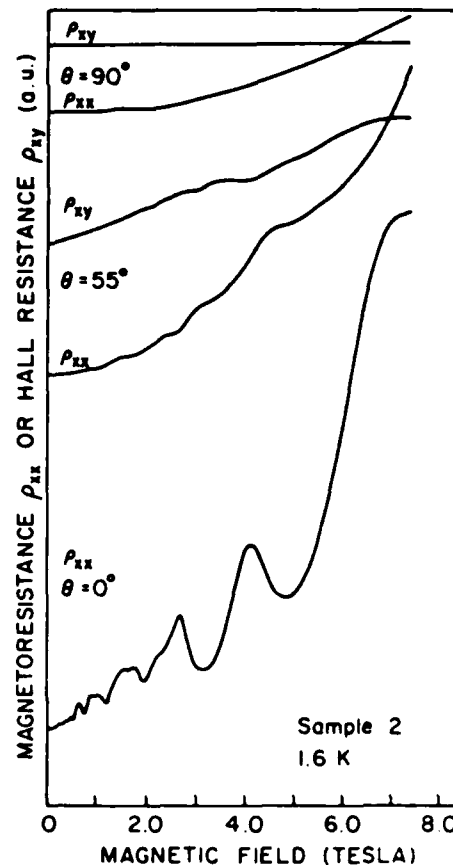

FIG. 3. Conduction band-edge bending picture of sample 1 drawn schematically according to the analysis in the text.

FIG. 4. Results of Shubnikov-de Haas effect measurement on sample 2, also shown are Hall resistance ρ_{xy}.

17

ed to be $n_s = 3.2 \times 10^{11}/cm^2$, in good agreement with the Hall data. In Fig. 4 there is additional structure at low field which we shall discuss elsewhere.

C. Cyclotron resonance experiments

1. Cyclotron resonance of the 2-DEG

Examples of cyclotron resonance spectra for a few fixed fields are shown in Fig. 6. In the figure, the main absorption peaks correspond to the cyclotron resonance of the 2-DEG, while the smaller peaks to the right correspond to the cyclotron resonance absorption of the donor-bound electrons. The frequencies of these peaks are plotted as a function of the magnetic field in Fig. 7. It is clear that the absorption peak frequency shifts proportionally to the magnetic field, and no deviation from linearity was observed in the range of the magnetic field used, indicating no coupling with LO phonon. Indeed, in the ternary $In_{0.53}GA_{0.47}As$ the GaAs-like LO mode and InAs-like LO-mode frequencies are 275 and 233 cm^{-1}, respectively.[18,19] The InP substrate TO-mode frequency is 307 cm^{-1}, so, it should be possible to observe the anticrossing of the 2-DEG cyclotron resonance at 233 cm^{-1}, only if we raised the magnetic field to about 11 T. From the slope of Fig. 7, using the relation $\omega_c = eB/m^*c$, we can extract a cyclotron resonance effective mass of $m^*_{CR} = 0.043\, m_0$ for the 2-DEG. The measurements on other samples showed that this value corresponds to 2-DEG densities $N_s = (3.0-3.7) \times 10^{11}/cm^2$, which are measured by Shubnikov-de Haas measurements. The band edge effective mass of electrons in $In_{0.53}Ga_{0.47}As$ is $m^* = 0.041\, m_0$.[20] The increase of the 2-DEG effective mass can be attributed to nonparabolicity of the conduction band.[21]

For the absorption spectra in Fig. 6, the linewidth $\Delta\omega$ can be expressed by

$$\Delta\omega = 2/\tau_q, \tag{5}$$

if we assume the line shape is Lorentzian. Over the range of magnetic fields used, the linewidths of resonances (FWHM) are $\Delta\omega = 10-11$ cm^{-1}, and are nearly independent of the field. Thus, Eq. (5) leads to a relaxation time $\tau_q = (1.0 \pm 0.1) \times 10^{-12}$ s for the 2-DEG. If we denote the low-field relaxation time as τ_c, which is deduced from the relation $\mu = e\tau_c/m^*$, then the ratio $\tau_q/\tau_c \approx 0.5$ for the range of magnetic field in Fig. 6.

2. Donor-bound electron cyclotron resonance

The upper line in Fig. 7 represents donor-bound electron cyclotron resonance in the InGaAs bulk region, which is caused by the transition Is$\rightarrow$(2p,m = +1) of the hydrogenic donor-bound electrons.[22,23] In the region where the magnetic field satisfies $(1/2)\hbar\omega_c/R^*_y \gg 1$, where R^*_y is the effective Rydberg of the donors in InGaAs, this line is approximately parallel to the 2-DEG cyclotron resonance line. If we extrapolate this impurity absorption line to zero field and approximately take this value as $(3/4)R^*_y$, then the ionization energy of the residual donor in the MOCVD grown InGaAs is $R^*_y = 2.95$ meV. According to the quasihydrogenic model of the donor in semiconductors
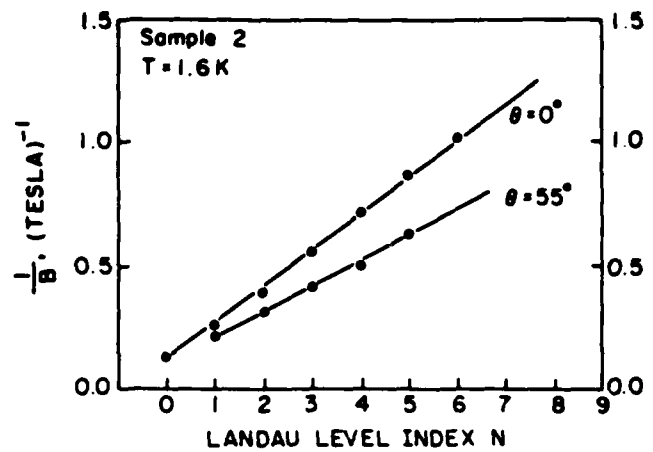
$$R^*_y = 13.6(m^*/m_0)(1/\epsilon_r^2). \tag{6}$$

FIG. 5. Reciprocal magnetic field, $1/B$, at maxima of the oscillations vs Landau quantum index for $\theta = 0°$ and $55°$.

If we take $m^* = 0.43\, m_0$, $\epsilon_r = 14$, then $R^*_y = 2.98$ meV, in good agreement with the experimental result. However, the residual donor impurity itself has not been identified yet.

IV. CONCLUSION

A high-qualtiy 2-DEG bound in an $In_{0.53}GA_{0.47}As/$ InP heterojunction was obtained for the first time by atmospheric pressure MOCVD using solid TMI as the indium source. Low-field Hall mobilities as high as $\mu_{300} = 12000$, $\mu_{77} = 83000$, $\mu_{4.2} = 92000$ cm^2/V-s have been obtained with the maximum mobility 98000 cm^2/V s at around 40 K. The two-dimensional nature of the electrons bound in the buffer layer heterointerface has been proved by Shubnikov-de Haas effect experiments, and the 2-DEG sheet density was measured to be $n_s = 3.2 \times 10^{11}/cm^2$ for sample 2, in good agreement with the results of 4.2-K Hall measurement. The effective mass of the 2-DEG is measured to be $m^*_{CR} = 0.043\, m_0$ for 2-DEG densities $(3.0-3.7) \times 10^{11}/cm^2$ by a cyclotron resonance experiment using far-infrared Fourier-transform spectroscopy. The relaxation time of the 2-DEG was estimated to be $(1.0 \pm 0.1) \times 10^{-12}$ s from the cyclotron resonance linewidth. The ionization energy of the residual
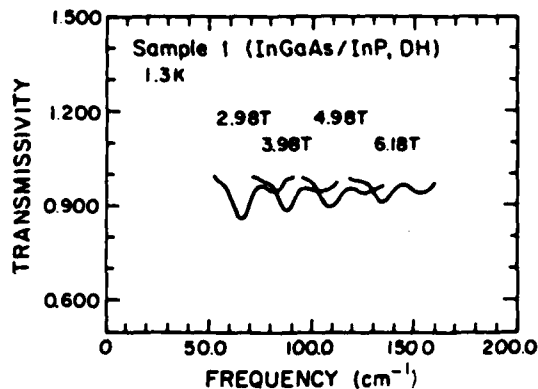

FIG. 6. Cyclotron resonance transmission spectra for several magnetic fields for sample 1.
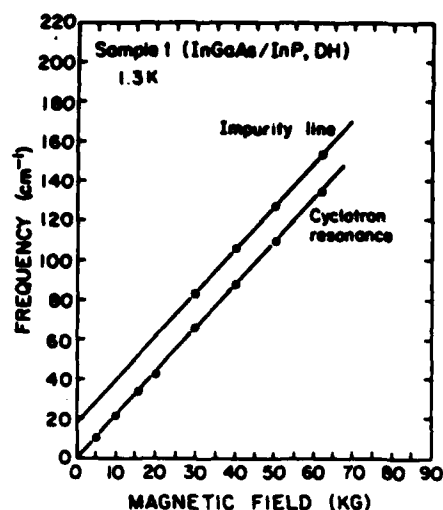
18

FIG. 7. Cyclotron resonance absorption peak frequency vs magnetic field for sample 1.

donors in MOCVD-grown $In_{0.53}Ga_{0.47}As$ was measured from the donor-bound electron cyclotron resonance. The measured ionization energy 2.95 meV is in good agreement with the theoretical result of the quasihydrogenic model.

[1]D. C. Tsui and A. C. Gossard, Appl. Phys. Lett. 38, 350 (1981).
[2]T. Mimura, K. Joshin, S. Hiyamizu, K. Hikosaka, and M. Abe, Jpn. J. Appl. Phys. 20, L598 (1981).
[3]A. B. Fowler, F. F. Fang, W. E. Howard, and P. J. Stiles, Phys. Rev. Lett. 16, 901 (1966).
[4]T. Ando, J. Phys. Soc. Jpn. 43, 1616 (1977).
[5]S. Hiyamizu, J. Saito, K. Nabu, and T. Ishikawa, Jpn. J. Appl. Phys. 22, L609 (1983).
[6]T. H. Windhorn, L. W. Cook, and G. E. Stillman, IEEE Electron Device Lett. EDL-3, 18 (1982).
[7]Y. Guldner, J. P. Vieren, P. Voisin, M. Voos, M. Razeghi, and M. A. Poisson, Appl. Phys. Lett. 40, 877 (1982).
[8]J. C. Portal, R. J. Nicholas, M. A. Brummell, M. Razeghi, and M. A. Poisson, Appl. Phys. Lett. 43, 293 (1983).
[9]M. Razeghi and J. P. Duchemin in Springer Series in Solid-State Sciences 53; Two-Dimensional Systems, Heterostructures, and Superlattices, Proceedings of the International Winter School, Mauterndorf, Austria, Feb. 26–Mar. 2, 1984, edited by G. Bauer, F. Kuchar, and H. Heinrich (Spring, Berlin, 1984), p. 100.
[10]M. Takikawa, J. Komeno, and M. Ozeki, Appl. Phys. Lett. 43, 280 (1983).
[11]L. D. Zhu, K. T. Chan, and J. M. Ballantyne, J. Cryst. Growth (to be published).
[12]K. T. Chan, L. D. Zhu, and J. M. Ballantyne, Appl. Phys. Lett. 47, 44 (1985).
[13]L. F. Eastman (private communication).
[14]F. Stern, Phys. Rev. B 12, 4891 (1972).
[15]James D. Oliver, Jr. and Lester F. Eastman, J. Electron. Mater. 9, 693 (1981).
[16]S. Hiyamizu, K. Nanbu, T. Mimura, T. Fujii, and H. Hashimoto, Jpn. J. Appl. Phys. 20, L378 (1981).
[17]R. Dingle, H. L. Störmer, A. C. Gossard, and W. Wiegmann, Appl. Phys. Lett. 33, 665 (1978).
[18]S. Yamazaki, A. Ushirokawa, and T. Katoda, J. Appl. Phys. 51, 3722 (1980).
[19]M. H. Brodsky and G. Lucovsky, Phys. Rev. Lett. 21, 990 (1968).
[20]T. P. Pearsall, R. Bisaro, P. Merenda, G. Laurencin, R. Ansel, J. C. Portal, C. Houlbert, and M. Quillec, Gallium, Arsenide and Related Compounds (Institute of Physics and Physical Society, London, 1979), p. 94.
[21]A. Raymond, J. L. Robert and B. Pistoulet, Gallium Arsenide and Related Compounds (Institute of Physics and Physical Society, London, 1979), p. 105.
[22]H. Hasegawa and R. E. Howard, Phys. Chem. Solids 21, 179 (1961).
[23]G. E. Stillman, C. M. Wolf, and J. O. Dimmock, Solid State Commun. 7, 921 (1969).

19

Dipole-dipole-interaction-induced line narrowing in thin-film vibrational-mode spectra

Z. Schlesinger

IBM Thomas J. Watson Research Center, Box 218, Yorktown Heights, New York 10598

L. H. Greene[*] and A. J. Sievers

Laboratory of Atomic and Solid State Physics and Materials Science Center,
Cornell University, Ithaca, New York 14853

Under certain circumstances the electric dipole interaction can reduce or eliminate the effects of spectral inhomogeneous broadening on an infrared absorption line of a thin film. The oscillating electric dipole moment must be oriented perpendicular to the film surface, and the dipole interaction, as measured by the frequency shift that it induces, must be larger than the width of the inhomogeneous frequency distribution. An example of this interaction-induced line narrowing is presented for a vibrational mode of a KReO₄ film, and the relevance of this mechanism to two-dimensional electron-gas subband transitions and adsorbate vibrational modes is considered.

Infrared-active modes oriented perpendicular ($\perp$) to the plane of a thin film may assume a collective nature due to the long-range (r^{-3}) electric dipole forces within the film. For these perpendicular modes, frequencies tend to be shifted upward and mode intensities do not obey ordinary sum rules. Analogous effects are found in a number of systems including thin films,[1,2] inversion layers in semiconductors,[3,4] and adsorbate systems.[5-8] Recent advances in the spectroscopy of adsorbate vibrational modes at monolayer and submonolayer coverages[9,10] as well as the heightened interest in two-dimensional (2D) electron systems enhance the importance of understanding these effects.

In this paper we study the ν_3 vibrational mode of a KReO₄ thin film. This system has a strong dipole-dipole interaction and exhibits unusual nonlinear behavior which has been discussed elsewhere.[11] Here we concentrate on linear properties and, in particular, show that the perpendicular mode linewidth is narrowed considerably due to the electric dipole-dipole interaction. The possibility that this interaction-induced line narrowing, for which there is a direct analogy in magnetic resonance,[12] has been observed previously in the two-dimensional electron gas on helium[13] is also explored briefly.

Let us begin with the experimental result. Noncrystalline or polycrystalline KReO₄ films are thermally evaporated from a powder onto various metal or transparent substrates. In Fig. 1 the transmission spectrum of a ≈ 1000 Å KReO₄ film on a KCl substrate is shown for TM polarized radiation incident at 45°. The polarization and angular dependencies of these absorption line strengths show clearly that the lower frequency (≈ 908 cm^{-1}) feature is due to parallel modes while the sharper line at ≈ 951 cm^{-1} is associated with the perpendicular modes. As we expect the film to be nominally isotropic, the substantial difference in the width and shape of the perpendicular and parallel mode absorptions is surprising. We will explain this difference without invoking any anisotropy, as a consequence of the collective (i.e., dipole-coupled) nature of the perpendicular mode oscillations in the thin-film system. (An excellent introduction to the properties of the vibrational modes of thin films and other smaller systems is given in Ruppin and Englman.[2])

The system under study consists of a thin film of thickness d, sandwiched between a substrate (index of refraction, n_3) and air ($n_1 = 1$). As we are interested in obtaining only the $q = 0$ (optical) response, we can model the film by a complex dielectric function $\epsilon_2(\omega)$. (To obtain finite q response more sophisticated approaches, such as the one described by Persson and Ryberg,[8] must be used.) For such a three-layer system the linearized equation for the change in the substrate reflectance due to the presence of the film is given in Ref. 14. From the appropriate Fresnel equation[15] one can derive the analogous equation for the change (due to the film presence) in the transmittance of TM polarized radiation

$$\frac{\Delta T}{T} = 2\omega \frac{d}{c} C_0 \{ C_\parallel \cos^2\theta \, \text{Im}[\epsilon_2(\omega)]$$
$$+ C_\perp \sin^2\theta \, \text{Im}[-\epsilon_2^{-1}(\omega)] \} , \qquad (1)$$
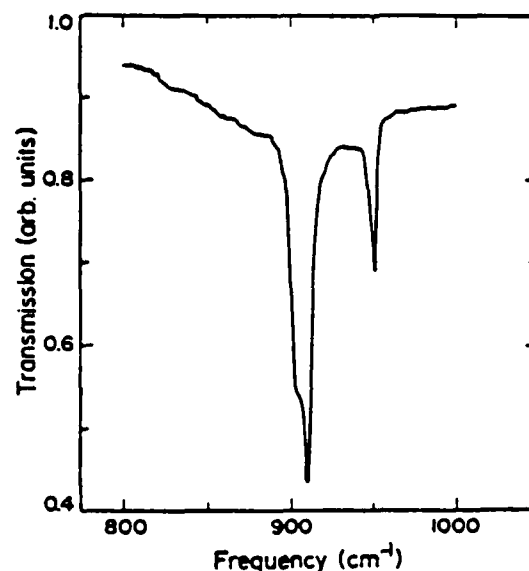

FIG. 1. Absorption lines associated with the ν_3 mode of ReO₄$^-$ in a KReO₄ film are shown for $\theta = 45°$. The broad resonance near 910 cm^{-1} is due to oscillations polarized in the film plane, while the sharper and weaker line near 950 cm^{-1} is due to perpendicular oscillations.

where ω and θ are the frequency and angle of incidence of the incident radiation, and

$$C_0 = \left[n_1 \left(- \frac{n_1^2}{n_3^2} \sin^2\theta \right)^{1/2} + n_3\cos\theta \right]^{-1} . \tag{2}$$

$$C_\| = \left[1 - \frac{n_1^2}{n_3^2} \sin^2\theta \right]^{1/2} \Big/ \cos\theta . \tag{3}$$

$$C_\perp = n_1^3 n_3 . \tag{4}$$

Although not really necessary for calculation Eq. (1) is heuristically useful since the term containing $\text{Im}[\epsilon_2(\omega)]$ is associated with absorption due to electric dipole oscillations in the plane of the film (parallel modes), while the $\text{Im}[-\epsilon_2^{-1}(\omega)]$ term is due to the perpendicular modes. We will now examine the resonances in these response functions for several simple models.

For a single mode Lorentz oscillator[16] (frequency ω_t, damping γ, mode strength ω_p^2) with static screening ϵ_∞

$$\epsilon_2(\omega) = \epsilon_\infty + \omega_p^2/(\omega_t^2 - \omega^2 - i\gamma\omega) . \tag{5}$$

$\text{Im}[\epsilon_2(\omega)]$ has a resonance at the frequency ω_t of width γ corresponding to the absorption due to the parallel mode. On the other hand, the longitudinal response function

$$\text{Im}[-\epsilon_2^{-1}(\omega)] = \text{Im}\left[\frac{\omega_p^2/\epsilon_\infty^2}{\omega_t^2 + \omega_p^2/\epsilon_\infty - \omega^2 + i\gamma\omega} \right] . \tag{6}$$

which is associated with the perpendicular oscillations, has its resonance at the higher frequency

$$\omega_l = \omega_t + \omega_p^2/\epsilon_\infty . \tag{7}$$

With respect to the parallel mode the perpendicular mode resonance is (1) shifted upward in frequency by approximately

$$\omega_s = \frac{\omega_p^2}{2\epsilon_\infty\omega_T} . \tag{8}$$

(2) weaker in intensity by ϵ_∞^2, and (3) equal in linewidth. (1) and (2) are consistent with the experimental results (Fig. 1); however, (3) is not since in the experiment we find that the parallel mode absorption is significantly broader than that associated with the perpendicular mode.

In order to explain this linewidth discrepancy let us consider the introduction of inhomogeneous broadening to $\epsilon_2(\omega)$, the simplest case of which involves a two oscillator dielectric function:

$$\epsilon_2(\omega) = \epsilon_\infty + \sum_{j=1}^{2} \frac{\omega_{pj}^2}{\omega_{tj}^2 - \omega^2 - i\gamma\omega} . \tag{9}$$

In this case $\text{Im}[\epsilon_2(\omega)]$, as shown in Fig. 2, has a doublet resonance with peaks at ω_{t1} and ω_{t2} corresponding to absorption due to parallel modes. Surprisingly, however, $\text{Im}[-\epsilon_2^{-1}(\omega)]$ does not mimic this doublet structure, but has only a single sharp resonance at a frequency between $\omega_{t1} + (\omega_{p1}^2 + \omega_{p2}^2)/\epsilon_\infty$ and $\omega_{t2} + (\omega_{p1}^2 + \omega_{p2}^2)/\epsilon_\infty$. This tendency of the resonance in $\text{Im}[-\epsilon_2^{-1}(\omega)]$ to remain narrow despite the inhomogeneous broadening in $\epsilon_2(\omega)$ is found to prevail whenever the perpendicular-parallel mode splitting ($\approx \omega_s$) is greater than the separation of the parallel modes ($\omega_{t1} - \omega_{t2}$).

It is now clear why a transmission spectrum calculated using Eqs. (1) and (9) can compare favorably to the data
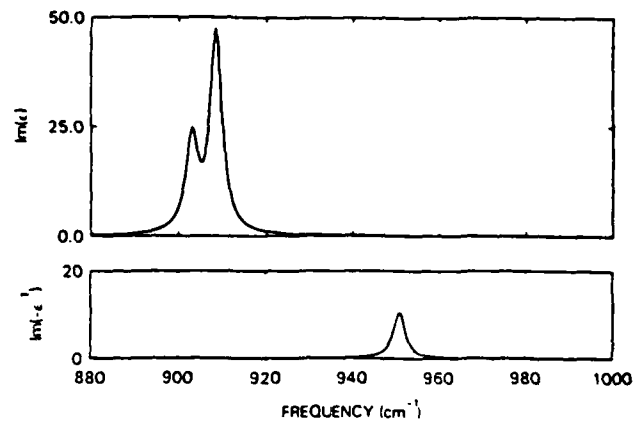
FIG. 2. Resonances of the two mode Lorentz oscillator dielectric function are shown as a function of frequency. In $\text{Im}(-\epsilon^{-1})$ the double resonance put into ϵ has coalesced into a single line.

shown in Fig. 1. The striking point is not that we can fit the data with Lorentz oscillators, but that the (doublet) structure introduced to fit the parallel modes does not produce a corresponding structure in the perpendicular absorption line.

Departing from the data of Fig. 1, we can explore this electric dipole-dipole-interaction narrowing by considering an inhomogeneously broadened line with a Gaussian profile, i.e.,

$$\epsilon_2(\omega) = \epsilon_\infty + \frac{\omega_p^2}{\sqrt{\pi}\Delta} \int_{-\infty}^{\infty} \frac{e^{-(\tilde{\omega}-\omega_t)^2/\Delta^2}}{\tilde{\omega}^2 - \omega^2 - i\gamma\omega} d\tilde{\omega} . \tag{10}$$

Here ω_t is the center frequency of the Gaussian packet and Δ and γ are the inhomogeneous and homogeneous linewidths, respectively. (We assume $\Delta > \gamma$.)

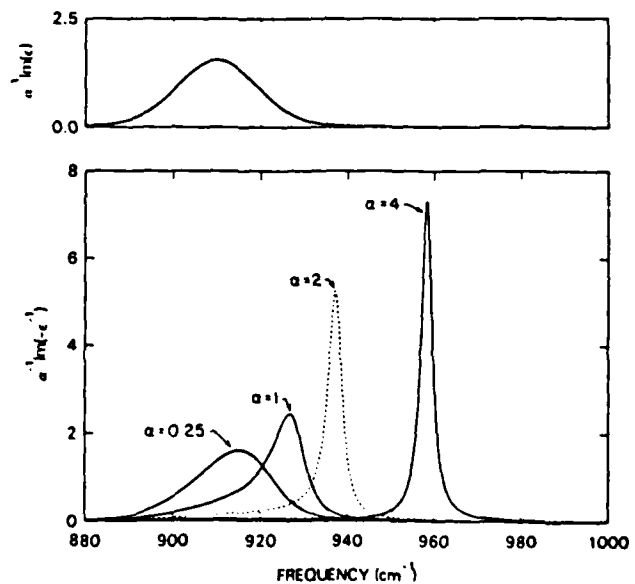The resonance in $\text{Im}[\epsilon(\omega)]$, which is associated with parallel mode absorption, always exhibits the full inhomo-

FIG. 3. Resonances of a Gaussian distribution of Lorentz oscillators are shown. The resonance in $\text{Im}(\epsilon)$ is Gaussian for all α. In contrast, the resonance in $\text{Im}(-\epsilon^{-1})$ crosses over from a broad Gaussian to the narrow Lorentzian in the neighborhood of $\alpha = 1$, as illustrated.

geneous width Δ, as shown in Fig. 3. The width and shape of the resonance in $\text{Im}[-\epsilon_2^{-1}(\omega)]$, however, depends on the dimensionless ratio of coupling strength to inhomogeneity:

$$\alpha = \omega_s/\Delta \ .$$

For the strongly coupled system $(\alpha \gg 1)$ the resonance exhibits the homogeneous width (γ) and shape, while in the weak-coupling regime $(\alpha \ll 1)$ the line is Gaussian of width Δ. An abrupt crossover occurs near $\alpha = 1$. The line shape and width of perpendicular modes thus depend critically on α.

This line narrowing may actually have been observed for the perpendicular (subband) excitations of electrons bound to the surface of He. In this system inhomogeneous broadening can be introduced in a controlled manner via a parallel magnetic field. It has been observed that with increasing areal electron density a remarkable narrowing of the resonant absorption line occurs.[13] Although an explanation in terms of changes in the velocity autocorrelation function has been put forward, dipole-dipole-interaction-induced narrowing should also be considered, especially since the observed line narrowing occurs for increasing α near[17] $\alpha = 1$.

In summary, we have shown that substantial differences observed in the linewidth and shape of parallel and perpendicular modes of KrReO$_4$ film can be accounted for by a dipole-dipole-interaction-induced narrowing of the perpendicular mode. In this collective mode individual molecules oscillate in phase at a single frequency despite having differing natural frequencies and thus the inhomogeneity inherent in the system is obscured. This interaction-induced line narrowing can occur in a wide variety of systems involving two-dimensional array of interacting dipole oscillators, including electrons on , planar arrays of metal particles, inversion layers, and adsorbate layers, as well as in thin films.

---

*Present address: Bell Communications Research, Murray Hill, NJ 07974.

[1] D. W. Bereman, Phys. Rev. 130, 2193 (1963); A. S. Barker, ibid. 136, A1290 (1963).

[2] R. Ruppin and R. Englman, Rep. Prog. Phys. 33, 149 (1970).

[3] W. B. Chen, Y. J. Chen, and E. Burstein, in Proceedings of the International Conference on Electronic Properties of Quasi-two Dimensional Systems, Providence, RI, 1975 [Surf. Sci. 58, 262 (1976)].

[4] S. J. Allen, Jr., D. C. Tsui, and B. Vinter, Solid State Commun. 20, 425 (1976).

[5] G. D. Mahan and A. A. Lucas, J. Chem. Phys. 68, 1344 (1978).

[6] H. Ibach and D. L. Mills, Electron Energy Loss Spectroscopy and Surface Vibrations (Academic, New York, 1982), Chap. 3.

[7] H. Pfnur, D. Menzel, F. M. Hoffman, A. Ortega, and A. M. Bradshaw, Surf. Sci. 93, 431 (1980).

[8] B. N. J. Persson and R. Ryberg, Solid State Commun. 36, 613 (1981); R. Ryberg, Phys. Rev. B 31, 2545 (1985); J. Chem. Phys. 82, 567 (1985).

[9] Y. J. Chabal, G. S. Higashi, and S. B. Christman, Phys. Rev. B 28, 4472 (1983).

[10] S. Chang, R. G. Tobin, P. O. Richards, and P. A. Thiel, Phys. Rev. Lett. 52, 648 (1984).

[11] L. H. Greene, Z. Schlesinger, and A. J. Sievers, Phys. Rev. B 28, 4863 (1983).

[12] S. Geschwind and A. M. Clogston, Phys. Rev. 108, 49 (1957).

[13] C. L. Zipel, T. R. Brown, and C. C. Grimes, Phys. Rev. Lett. 57, 1760 (1975).

[14] J. D. E. McIntyre and D. E. Aspnes, Surf. Sci. 24, 417 (1971).

[15] Z. Schiesinger, Ph.D. thesis, Cornell University, 1982 (unpublished).

[16] F. Wooten, Optical Properties of Solids (Academic, New York, 1972).

[17] To obtain α from microscopic quantities one can use $\omega_p^2 = 4\pi n e^2/m$ for the multilayer thin-film system, where n is the density of oscillators, e the effective change, and m the effective mass of the vibrational mode. 2D systems, such as electrons on He or adsorbates at monolayer or submonolayer coverage, may be handled somewhat differently. The dipole sum (r_{ij}^{-3}) is more or less independent of structure for close-packed 2D lattices and it is then not a bad approximation to use $\omega_p^2 \approx 8.9 n_s^{3/2} e^2/m$ (see Ref. 6), where n_s is the areal density (coverage). The situation of random partial coverage of such a lattice is treated in Ref. 5; $\omega_p^2 = 8.9 \Theta \bar{n}_s^{3/2} e^2/m$ is a reasonable approximation where $\bar{n}_s$ is the areal density at full coverage and Θ is the fractional coverage.

Surface-reconstruction-induced changes in free-carrier scattering from the W(100) surface: An infrared surface-electromagnetic-wave study

D. M. Riffe, L. M. Hanssen, and A. J. Sievers

Laboratory of Atomic and Solid State Physics and Materials Science Center, Cornell University, Ithaca, New York 14853-2501

(Received 10 February 1986)

Using the infrared-absorption technique of surface-electromagnetic-wave spectroscopy (SEWS) we have studied the effects of H_2 and D_2 chemisorption on the SEW attenuation coefficient α in the 10-μm region between 165 and 350 K. The change in α at room temperature has also been measured for N_2, O_2, and CO adsorption. The coverage (Θ) dependence of α for N_2, O_2, and CO is fairly simple [either a monotonic increase (N_2) or a peak at some intermediate coverage (O_2, CO)] and points to changes in free-carrier (FC) surface scattering as the dominant α-changing mechanism. Much richer structure in $\alpha(\Theta)$ upon H_2 and D_2 adsorption is observed: A small peak followed by a sharp dip at $\Theta = 0.42$ monolayer (ML) ($\Theta = 2$ monolayers $\equiv$ saturation), a broad maximum at $\Theta = 1.28$ ML, and a value at $\Theta = 2.0$ ML higher than for the clean surface. For $\Theta > 0.42$ ML the variations are dominated by reconstruction-induced changes in FC scattering from the surface. The difference in α between $\Theta = 1.28$ ML and saturation indicates that the $\Theta = 1.28$ ML disordered surface phase and the $\Theta = 2.0$ ML $p(1 \times 1)$-D phase are temperature independent between 165 and 300 K. Adsorbate-induced quenching of the W(100) 0.3-eV intrinsic surface states also contributes to the changes in α; the associated loss of oscillator strength is most apparent in a strong frequency dependence of α relative to the clean surface for D_2 adsorption. In addition, it is possible that a decrease in relaxation of the W(100) surface as Θ approaches 0.42 ML for H_2 or D_2 has some effect on the SEW attenuation by influencing the amount of FC interband scattering at the metal-vacuum interface.

I. INTRODUCTION

In 1952 Holstein[1] showed with a simple physical argument that the infrared (ir) absorptivity at a metal surface is larger if the conduction electrons colliding with the surface are diffusely rather than specularly reflected. The next year Dingle further developed the theory of the anomalous skin effect[2,3] from the formal equations of Reuter and Sondheimer[4] and applied his theory[5] to a large group of optical data which resulted in qualitative agreement as long as the electronic scattering from the surface was assumed diffuse. Other experimental results on the absorption of electromagnetic radiation[6-11] also indicate diffuse surface scattering. However, Bennett *et al.*,[12-14] using supersmooth substrates for ultrahigh vacuum (UHV) evaporated Au, Ag, and Al films measured in a dry N_2 atmosphere, were able to obtain ir reflection results which were consistent with specular scattering. Furthermore, by increasing the roughness of the substrate[14] they were able to increase the value of the diffuse scattering and thereby decrease the reflectivity. Their results suggest that a sample of sufficient quality can exhibit specular scattering.

Although the early prejudice was that only totally diffuse scattering was possible, in spite of a small amount of experimental evidence to the contrary,[15] many more recent experiments[16-22] show that specular scattering is possible for atomically smooth surfaces and that contamination due to chemisorption, which is necessarily present in all but careful UHV studies, need not inhibit all of the specular electronic reflection from the surface. The prob-

lem has been and continues to be to identify specularity in a quantitative manner. With the development of UHV surface probes has come the realization that surface reconstruction is a natural phenomenon which can be triggered in a variety of ways.[23] In this paper we describe our infrared investigation of free-carrier scattering at a metal surface as a function of adsorbate- and temperature-induced surface reconstruction.

The W(100)-H surface has been studied by a variety of UHV techniques which has enabled a fairly detailed structural picture to develop. In spite of the large quantity of data about this system no study has directly dealt with the interaction of the tungsten conduction electrons with the surface upon H_2 adsorption. Although optical absorption studies have been done on this system they have either concentrated on energies above 0.6 eV where interband transitions dominate the optical response,[24,25] or they have addressed only the question of the vibrational response of the adsorbate-adsorbent system.[26,27] Here we use the ir absorption technique of surface electromagnetic wave spectroscopy (SEWS) in the 125 meV (1000 cm^{-1}) region to study the surface scattering phenomenon.

We find that for H_2 and D_2 adsorption the largest contribution to the change in absorptivity in this energy range can be attributed to variations in the free-carrier scattering from the surface caused by adsorbate-induced surface reconstruction. In addition there is a contribution due to the quenching of intrinsic surface states (ISS) located near 0.3 eV which are inherent to this surface. In the next section we discuss background information on free-carrier contributions to the SEW attenuation coefficient with an

emphasis on the surface-assisted ir absorption process. In Sec. III the experimental details are presented. The results for the change in the SEW attenuation coefficient are described in Sec. IV: Room temperature (RT) exposure and coverage dependence for H_2 and D_2 is presented along with the frequency dependence and temperature dependence of D_2-induced variations. In addition, room temperature exposure results are presented for adsorption of N_2, O_2, and CO. In Sec. V we discuss these results and show that changes in the bulk Drude parameters in a small region (several lattice constants) near the surface are too small to account for the data. We then discuss the variations in attenuation in terms of the 0.3-eV ISS and the surface-assisted absorption process. The concluding section summarizes our results on electronic surface scattering from the W(100) surface.

II. FREE-CARRIER CONTRIBUTIONS TO THE SEW ATTENUATION COEFFICIENT

A. Drude model

The ability of any metal such as tungsten to absorb infrared radiation at room temperature depends upon the behavior of the conduction electrons within a skin depth δ (≈ 100 Å) of the surface. More specifically, in the Drude model, the conduction electron contribution α_{ce} to the SEW attenuation coefficient α for a metal-vacuum interface is related to the relaxation time τ of the charge carriers within δ by

$$\alpha_{ce} = \left[\frac{\omega}{\omega_p}\right]^2 \frac{1}{c\tau} \quad (\omega \ll \omega_p) ,$$

where ω is the frequency, ω_p the plasma frequency (both in rad/sec), and c the speed of light.[28] In the infrared near room temperature there are three contributions to $1/\tau$ which must be considered: the electron-electron scattering rate $1/\tau_{e-e}$, the electron-phonon scattering rate $1/\tau_\phi$, and an effective scattering rate due to collisions with the surface $1/\tau_s$. These processes are often treated as independent so that

$$\frac{1}{\tau} = \frac{1}{\tau_{e-e}} + \frac{1}{\tau_\phi} + \frac{1}{\tau_s} ;$$

hence, we first consider each one separately.

1. Electron-electron scattering

The electron-electron scattering rate has been theoretically considered by Gurzhi[29,30] and Lawrence.[31] Both authors have derived expressions for the scattering rate of the form

$$\frac{1}{\tau_{e-e}} = K\left[(k_B T)^2 + \left[\frac{\hbar\omega}{2\pi}\right]^2\right] .$$

Gurzhi's order-of-magnitude expression has $K \sim \omega_p / (\hbar\omega_p)^2$ which for tungsten is $\approx 2 \times 10^{14}$ s^{-1}eV^{-2}. [See Table I for ω_p (Ref. 32) and other ir parameters for W.] Lawrence's expression, which works fairly well for the noble metals Cu and Ag, yields values of $K \leq 10^{15}$ s^{-1}eV^{-2}.

TABLE I. Room-temperature ir parameters for W.

Parameter	Value at 1000 cm^{-1}
ρ_{dc} [a]	5.59 $\mu\Omega$ cm
$\hbar\omega_p$ [b]	7.0 eV
v_F/c [c]	4.0×10^{-3}
v_F/ω	63 Å
δ [d]	140 Å
$1/\tau_{e-e}$ [e]	1.4×10^{13} s^{-1}
$1/\tau_\phi$ [f]	5.3×10^{13} s^{-1}
$1/\tau_s$ [g]	$(1-p)1.6 \times 10^{13}$ s^{-1}
ϵ_0 [h]	70

[a]Reference 41.   [e]Reference 34.
[b]Reference 32.   [f]See text.
[c]Reference 52.   [g]Reference 1.
[d]Reference 50.   [h]Reference 62.

Experimentally, the ω^2 and T^2 signatures allow $1/\tau_{e-e}$ to be determined from temperature-dependent emissivity measurements. For the transition metals Mo, V, Ta,[33] and W (Refs. 33 and 34) $1/\tau_{e-e}$ appears to be substantially larger than either of the theoretical estimations predict. In particular, for tungsten Wojcik et al.[34] have determined a value of $K = 1.4 \times 10^{16}$ s^{-1}eV^{-2}.[35] At room temperature and 1000 cm^{-1} this yields a value of $1/\tau_{e-e} = 1.4 \times 10^{13}$ s^{-1} which implies $\alpha_{e-e} = 0.15$ cm^{-1}.

2. Electron-phonon scattering

At zero frequency near room temperature electron-phonon scattering is the dominant relaxation mechanism for the free carriers and provides the major contribution to the dc resistivity $\rho_{dc} = 4\pi/[\omega_p^2\tau(0)]$.[36] For $\omega \neq 0$ an extra decay mechanism exists due to the spontaneous emission of phonons which is absent in the zero-frequency limit.[37-39] This spontaneous emission process can produce a significant addition to the dc relaxation rate $1/\tau_\phi(0)$ for $\hbar\omega \geq 2k_B T$ and $\hbar\omega \geq 2k_B\Theta_D$ (Θ_D denotes the Debye temperature of metal).[39]

In the limits $\hbar\omega \gg k_B T$ and $\hbar\omega \gg k_B\Theta_D$ Holstein's[37,38] and Gurzhi's[39] results indicate at high temperatures ($T \gg \Theta_D$) that $1/\tau_\phi = 1/\tau_\phi(0)$. But as the temperature is lowered the spontaneous emission process gains increasing importance in the ir absorptivity until $T = 0$, at which point it constitutes the only lattice vibrational decay mechanism of the electrons. For temperatures which are not too low ($T \geq \Theta_D/4$) the relationship between the ir and dc relaxation rates is well represented by a second-order expansion in $(\Theta_D/T)^2$:

$$\frac{1}{\tau_\phi} = \frac{1}{\tau_\phi(0)}\left[1 + \frac{2}{18}\left[\frac{\Theta_D}{T}\right]^2 + \frac{11}{3240}\left[\frac{\Theta_D}{T}\right]^4\right]. \quad (1)$$

For tungsten $\Theta_D = 310$ K,[40] so a 12% correction to the dc rate results in the ir at room temperature.

Since $1/\tau_\phi(0)$ and $1/\tau_{e-e}(0)$ are the only significant RT contributions to ρ_{dc}, the electron-phonon relaxation rate can be calculated from ρ_{dc},[41] ω_p, $1/\tau_{e-e}(0)$,[42] and Eq. (1). Thus $1/\tau_\phi = 5.3 \times 10^{13}$ s^{-1} which implies $\alpha_\phi = 0.55$ cm$^{-1} \approx 3.7\alpha_{e-e}$ at 1000 cm^{-1}.

3. Electron-surface scattering

In the surface-assisted optical absorption process it is important to distinguish between scattering events which conserve the tangential velocity $v_{||}$ of the impinging electrons, which is defined as specular scattering, and those events which do not since $v_{||}$ conserving events contribute negligibly to the overall absorption.[1] The causes of non-specular scattering can be conveniently divided into two categories.

The first category, which was considered by Holstein and Dingle, is composed of causes which are classified as surface disorder and leads to diffuse scattering. For a single crystal examples of such inhomogeneities are missing or extra atoms in the top layer, steps in the surface due to slight misalignment along a crystallographic axis, or, as is relevant to our discussion, adsorption of molecules onto the surface.

Nonspecular scattering also arises because of the complex nature of real Fermi surfaces and is present even in single crystals with perfect surfaces.[43-46] We refer to this process as surface umklapp scattering. To illustrate this for tungsten a slice of the Fermi surface,[47] normal to the (001) direction, is drawn in Fig. 1. It is composed of electron "jacks" and hole "octahedrals" and "ellipsoids." An electron located on the Fermi surface at point A will strike the (100) metal-vacuum interface at an incident angle of 45°. If the sample surface has the same periodicity as the lattice then the electron must be reflected to either
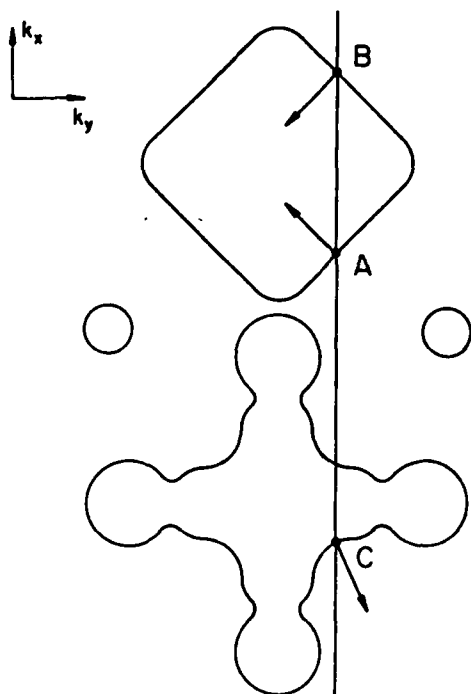

FIG. 2. α/α_ϕ versus frequency. The dashed lines show various contributions in the Drude model $(\alpha_\phi, \alpha_{e-e})$ with Holstein's approximation for diffuse surface scattering $(\alpha_{s,d})$. The solid lines are curves calculated from Dingle's anomalous skin effect equations.

FIG. 1. A slice of the W Fermi surface perpendicular to the (001) direction. An electron on the Fermi surface at point A (the vector indicates the direction of the electron's velocity) incident on the (100) metal-vacuum interface can be reflected to either point B or C with no change in tangential crystal momentum. Scattering into B is specular while scattering into C is a surface umklapp process.
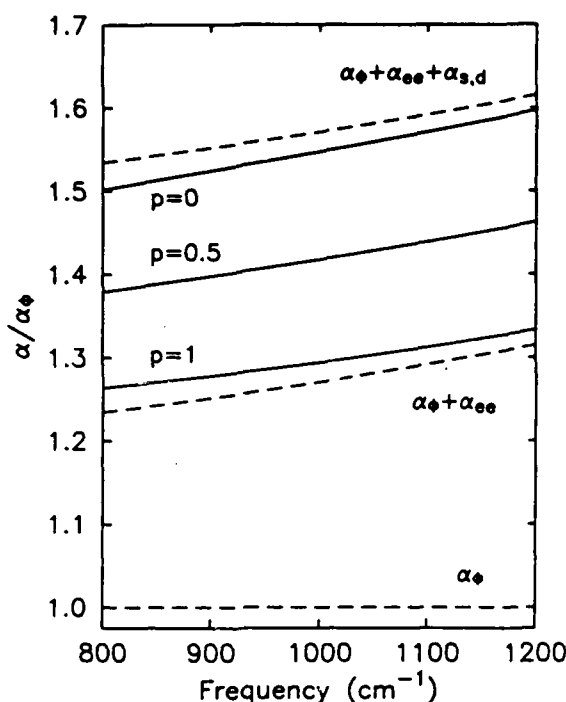
point B or C since the tangential crystal momentum $\hbar k_{||}$ is necessarily conserved. If it emerges in the state B then the scattering is specular since the tangential velocity is also conserved. Interband scattering from the free-carrier (FC) electron band to the FC hole band into the state C, however, results in a large change in the velocity parallel to the crystal surface, which contributes to ir absorption. An atomically perfect surface, therefore, need not appear perfectly specular.

The overall scattering behavior of conduction electrons from the surface is phenomenologically described by the Fuch's specularity parameter p.[48] If all the electrons are reflected with no tangential velocity change then $p=1$. $p=0$ indicates that the electrons are randomly scattered into all possible scattering angles. Other types of behavior can be characterized by a value of p between 0 and 1 which indicates the effective specularity of the outgoing electrons. For example, if all the electrons are reflected into angles near the specular direction then p is close to 1 even though there is no true specular scattering occurring.[49]

In order for the amount of specularity to have a major effect on the absorptivity of an optically thick sample two conditions must apply. The first is that the mean-free path l_0 of the electrons must be at least comparable to the classical skin depth δ (Ref. 50) of the metal. If $l_0 \ll \delta$ then bulk scattering dominates the absorptivity. The other condition is that the energy $\hbar\omega$ of the impinging radiation be below the region where interband transitions dominate the optical response of the metal. For good conduc-

tors at room temperature the range between 100 and 4000 cm^{-1} generally satisfies these two conditions,[51] below which $l_0 \ll \delta$ and above which interband transitions have the largest effect.

Within this range of frequencies there are two regions separated by $\delta = v_F/\omega$ (Ref. 52) (v_F is electronic velocity at Fermi surface). If the skin depth δ is much larger than the distance traveled by an electron in one cycle of the field then the dielectric function is local in space and the surface and bulk contributions can be separated.[1] In this case the surface contribution to the free-carrier response is characterized by a scattering rate

$$\frac{1}{\tau_s} = (1-p)\frac{3}{8}\frac{v_F}{c}\omega_p .$$

For tungsten this equals $(1-p)1.6\times 10^{13}$ s^{-1} which implies $\alpha_s = (1-p)0.16$ cm^{-1} at 1000 cm^{-1}. In the diffuse limit $\alpha_{s,d} \approx 0.3\alpha_\phi$. In Fig. 2 α_ϕ, $\alpha_\phi + \alpha_{e-e}$, and $\alpha_\phi + \alpha_{e-e} + \alpha_{s,d}$ normalized by α_ϕ are plotted versus frequency.

B. Anomalous skin effect

Since for tungsten at 1000 cm^{-1}, $\delta \approx 2v_F/\omega$, Holstein's local description of the surface-assisted absorption process is not quite valid. Also, because SEW's are a p-polarized (TM) wave the effect on the absorptivity of microscopic fields located at the surface[53] must be considered along with the nonlocality of the dielectric function. Fortunately, as Kleiwer and Fuchs have shown,[54,55] for ω_p and τ appropriate for W near $\bar{\nu} = 1000$ cm^{-1} the surface impedance $\hat{z}$ for non-normal incidence is independent of the polarization of the radiation and is essentially equivalent to that given by the theory of the anomalous skin effect as developed by Reuter and Sondheimer (RS).[4]

In the frequency region of interest Dingle[2,3] has calculated, using RS's equations, an expression for the surface impedance $\hat{z}$ which is appropriate for W at room temperature. Using the general relationship that $\alpha = -2(\omega/c)r_n x_n$ (Ref. 56) where r_n (x_n) is the real (imaginary) part of the normalized surface impedance $\hat{z}_n = \hat{z}/(4\pi/c)$ we have plotted, also in Fig. 2, α/α_ϕ for several values of p for the frequency region covered in our measurements. In the $\delta \gg v_F/\omega$ limit the results for $p=0$ and 1 approach the Drude-Holstein results for $(\alpha_\phi + \alpha_{e-e} + \alpha_{s,d})/\alpha_\phi$ and $(\alpha_\phi + \alpha_{e-e})/\alpha_\phi$, respectively.

III. EXPERIMENTAL

A. Sample details

The tungsten sample (6.1 cm$\times$0.6 cm$\times$0.17 cm) was oriented, spark cut, and then polished on both of its largest sides. Two gratings, used for coupling free-space radiation to the SEW's, were then etched into one of the polished surfaces with standard photolithographic techniques utilizing type J photoresist and a 5:1 mixture of HF and HNO_3 are the etchant. The 32-μm spacing gratings are an estimated 10 μm deep and are separated by 5 cm. The large distance between the gratings enhances the already high sensitivity SEWS affords over conventional reflec-

tion absorption spectroscopy when using a strong ir source such as a laser.[57]

The sample is mounted on a Huntington 600-XYZTRC manipulator in the UHV system and is thermally connected to a liquid-N$_2$ cooling assembly as shown in Fig. 3. Two feedthroughs on the manipulator flange are connected on the inside via a stainless-steel tube (f) through which liquid-N$_2$ flows. At the lowest point of the tube a copper block (h) is clamped onto it. Attached to the copper block two 0.025-cm-thick flexible, annealed copper strips (e) run down to the sample mount where they are sandwiched in place. The sandwich is necessary to electrically isolate the sample during cleaning or thermal desorption runs [since it is placed at high voltage via tantalum leads (l)] from the liquid-N$_2$ tube which is at ground. The sandwich consists of a stainless-steel block (j) which is connected to and held by the manipulator shaft (g), the copper cooling strips (e), a 1.9-cm-diam$\times$0.2-cm-thick sapphire flat (d), a 0.025-cm Ta sheet piece (c) indirectly connected to the sample, and a macor piece (i) for insulating the screws (k) which are
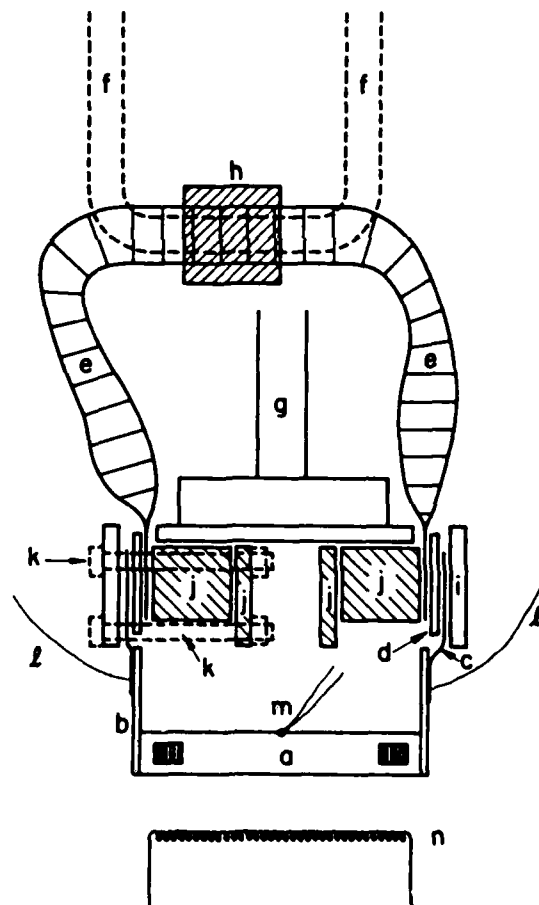
FIG. 3. A front sketch of the W sample mount. The sample (a) is thermally connected to the liquid-N$_2$ cooling feedthrough tube (f) via Ta rods (b), Ta sheets (c), sapphire flats (d), Cu sheet (e), and a Cu block (h). Macor pieces (i) and the sapphire flats electrically isolate the sample from ground during e-beam heating which is provided by the Ta filament (n) and the high-voltage Ta leads (l). Temperature is monitored with a W-Re(3 at. %)−W-Re(25 at. %) thermocouple (m).

used to squeeze the sandwich together (only shown dashed on left-hand side). The Ta strips are spotwelded to the Ta rods (b) which are electron-beam welded to the ends of the tungsten sample (a). By maintaining a constant flow of cold N_2 gas (or liquid) through the stainless-steel tube the sample cools from 2500 K to room temperature in 8 min and to 165 K in 25 min.

Sample temperature is measured with a W-Re(3 at. %)—W-Re(25 at. %) thermocouple (tc) (m) which is spotwelded to the center of the top edge of the sample. Above 298 K standard tables were used to determine the temperature, but below this the tc was calibrated against a Chromel-Alumel tc. This calibration differed by no more than $\pm 2.0\,^{\circ}$C from the curve published by Sandstrom and Withrow.[58]

Before any measurements were made the sample was baked in 1×10^{-7} Torr of O_2 for about 20 h at 1520 K (with periodic flashes to 2300 K) via electron bombardment heating from a Ta filament (n) directly beneath the sample. After this treatment, the low-temperature $(\sqrt{2} \times \sqrt{2})R\,45^{\circ}$ low-energy electron diffraction (LEED) pattern was observed, indicating that this procedure was sufficient to remove any C from the surface.[59] Before each experimental run the sample was again flashed to 2300 K to remove any contaminants, and the low-temperature LEED pattern was periodically observed as a check against subsequent C buildup.

B. Optical layout

The 32-μm spacing of the gratings was chosen so that the SEW's and free-space radiation couple near an angle of 45° at 1000 cm^{-1} as shown in Fig. 4. S-polarized (TE) radiation from a CO_2 laser (either $^{13}CO_2$ or $^{12}CO_2$) is sent through a chopper (C) and then a half-wave plate (WP) which is set to produce p-polarized (TM) radiation. (Because SEW's are a TM wave they only couple to TM free-space radiation.) Most of the radiation passes through a beam splitter (BS) and enters the vacuum chamber through a BaF_2 window ($W1$). A 40-cm focal length (FL) lens ($L2$) is used to focus the radiation onto the input grating where the SEW's are generated. The surface waves then travel the 5 cm across the W(100) surface to the output grating where they are converted back to free-space radiation which travels through another BaF_2 window ($W2$) and impinges on a liquid-N_2-cooled HgCdTe photoconductive detector ($D2$).

Although the free-space radiation generated at the output grating is well collimated its angle of departure changes as the frequency of radiation is changed. $L3$ is a 10-cm FL lens which images the output grating onto $D2$ and hence minimizes the need to realign the detector whenever the laser frequency is changed. The mirror ($M3$) mounted on a translation stage also minimizes problems in maximizing the detected signal whenever a new laser line is selected since translating $M3$ perpendicular to the axis of $L2$ changes the angle of incidence without altering the position of the incoming radiation on the sample.

The radiation which does not pass through the beam splitter is focused onto a pyroelectric detector ($D1$) by $L1$. The output signals of $D1$ and $D2$ are sent to separate
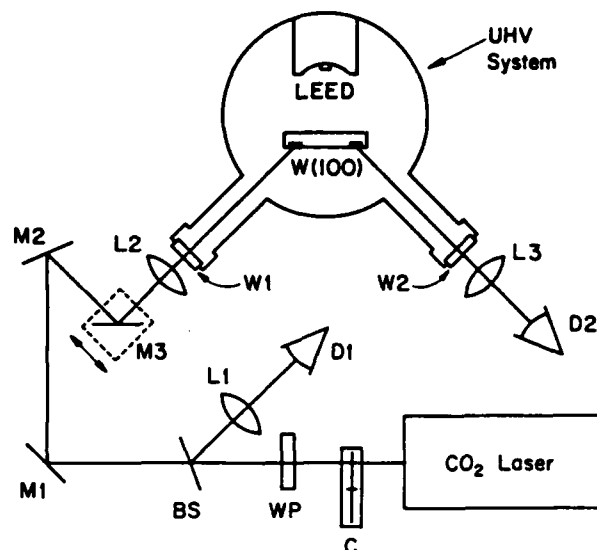

FIG. 4. Top view of the optical setup. A chopped CO_2 laser beam is sent into the sample chamber through a BaF_2 window ($W1$) and strikes the input grating of the sample. A HgCdTe detector ($D2$) is used to measure the transmitted intensity of free-space radiation generated at the output grating by SEW's which have traveled across 5 cm of the front (100) surface. LEED can be performed on the rear surface as ir measurements are made on the front. The ratio of the phase detected signals from $D2$ and the reference pyroelectric detector $D1$ are recorded on a chart recorder.

lock-ins tuned to the chopper frequency and their outputs are ratioed and recorded.

C. Experimental procedure

A typical experimental run consists of the following: The sample assembly is first cooled down as far as possible to insure as rapid cooling as possible from high temperatures. The sample is then flashed to 2300 K and allowed to cool to the desired adsorption temperature at which time the Ta filament is turned on and its current adjusted so that it radiatively stabilizes the sample temperature. Gas is then leaked into the chamber (typically at 5×10^{-9} Torr initially) and the SEW signal is monitored as a function of exposure. The change in the SEW attenuation coefficient α between two coverages Θ_i and Θ_f is calculated from $\Delta\alpha = -[1/(5 \text{ cm})]\ln(1 + \Delta I / I_0)$ where ΔI is the change in the detected intensity I_0 between Θ_i and Θ_f.

IV. RESULTS

A. H_2 and D_2 adsorption

The features in $\Delta\alpha$ versus exposure are highly non-monotonic and are qualitatively the same at all frequencies studied from 886 to 1088 cm^{-1}. Figure 5 shows two typical room-temperature runs, one for H_2 and one for D_2. Initial absorption results in a small, but significant, rise in α followed by a sharp minimum at an uncorrected gauge exposure of 0.100 ± 0.004 (0.140 ± 0.006) langmuir
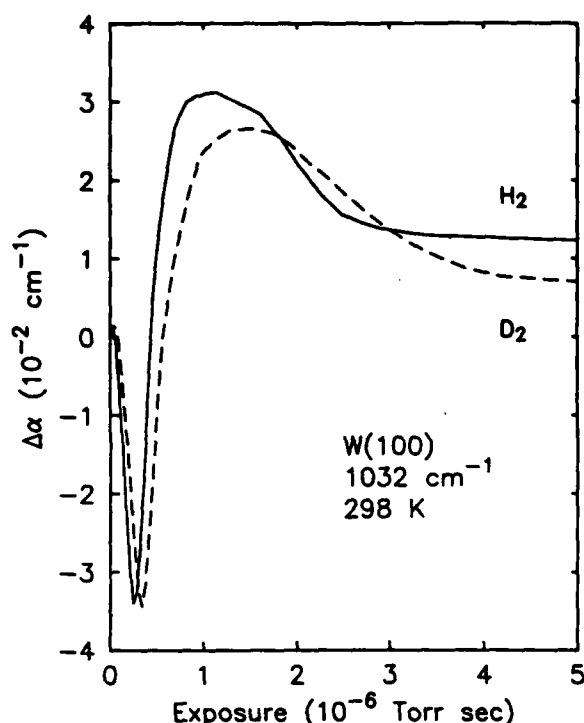
FIG. 5. Change in α versus exposure for H_2 and D_2 at a laser frequency of 1032 cm^{-1} and a temperature of 298 K. The exposure is a corrected value obtained by multiplying the ion gauge pressure by 2.3.
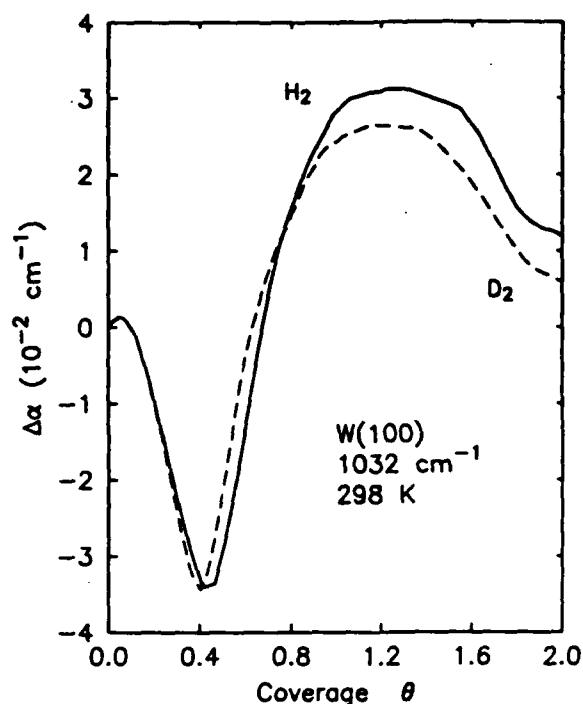
FIG. 6. Change in α versus coverage for H_2 and D_2 at a laser frequency of 1032 cm^{-1} and a temperature of 298 K. Coverage is determined from partial coverage thermal desorption measurements.

(L) for H_2 (D_2) (1 L $\equiv 10^{-6}$ Torr sec). This is followed by a rise to a broad maximum at 0.45±0.04 (0.59±0.05) L. (These exposure values are averages of all room-temperature runs.) As the surface becomes saturated α decreases to a final value above the zero coverage value with $\alpha_{H_2} > \alpha_{D_2}$. The stronger absorption for H_2 is mainly due to the W_2-H symmetric stretch (ν_1) which has been previously reported.[27] Note that the ratio of exposures at minimum α between D_2 and H_2 runs is 1.40±0.09, in good agreement with previous results that the sticking coefficient is the same for both isotopes.[60]

In order to convert exposure to coverage we use thermal desorption measurements which show that the coverage at the minimum is $\Theta = 0.42\pm0.04$ ML. Using this as a calibration point and the fact that the sticking coefficient is well represented by $s = C(1-\Theta/2)$ (Refs. 60 and 61) where C is a constant, the coverage for a given exposure is determined. $\Delta\alpha$ vs D_2 and H_2 coverage is shown in Fig. 6 for the same data shown in Fig. 5. The broad maximum now occurs at a coverage of $\Theta = 1.28\pm0.08$ ML.

Figure 7 shows the experimental results for $\Delta\alpha/\alpha_\phi$ for D_2 adsorption between various features (zero coverage, $\Theta = 0.42$ ML dip, $\Theta = 1.28$ ML peak and saturation) as a function of frequency. Data for D_2 instead of H_2 is presented in order to eliminate complications caused by the ν_1 mode absorption which is centered at 1070 cm^{-1} for the $p(1\times1)$-H state. Note that the data labeled B and C actually show a decrease in $|\Delta\alpha/\alpha_\phi|$ as ω increases while the data labeled A, D, and E show an increase.

The same basic features in $\Delta\alpha$ versus coverage for D_2
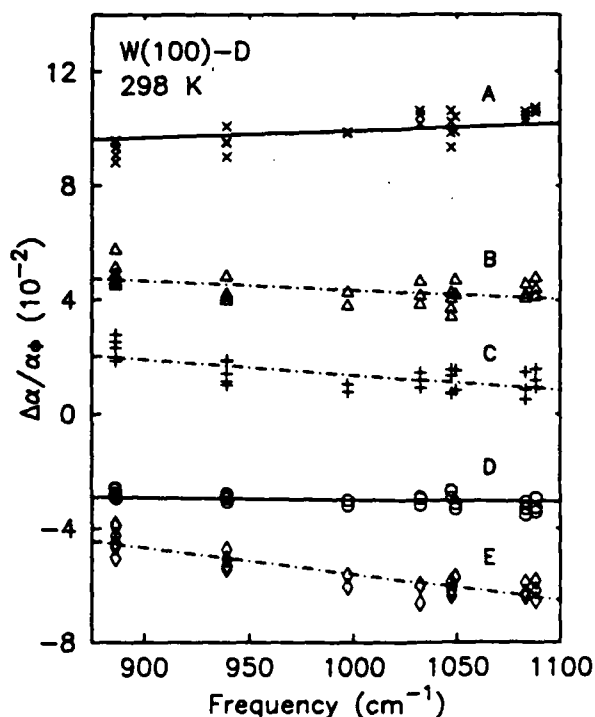
FIG. 7. Change in α versus frequency for D_2 adsorption between various initial (Θ_i) and final (Θ_f) coverages. Curve A, $\Theta_i = 0.42$ ML, $\Theta_f = 1.28$ ML; curve B, $\Theta_i = 0$ ML, $\Theta_f = 1.28$ ML; curve C, $\Theta_i = 0$ ML, $\Theta_f = 2.0$ ML; curve D, $\Theta_i = 1.28$ ML, $\Theta_f = 2.0$ ML; curve E, $\Theta_i = 0$ ML, $\Theta_f = 0.42$ ML. The solid lines are fits to the theory of the anomalous skin effect [Eq. (4)], while the dot-dashed lines are linear guides to the eye.

FIG. 8. Change in α between various coverages as a function of temperature. Curve A, $\Theta_i = 0.42$ ML, $\Theta_f = 1.28$ 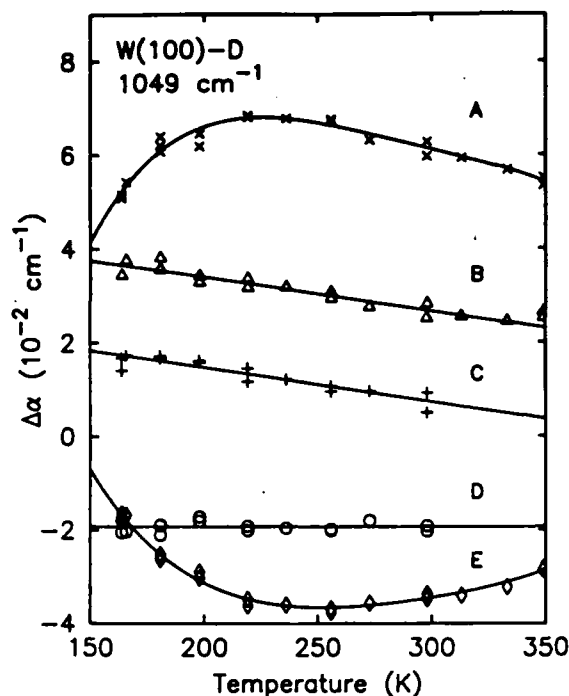ML; curve B, $\Theta_i = 0$ ML, $\Theta_f = 1.28$ ML; curve C, $\Theta_i = 0$ ML, $\Theta_f = 2.0$ ML; curve D, $\Theta_i = 1.28$ ML, $\Theta_f = 2.0$ ML; curve E, $\Theta_i = 0$ ML, $\Theta_f = 0.42$ ML.
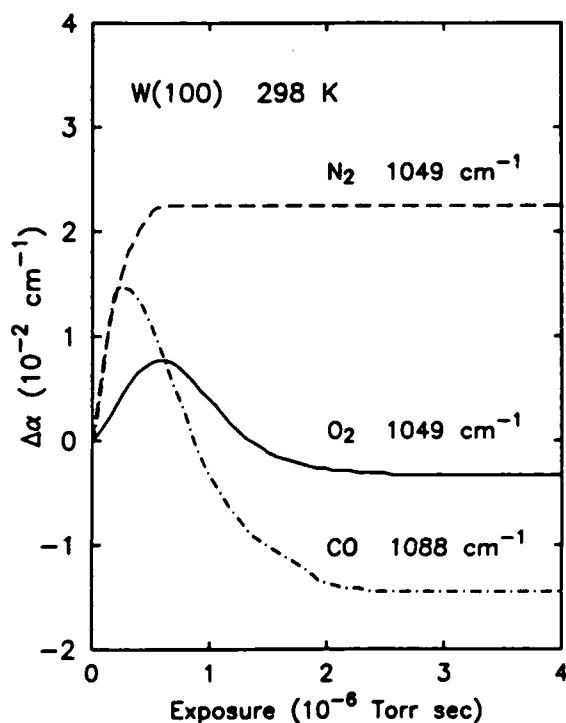

FIG. 9. $\Delta\alpha$ versus exposure for N_2, O_2, and CO at room temperature. The exposure is uncorrected in all cases.

and H_2 are present from 165 to 350 K. The temperature dependence of these changes for D_2 is shown in Fig. 8. We have drawn curves through the data labeled A and E as guides to the eye. The curves through B and C are linear fits below 300 K while a constant fit is shown for D. Above RT there is no data for $\Theta = 2.0$ ML since D_2 partially desorbs above 300 K.

B. Other gases

The rather complex nature of the coverage dependence of $\Delta\alpha$ for H_2 and D_2 prompted a look at the adsorption of other gases to see what similarities and differences might exist. Figure 9 shows RT results for adsorption of N_2, O_2, and CO onto the W(100) surface as a function of exposure. In each case the coverage dependence of the absorption is much simpler than for H_2 or D_2.

V. DISCUSSION

A. Changes in modified Drude parameters at the surface

Although tungsten is a transition metal, bulk ir data are well described by an appropriate plasma frequency ω_p, relaxation time τ, and high-frequency interband contribution ϵ_0 (Ref. 62) in a modified Drude model. One possible consequence of chemisorption is the alteration of these parameters in a small region (1 or 2 atomic layers) near the surface. Since the three-layer model of McIntyre and Aspnes[63] works well in interpreting the results of the W_2-H ν_1 mode absorption, we use it here to show that changes in the SEW attenuation coefficient α due to such effects are too small to account for the data.

For a sufficiently thin ($d/2\delta \ll 1$) layer of thickness d, the attenuation due to the layer can be written as

$$\alpha_l = 8\pi^2\tilde{\nu}^2 d \, \text{Im} \left[\frac{1}{(-\hat{\epsilon}_m)^{1/2}} \left[\frac{\hat{\epsilon}_l - 1}{\hat{\epsilon}_l} + \frac{\hat{\epsilon}_l}{-\hat{\epsilon}_m} \right] \right] , \qquad (2)$$

where ϵ_m (ϵ_l) is the dielectric function of the metal (layer) and $\tilde{\nu}$ is the frequency (cm^{-1}).[64] If we assume a modified Drude response

$$\hat{\epsilon}_k = \epsilon_{0,k} + i \left| \frac{\omega_{p,k}}{\omega} \right|^2 \frac{\omega\tau_k}{1 - i\omega\tau_k} \qquad (3)$$

for the metal ($k = m$) and the layer ($k = l$), then the above effects correspond to altering $\omega_{p,l}$, τ_l, and $\epsilon_{0,l}$.

The change in α due to modifying the plasma frequency in a thin layer calculated from Eq. (2) and Eq. (3) is given by

$$\Delta\alpha = -\alpha_{ce} \frac{\Delta(\omega_{p,l}^2)}{\omega_{p,m}^2} \frac{d}{2\delta} .$$

Assuming that one conduction electron is tied up in each W–H bond this yields $\Delta\alpha = 1.5 \times 10^{-2}\Theta$ cm^{-1} at 1032 cm^{-1}. While this can account for the size of $\Delta\alpha$ at saturation it fails at lower coverages. Nor does it seem likely that the many variations in the sign of $\Delta\alpha$ as Θ in-

29

creases can be explained since all of the H is located at the bridge site[65] implying that the adsorbate-substrate bonding is basically the same at all coverages.

If instead $\epsilon_{0,l}$ is changed and $\omega_{p,l}^2$ is held at a fixed value on the order of $\omega_{p,m}^2$, then α is altered even less. In this case

$$\Delta\alpha = 3\alpha_{ce}\frac{\omega^2}{\omega_{p,m}^2}\Delta\epsilon_{0,l}\frac{d}{2\delta}$$

$$\approx 7\times 10^{-4}\Delta\epsilon_{0,l}\frac{d}{2\delta}\ \text{cm}^{-1}\ .$$

Since $d/(2\delta)\approx 10^{-2}$ and the maximum in $\Delta\epsilon_{0,l}\approx 10^2$ (Ref. 66) we have result which is 2 orders of magnitude too small.

The largest excursion in α as the electron-phonon or electron-electron interaction is altered in a thin layer near the surface occurs as $\omega\tau_l$ increases from $\sim 7\times 10^{-2}$ to ~ 10 and results in $\Delta\alpha = 3\times 10^{-2}$ cm^{-1} for $d=3$ Å (≈ 2 atomic layers). While this is nearly large enough to be a possible explanation, more reasonable variations in τ_l, on the order of $\Delta\tau_l/\tau = 0.1$ cannot account for the size of the changes observed here. Hence it appears that changes in bulk parameters near the surface are insufficient to account for the SEWS observations.

B. Surface-assisted free carrier absorption: $\Theta > 0.42$ ML

The coverage region for $\Theta > 0.42$ ML shows best the free-carrier absorption effect for H$_2$ and D$_2$ adsorption. This is due to the fact that for $\Theta < 0.42$ ML the 0.3-eV intrinsic surface states are not yet quenched[67,68] and still contribute to optical absorption.[24] For this reason we first concentrate on $\Theta > 0.42$ ML.

Between $\Theta = 0.42$ and 2.0 ML the coverage dependence of the SEW attenuation coefficient (see Fig. 6) is similar to results for resistivity changes upon molecular adsorption onto thin metallic films.[69-71] In a number of these cases Wissmann[70] has demonstrated that the Fuchs theory of diffuse surface scattering[48] applies. The general features of the changes in resistivity upon chemisorption observed in these studies are as follows: Initial adsorption increases the diffuse scattering due to the randomness of adatom placement and leads to an initial increase in the resistivity. For some systems the diffuseness is a maximum at saturation, but for others there is a peak at some intermediate coverage(s). Such behavior is not unexpected since a saturated layer is often more uniform than one at intermediate coverages. A useful analogy is the Nordheim peak[72] in resistivity of a binary alloy A_xB_{1-x} as x is increased from zero to unity. In fact, a recent calculation including the effects of multiple scattering[73] has predicted the existence of such a maximum for an atomically smooth surface contaminated by adsorbed atoms. We also note a general experimental trend that the saturated coverage resistivity is consistently higher than the clean surface resistivity. The striking similarity between the W(100)-H (and -D) attenuation coefficient coverage dependence and the resistivity coverage dependence of thin gas covered films strongly points to changes in dif-

fuse surface scattering as the dominant mechanism for $\Theta > 0.42$ ML.

This interpretation is corroborated by other experimental results on this system. Figure 10 compares the SEW results with the mainly LEED-derived phase diagram[23,60,74,75] for the W(100)-H surface. (Henceforth we use H generically unless specifically referring to D.) At $\Theta = 0.42$ ML, where α is a minimum, the surface is reconstructed in what is known as the incommensurate-$c(2\times2)$-H phase which is characterized by $\frac{1}{2}$ order spots split into a quartet along the $\pm(10)$ and $\pm(01)$ directions. As more gas is added the spots of the $\frac{1}{2}$ order quartet streak along directions perpendicular to their splitting (the streaking is apparent at $\Theta = 0.48$ ML for our sample) and then eventually disappear, indicating a loss of order in the one dimension followed by a loss of order in both dimensions. These LEED changes, signaling the onset of disorder, are accompanied by a sharp rise in the SEW attenuation until the maximum at $\Theta = 1.28$ ML. The subsequent fall in α as the surface approaches the well ordered $p(1\times1)$-H state at saturation occurs concurrently with a decrease in the diffuse LEED background. The high degree of order at saturation is also reflected in high-energy ion scattering[76] results which show
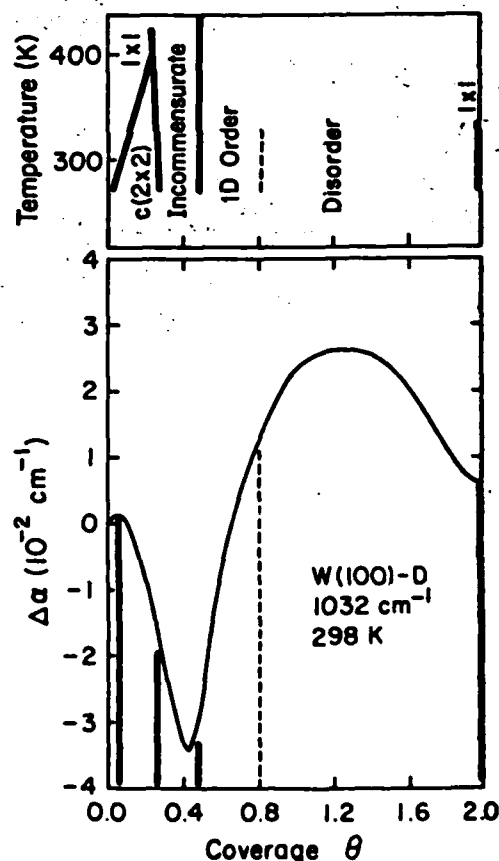

FIG. 10. The LEED determined phase diagram and $\Delta\alpha$ versus coverage for W(100)-D. The sharp dip occurs for the split-$c(2\times2)$ phase while the broad maximum occurs for the disordered state. The boundaries on the incommensurate-$c(2\times2)$ phase were determined from our LEED and thermal desorption measurements.

that the top layer is unreconstructed and in ir vibra⁺ional spectra which show that the v_1 and $2v_2$-β_1 absorption features are their sharpest at $\Theta = 2.0$ ML.[77]

The same basic coverage dependence also appears in the SEW data for the absorption of CO and O_2 as shown in Fig. 9: an initial rise in α followed by a peak at some intermediate coverage and a decrease towards saturation. Although the 0.3-eV ISS are quenched by adsorption of these gases, the quenching occurs more gradually;[67,68,78] hence the loss of the associated oscillator strength can be approximated by a slowly decreasing background. This appears to result in a smaller value of α at saturation compared with zero coverage. Nitrogen adsorption, on the other hand, shows no decrease in α after the initial rise, suggesting that disorder is a maximum at saturation for this system. These observations for the other gases further support the thesis that changes in diffuse surface scattering are being observed on the W(100) surface.

It should also be noticed that the variations in α for H_2 and D_2 are at least twice as large as for the other adsorbates. This seems strange since it is expected that the larger atoms should have a higher cross section for electronic scattering and suggests that it is the direct interaction of the free carriers with the reconstructed top W layer by H or D which results in the changes in α for these two systems.

In order to determine the amount the specularity changes we use the theory of the anomalous skin effect as developed by Dingle.[2,3] For the limited frequency range of our study Dingle's results can be summarized by the following equation:

$$\Delta\alpha/\alpha_{\phi} = -[0.253 + 6.3 \times 10^{-5}(\tilde{v} - 1000)]\Delta p , \qquad (4)$$

where $\tilde{v}$ is the frequency expressed in cm^{-1}. Using this equation we have determined the change in p between $\Theta_i = 0.42$ ML and $\Theta_f = 1.28$ ML to be $\Delta p = -0.39$ and between $\Theta_i = 1.28$ ML and $\Theta_f = 2.0$ ML to be $\Delta p = +0.11$. The fits are shown in Fig. 7 as the solid lines through the data labeled A and D. Although the frequency dependence of the data is slightly stronger than the theory, both show an increase in $|\Delta\alpha/\alpha_{\phi}|$ as ω increases.

The temperature dependence of the variations in α in this coverage range are interesting. The data labeled D in Fig. 8 shows that $\Delta\alpha$ between $\Theta_i = 1.28$ ML and $\Theta_f = 2.0$ ML is temperature independent from room temperature down to 165 K. This indicates that both of these phases are independent of temperature over this range, since it seems unlikely that the disordered and $p(1 \times 1)$-D states would change α in the same manner with temperature if there did exist a change in either one.

Using the value of α at $\Theta_f = 1.28$ ML as a reference the curve labeled A shows that as the temperature is lowered the relative attenuation at $\Theta_i = 0.42$ ML decreases until approximately 200 K where there begins a dramatic increase as the temperature is lowered further. The slow decrease suggests that the specularity for this phase increases slightly but that below 200 K it sharply drops off. Such a sharp drop in specularity may be associated with immobility of the adsorbate, as suggested by Barker et al.,[74] which hinders complete formation of the surface

phase. This immobility seems also apparent in other ir measurements where low-coverage, low-temperature modes are observed to be much broader than at room temperature.[79]

C. Surface umklapp scattering and the intrinsic surface states: $\Theta < 0.42$ ML

For $\Theta < 0.42$ ML it is apparent that something else besides surface assisted absorption contributes to the ir response. This is best seen in the frequency dependence of the changes in α for $\Theta_i = 0$ ML shown in curves B, C, and E of Fig. 7. For $\Theta_f = 1.28$ and 2.0 ML (curves B and C, respectively) $|\Delta\alpha/\alpha_{\phi}|$ shows a decrease as frequency increases while $|\Delta\alpha/\alpha_{\phi}|$ for $\Theta_f = 0.42$ ML (curve E) shows a much stronger dependence on frequency than curves A and D which show good agreement with the anomalous skin effect.

The resultant strong negative slope of $\Delta\alpha/\alpha_{\phi}$ versus frequency from these three $\Theta_i = 0$ ML curves can be understood in terms of the D_2 induced quenching of the 0.3-eV intrinsic surface states. As pointed out by Anderson et al.,[24] the good correlation of the surface reflectance spectroscopy (SRS) transition energies with the ultraviolet photoemission determined energy levels strongly suggests that the optical transitions from surface electronic states involve final-state energies located just above the Fermi level. Although the SRS measurements only probed transitions down to ≈ 0.6 eV the data show a contribution from these intrinsic states up to ≈ 0.8 eV, an indication that these states are rather broad. It is therefore reasonable to expect a contribution from the same states at 1000 cm^{-1} (0.125 eV). The strong frequency dependence is thus due to the fact that our measurements probe the low-frequency tail of these states where the absorption strength is rapidly changing.

Exactly how much these states contribute to the response is an open question and cannot be determined from this study. The simplest assumption is that all of the decrease in attenuation, after the small initial rise, is due to the quenching of optical transitions associated with the removal of the surface states. Another, perhaps more interesting, possibility is that some part of the large negative excursion in α is caused by the surface-enhanced free-carrier absorption effect. Although surface disorder is an unlikely explanation there is the possibility that surface umklapp processes play a role.

Surface disorder is largely ruled out by LEED observations in this coverage region.[23,60,74,75,80] The clean surface shows a mostly $p(1 \times 1)$ order (unreconstructed) with a hint of $\frac{1}{2}$ order spots. At a very small value of Θ the $\frac{1}{2}$ order spots sharpen considerably as the surface enters the $c(2 \times 2)$-H phase. With further coverage the $\frac{1}{2}$ order spots split into a quartet as described above as the incommensurate–$c(2 \times 2)$-H state is formed, with the magnitude of the splitting linearly proportional to the coverage beyond which the splitting begins to occur ($\Theta \approx 0.26$ ML for our sample). Although there is some debate about the state of the room-temperature clean surface (ordered versus disordered), both of the hydrogen stabilized phases definitely show long-range order.

At first glance one might assume that the appearance of $\frac{1}{2}$ order LEED spots would necessarily be associated with the opening up of more free-carrier nonspecular scattering channels. A look at Fig. 11, in which a slice of the Fermi surface[47] is drawn perpendicular to the (100) direction, indicates that this is not a large effect for W. A change in $k_{\parallel}$ corresponding to a $(\frac{1}{2} \frac{1}{2})$ LEED beam is drawn and shows for the majority of free carriers that such a change in parallel momentum is impossible since this momentum transfer connects relatively few states on the Fermi surface. Therefore, a $c(2 \times 2)$ structure should not significantly increase the diffuse surface scattering.

What may be occurring, though, is a change in the amount of surface umklapp scattering caused by adsorbate-induced changes in the relaxation of the W(100) surface. Since changes in reconstruction (periodicity parallel to this surface) can change the outgoing electrons' $k_{\parallel}$ it seems reasonable that a change in the first interatomic layer spacing (relaxation) could effect the outgoing $k_{\perp}$ and hence change the relative amount of electrons which are specularly reflected. Such a change in the relaxation of the first layer has been reported by King and Thomas[60] in their LEED study of this system. As Θ increases to ≈ 0.40 ML their Fig. 16 shows a sharp increase in the first W interlayer spacing of $\sim 2\%$, with much smaller subsequent variations as the surface becomes saturated.

The temperature dependence of $\Delta\alpha$ for the clean surface and a calculation by Fu et al.[81] lend mild support to this idea. Their calculation suggests that as the low-temperature $(\sqrt{2} \times \sqrt{2})R 45°$ clean surface phase [which is quite similar to the $c(2 \times 2)$-H phase] is formed from the $p(1 \times 1)$ RT state the top layer spacing also increases (by $\sim 4\%$) to an unrelaxed position. A look at curves B and C of Fig. 8 shows that this phase transition is also accompanied by a decrease in the surface contribution to α, fur-

ther indicating that surface relaxation may be related to specularity through the surface umklapp mechanism.

Although the results of Fu et al. are consistent with a surface umklapp scattering explanation of the linear decrease in the clean surface contribution to α, another mechanism, related to the surface Debye temperature of W, may be responsible. The dynamical LEED data of Heilmann et al.[82] indicate that the high-temperature $p(1 \times 1)$ clean surface has an effective surface Debye temperature $\Theta_{D,S} = 210 \pm 40$ K while the low-temperature $(\sqrt{2} \times \sqrt{2})R 45°$ phase has an effective $\Theta_{D,S} = 400 \pm 100$ K. Since in the temperature range of interest the electron-phonon relaxation rate $1/\tau_\phi \propto 1/\Theta_D^2$,[36] a change in $\Theta_{D,S}$ should effect the electron-phonon scattering in a thin layer near the surface. Using Eqs. (2) and (3) to estimate the change in α caused by the LEED determined increase in $\Theta_{D,S}$ yields $\Delta\alpha = -(8.0 \pm 3.0) \times 10^{-3}$ cm^{-1} at 1049 cm^{-1} for a thickness equal to one interlayer spacing (1.6 Å). Experimentally, the change in α for the clean surface in going from 300 to 165 K is 1.0×10^{-2} cm^{-2}. The fact that the experimental and calculated values of $\Delta\alpha$ are not significantly different lends support to the idea that the change in $\Theta_{D,S}$ may be a possible explanation for the clean surface temperature dependence of $\Delta\alpha$.

Lastly, we note that initial adsorption results in a small, but perceptible, rise in α. It seems reasonable to suppose that this is due to an increase in diffuse surface scattering caused by a small increase in disorder of the surface due to random placement of the hydrogen before the $c(2 \times 2)$ order becomes long range.

VI. SUMMARY

We have investigated the behavior of changes in the attenuation coefficient of 10-μm SEW's caused by D$_2$ and H$_2$ adsorption on W(100). The variations have been discussed in terms of changing Drude parameters of the metal in a small region of the surface, the quenching of 0.3-eV intrinsic surface states, and surface-assisted free-carrier absorption. Changes in the Drude parameters of W in a thin layer near the surface are generally too small to account for the size of the observed variations.

For $\Theta > 0.42$ ML there are four main experimental points which contribute to an interpretation that the variations in α are mainly the result of changes in the specularity of scattered free carriers caused by adsorbate-induced reconstruction of the W(100) surface atoms. The four points are as follows: (1) The maximum variation in α is quite large, i.e., it is 10 times larger than the W$_2$-H symmetric stretch contribution to α (Ref. 27) and at least 2 times larger than variations observed for CO, O$_2$, and N$_2$ adsorption. (2) A coverage dependence for α is observed which is similar to resistivity measurements on gas-covered films.[69-71] (3) There exists a high degree of correlation between the LEED deduced structures[60] and the variations. (4) The induced changes are broadband: they are observed over the entire range of frequencies studied from 886 to 1088 cm^{-1}, and they are fit well by the theory of the anomalous skin effect[2,3] with realistic values of changes in the Fuchs specularity parameter.[48]
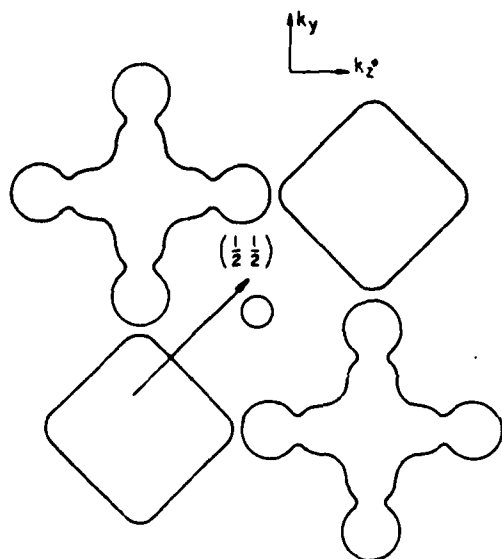
In this coverage range our results show that the

FIG. 11. A slice of the W Fermi surface perpendicular to the (100) direction, illustrating that a change in k corresponding to a $(\frac{1}{2} \frac{1}{2})$ LEED beam is forbidden for the majority of free carriers.

$\Theta = 1.28$ ML disordered surface phase and the saturation $p(1 \times 1)$-D phase are independent of temperature between 165 and 300 K. Also, the previously reported[74] immobility of the adsorbate below 200 K seems apparent for D_2 adsorption.

In the coverage range of $\Theta < 0.42$ ML it is shown that surface scattering is not the only mechanism for these broadband changes. Although the exact contribution of the 0.3-eV intrinsic surface states to the optical response at 10 μm is not known, it seems clear that they play some role. We suggest that surface umklapp scattering[43-46] may have some contribution to the large negative change

in α as Θ approaches 0.42 ML. In addition, the surface umklapp mechanism and/or a changing surface Debye temperature are possible explanations for the $\Theta = 0$ ML temperature dependence of $\Delta\alpha$.

ACKNOWLEDGMENTS

[1] T. Holstein, Phys. Rev. 88, 1427 (1952).

[2] R. B. Dingle, Physica 19, 311 (1953).

[3] R. B. Dingle, Physica 19, 729 (1953).

[4] G. E. H. Reuter and E. H. Sondheimer, Proc. R. Soc. London, Ser. A 195, 336 (1948).

[5] R. B. Dingle, Physica 19, 348 (1953).

[6] R. G. Chambers, Proc. R. Soc. London, Ser. A 215, 481 (1952).

[7] M. A. Biondi, Phys. Rev. 102, 964 (1956).

[8] E. W. Johnson and H. H. Johnson, J. Appl. Phys. 36, 1286 (1965).

[9] A. P. Lenham and D. M. Treherne, J. Opt. Soc. Am. 56, 683 (1966).

[10] M. A. Biondi and A. I. Guobadia, Phys. Rev. 166, 667 (1968).

[11] J. A. McKay and J. A. Rayne, Phys. Rev. B 13, 673 (1976).

[12] R. H. Doremus, J. Appl. Phys. 36, 2853 (1965).

[13] H. E. Bennett and J. M. Bennett, in Optical Properties and Electronic Structure of Metals and Alloys, edited by F. Abelès (North-Holland, Amsterdam, 1966), p. 175.

[14] H. E. Bennett, J. M. Bennett, E. J. Ashley, and R. J. Motyka, Phys. Rev. 165, 755 (1968).

[15] D. K. C. MacDonald and K. Sarginson, Proc. R. Soc. London, Ser. A 203, 223 (1950).

[16] E. J. Gillham, J. S. Preston, and B. E. Williams, Philos. Mag. 46, 1051 (1955).

[17] A. E. Ennos, Brit. J. Appl. Phys. 8, 113 (1957).

[18] M. S. P. Lucas, Appl. Phys. Lett. 4, 73 (1964).

[19] M. S. P. Lucas, Thin Solid Films 2, 337 (1968).

[20] D. C. Larson and B. T. Boiko, Appl. Phys. Lett. 5, 155 (1964).

[21] A. J. Learn and R. S. Spriggs, J. Appl. Phys. 34, 3012 (1963).

[22] K. L. Chopra, L. C. Bobb, and M. H. Francombe, J. Appl. Phys. 34, 1699 (1963).

[23] See, e.g., P. J. Estrup, in Chemistry and Physics of Solid Surfaces V, edited by R. Vanselow and R. Howe (Springer-Verlag, New York, 1984).

[24] J. Anderson, G. W. Rubloff, M. A. Passler, and P. J. Stiles, Phys. Rev. B 10, 2401 (1974).

[25] J. B. Restorff and H. D. Drew, Surf. Sci. 88, 399 (1979).

[26] Y. J. Chabal, Phys. Rev. Lett. 55, 845 (1985).

[27] D. M. Riffe, L. M. Hanssen, A. J. Sievers, Y. J. Chabal, and S. B. Christman, Surf. Sci. 161, L559 (1985).

[28] For a review of the properties of surface electromagnetic waves see, e.g., G. N. Zhizhin, M. A. Moskalova, E. V. Shomina, and V. A. Yakovlev, in Surface Polaritons, edited by V. M. Agranovich and D. L. Mills (North-Holland, New York, 1982), pp. 93-143.

[29] R. N. Gurzhi, Zh. Eksp. Teor. Fiz. 35, 965 (1958) [Sov. Phys.—JETP 8, 673 (1959)].

[30] R. N. Gurzhi, M. Y. Azbel, and H. P. Lin, Fiz. Tverd. Tela (Leningrad) 5, 759 (1963) [Sov. Phys. Solid State 5, 554 (1963)].

[31] W. E. Lawrence, Phys. Rev. B 13, 5316 (1976).

[32] The value of $\hbar\omega_p$ in Table I was determined from an SEW interferrometric measurement on the sample used in this study; see L. M. Hanssen, Ph.D. Thesis, Cornell University, 1985; and L. M. Hanssen, D. M. Riffe, and A. J. Sievers (unpublished). A value of 6.0 eV has been obtained from the data of J. M. Weaver, C. G. Olson, and D. W. Lynch by M. A. Ordal et al., Appl. Opt. 22, 1099 (1983).

[33] S. X. Cheng and A. J. Sievers (unpublished).

[34] L. A. Wojcik, A. J. Sievers, G. W. Graham, and T. N. Rhodin, J. Opt. Soc. Am. 72, 149 (1982).

[35] This is essentially the same as the value determined by Cheng and Sievers in Ref. 33.

[36] F. J. Blatt, Physics of Electronic Conduction in Solids (McGraw-Hill, New York, 1968), pp. 183-196.

[37] T. Holstein, Phys. Rev. 96, 535 (1954).

[38] A brief derivation of Holstein's results is contained in the Appendix of Ref. 11.

[39] R. N. Gurzhi, Zh. Eksp. Teor. Fiz. 33, 660 (1957) [Sov. Phys.—JETP 6, 506 (1958)].

[40] N. W. Ashcroft and N. D. Mermin, Solid State Physics (Saunders College, Philadelphia, 1976), p. 461.

[41] C. J. Smithells, Tungsten (Chapman and Hall, London, 1952), p. 180.

[42] See previous section.

[43] P. J. Price, IBM J. Res. Dev. 4, 153 (1960).

[44] A. B. Pippard, The Dynamics of Conduction Electrons (Gordon and Breach, New York, 1965), pp. 46-51.

[45] R. F. Greene, in Solid State Surface Science (M. Dekker, New York, 1969), Vol. 1, pp. 87-132.

[46] A. F. Andreev, Usp. Fiz. Nauk 105, 113 (1971) [Sov. Phys.—Usp. 14, 609 (1972)].

[47] D. M. Sparlin and J. A. Marcus, Phys. Rev. 144, 484 (1966).

[48] K. Fuchs, Proc. Cambridge Philos. Soc. 34, 100 (1938).

[49] R. F. Greene, Phys. Rev. 141, 687 (1966).

[50] For tungsten at 10 μm $\delta \approx c/(2\omega_p)$.

[51] See, e.g., F. Wooten, Optical Properties of Solids (Academic, New York, 1972).

[52] The Fermi velocity is estimated from the ir plasma frequency assuming a spherical Fermi surface; see, e.g., N. W. Ashcroft and N. D. Mermin, Solid State Physics (Saunders College, Philadelphia, 1976), Chap. 2.

[53] P. J. Feibelman, Prog. Surf. Sci. 12, 287 (1982).

[54] K. L. Kliewer and R. Fuchs, Phys. Rev. 172, 607 (1968).

[55] J. M. Keller, R. Fuchs, and K. L. Kliewer, Phys. Rev. B 12, 2012 (1975).

[56]A. J. Sievers and Z. Schlesinger, J. Phys. (Paris) **44**, C10-13 (1983).

[57]Y. J. Chabal and A. J. Sievers, Phys. Rev. B **24**, 2921 (1981).

[58]D. R. Sandstrom and S. P. Withrow, J. Vac. Sci. Technol. **14**, 748 (1977).

[59]K. Yonehara and L. D. Schmidt, Surf. Sci. **25**, 238 (1971).

[60]D. A. King and G. Thomas, Surf. Sci. **92**, 201 (1980).

[61]T. E. Madey, Surf. Sci. **36**, 281 (1973).

[62]The value of ϵ_0 in Table I was obtained by L. V. Nomerovannaya, M. M. Kirillova, and M. M. Noskov, Zh. Eksp. Teor. Fiz. **60**, 748 (1971) [Sov. Phys.—JETP **33**, 405 (1971)] using ellipsometric techniques. A similar value can be obtained from the data of J. H. Weaver *et al.* in the paper by M. A. Ordal *et al.* (see Ref. 32).

[63]J. D. McIntyre and D. E. Aspnes, Surf. Sci. **24**, 417 (1971).

[64]Z. Schlesinger and A. J. Sievers, Phys. Rev. B **26**, 6444 (1982).

[65]M. R. Barnes and R. F. Willis, Phys. Rev. Lett. **41**, 1729 (1978).

[66]This value of $\Delta\epsilon_{0,l}$ is estimated from the value of $\epsilon_{0,m} = 70$ (see Ref. 62).

[67]B. J. Waclawski and E. W. Plummer, Phys. Rev. Lett. **29**, 783 (1972).

[68]B. Feuerbacher and B. Fitton, Phys. Rev. Lett. **29**, 786 (1972).

[69]J. W. Geus, in *Chemisorption and Reactions on Metallic Films*, edited by J. R. Anderson (Academic, New York, 1971), Vol. 1, p. 327, and references therein.

[70]P. Wissmann, in *Springer Tracts in Modern Physics*, edited by G. Höhler (Springer-Verlag, New York, 1975), Vol. 77, and references therein.

[71]C. Pariset and J. P. Chauvineau, Surf. Sci. **47**, 543 (1975).

[72]N. F. Mott and H. Jones, *The Theory of the Properties of Metals and Alloys* (Dover, New York, 1958), p. 297.

[73]D. Lessie, Phys. Rev. B **20**, 2491 (1979).

[74]R. A. Barker and P. J. Estrup, J. Chem. Phys. **74**, 1442 (1981).

[75]A. H. Smith, R. A. Barker, and P. J. Estrup, Surf. Sci. **136**, 327 (1984).

[76]I. Stensgaard, L. C. Feldman, and P. J. Silverman, Phys. Rev. Lett. **42**, 247 (1979).

[77]Y. J. Chabal, J. Electron Spectrosc. Relat. Phenom. **38**, 159 (1986).

[78]E. W. Plummer and J. W. Gadzuk, Phys. Rev. Lett. **25**, 1493 (1970).

[79]Y. J. Chabal (private communication).

[80]R. A. Barker and P. J. Estrup, Phys. Rev. Lett. **41**, 1307 (1978).

[81]C. L. Fu, A. J. Freeman, E. Wimmer, and M. Weinert, Phys. Rev. Lett. **54**, 2261 (1985).

[82]P. Heilmann, K. Heinz, and K. Müller, Surf. Sci. **89**, 84 (1979).

INFRARED OBSERVATION OF ADSORBATE INDUCED CHANGES IN FREE CARRIER SURFACE SCATTERING

D.M. RIFFE, L.M. HANSSEN and A.J. SIEVERS

Laboratory of Atomic and Solid State Physics and Materials Science Center, Cornell University, Ithaca, NY 14853-2501, USA

Changes in the surface electromagnetic wave attenuation coefficient α upon chemisorption of N_2, O_2, CO, H_2, and D_2 onto W(100) have been measured at room temperature near 10 μm. The size as well as the coverage dependence of the variations point to changes in the amount of diffuse free carrier surface scattering as the dominant α-altering mechanism.

1. Introduction

In 1938 Fuchs [1] showed that the DC resistivity of a thin metallic film is larger if the conduction electrons colliding with the surface are diffusely rather than specularly reflected. This result was later extended into the infrared (IR) by Dingle [2] who calculated that diffuse surface scattering also leads to higher absorption by a metal than does specular reflection of the charge carriers. With the subsequent advent of ultrahigh vacuum (UHV) techniques came the experimental possibility of controlling the disorder of the surface by atomic or molecular adsorption and thereby changing the amount of diffuse electronic scattering at the surface. Since then there have been numerous investigations which have measured adsorbate induced resistivity variations of thin films [3,4]. For many of these studies it has been demonstrated that the Fuchs theory applies [3]. Conspicuously absent, though, are equivalent IR measurements. In this paper we report the results of such infrared measurements on the W(100) surface.

The IR absorption technique utilized in the present study consists of measuring the change in the surface electromagnetic wave (SEW) attenuation coefficient α upon chemisorption of N_2, O_2, CO, H_2, and D_2. Broad-band changes in α are observed upon adsorption of each of these gases. The size and coverage dependence of the measured variations suggest that adsorbate induced changes in electronic surface scattering provide the dominant contribution to the observed variations in α.

After a brief description of the experimental details in section 2 the results for room temperature (RT) adsorption of the five gases are presented in section 3. The discussion of the results (section 4) is divided into two main parts. In section 4.1 we discuss, rather generally, possible contributions to the measured changes in α in terms of the three-layer model of McIntyre and Aspnes [5]. Then in section 4.2 the discussion focuses on the α variations for each of the W(100)–adsorbate systems individually. The last section summarizes our results on adsorbate induced changes in the SEW attenuation coefficient.

2. Experimental

Experimental details are more thoroughly described elsewhere [6]. Briefly, radiation in the 10 μm region from a line-tunable gas laser (either $^{13}CO_2$ or $^{12}CO_2$) is coupled to SEW's via a grating etched in the sample surface. The SEW's travel a distance $L = 5$ cm along the smooth W(100)–vacuum interface before another grating couples them back to free space radiation which is detected with a HgCdTe photoconductive detector. The absorption measurement is performed by monitoring the intensity at the detector as gas is adsorbed onto the surface. Any change in α is calculated from

$$\Delta\alpha = -L^{-1} \ln(I/I_0),$$

where I_0 is the zero-coverage detected intensity. Initial adsorption pressures varied between 5×10^{-9} and 10^{-7} Torr above a background base pressure of typically 8×10^{-11} Torr.

3. Results

In fig. 1 we have plotted the change in α ($\Delta\alpha$) versus exposure for adsorption of the five different molecules, N_2, O_2, CO, H_2, and D_2, onto W(100) at various frequencies near 10 μm. The exposure is determined from uncorrected ion gauge pressure readings. Initial adsorption results in an increase in attenuation for all five gases. For N_2 $\Delta\alpha$ reaches a plateau at an exposure of 0.53 ± 0.03 langmuir (L). CO and O_2 adsorption results in qualitatively similar variations in α: a peak at some intermediate exposure [0.36 ± 0.07 (0.6 ± 0.1) L for CO (O_2)] with a final value of α less than at zero coverage. Chemisorption of H_2 and D_2 yields much richer structure in $\Delta\alpha$. After the small initial rise a sharp dip appears at 0.100 ± 0.004 (0.140 ± 0.006) L for H_2 (D_2) followed by a broad maximum at 0.45 ± 0.04 (0.59 ± 0.05) L. As the surface becomes saturated α decreases to a value which is still larger than for the clean surface.
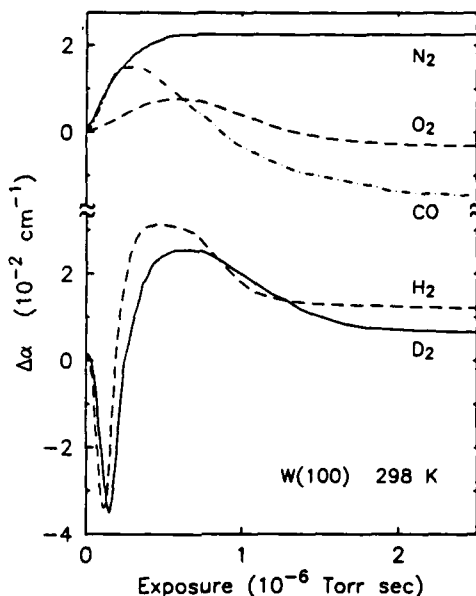
36

Fig. 1. Change in α ($\Delta\alpha$) versus exposure for N_2, O_2, CO, H_2, and D_2 adsorption onto W(100) at room temperature for typical runs near 1000 cm^{-1}. Laser frequencies used for runs shown: N_2 and O_2, 1049 cm^{-1}; CO, 1088 cm^{-1}; H_2 and D_2, 1032 cm^{-1}.

Fig. 2 shows the same $\Delta\alpha$ data of fig. 1 plotted versus coverage instead of exposure. For D_2 and H_2 the coverage is determined using our thermal desorption (TD) data which indicate that the sharp dip in α corresponds to $\theta = 0.21 \pm 0.02$ (θ is the fraction of saturation coverage) along with the previous results that saturation corresponds to 2×10^{15} atoms/cm^2 [7] and that the sticking coefficient σ varies as $1 - \theta$ [8,9]. Flash desorption results are also used to obtain the CO coverage. At room temperature CO adsorbs into two classes of states labeled α and β [10]. Saturated β corresponds to 5.0×10^{14} molecules/cm^2 [11] while TD data show that for RT adsorption onto our sample $\theta_\alpha \approx 0.5\theta_\beta$ which implies $\theta_{sat} \approx 7.5 \times 10^{14}$ molecules/cm^2. By assuming the form of $\sigma(\theta)$ as measured by Clavenna and Schmidt [10] the coverage versus exposure is determined. Both the H_2–D_2 and CO TD results indicate that during exposure the pressure at the sample is higher than at the ionization gauge by a factor of ~1.4. Using this fact, previously determined forms of $\sigma(\theta)$ for N_2 [12] and O_2 [13], and saturation coverage values of 3×10^{14} and 6×10^{14} molecules/cm^2 for N_2 [12,14] and O_2 [13] respectively, coverage versus measured exposure is calculated for these two gases.

Since the two classes of CO states, α and β, are easily identifiable in TD spectra, an attempt was made to try and separate out the contribution to $\Delta\alpha$
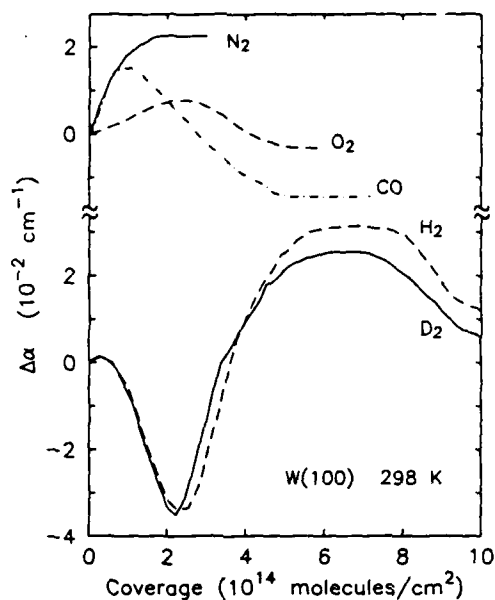
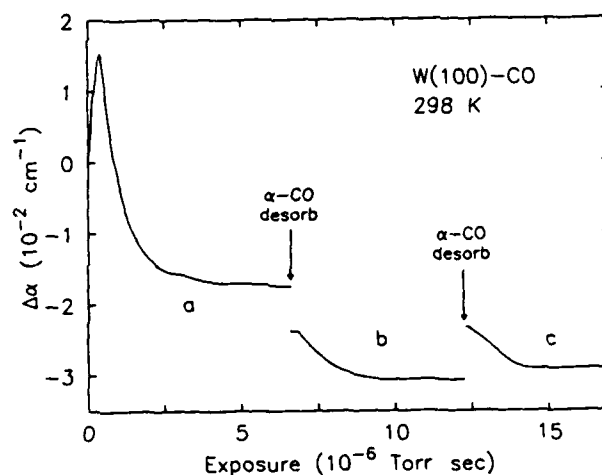Fig. 2. Change in α ($\Delta\alpha$) versus molecular coverage for the same data shown in fig. 1.

Fig. 3. Change in α ($\Delta\alpha$) versus CO exposure at room temperature and 1088 cm^{-1} showing the effects of α-CO desorption and readsorption. $\Delta\alpha$ upon CO adsorption onto a clean surface is shown in curve a. At 6.6 L, CO exposure was stopped, the sample flashed to ~ 700 K and recooled to RT, resulting in the drop in $\Delta\alpha$ shown as the discontinuity between curves a and b. CO was then re-admitted to the UHV chamber where upon $\Delta\alpha$ decreased as shown in curve b. At 12.3 L exposure was again stopped, the sample thermally cycled to ~ 700 K and back to RT, and then re-exposed to CO resulting in curve c.

from each class as shown in fig. 3. After saturating the clean surface with CO at room temperature (curve a) the α-CO was thermally desorbed ($T_{\text{max}} \approx 700$ K) and the sample recooled to RT whereupon it was re-exposed to CO, giving the change in attenuation shown in curve b. The sample was again thermally cycled to ~ 700 K and back to RT and re-exposed to CO, resulting in a change in attenuation essentially identical to curve b as shown in curve c.

4. Discussion

4.1. Contributions to $\Delta\alpha$

For a metal with chemisorbed molecules the standard model used to describe the IR response is the three-layer model of McIntyre and Aspnes [5] which describes the surface region between vacuum and the bulk metal by an isotropic, uniform dielectric layer. The effect of the adsorbed molecules on the IR response, then, is either to alter the dielectric function $\hat{\epsilon}_d$ of the layer by changing the vibrational or electronic structure at the surface, or to change the effective dielectric function $\hat{\epsilon}_m$ of the metal by changing the nature of the free carrier surface scattering.

4.1.1. Changes in $\hat{\epsilon}_d$

Several possible mechanisms for changing $\hat{\epsilon}_d$ can be ruled out. Previous IR and electron energy loss spectroscopy (EELS) measurements eliminate surface vibrations as a contribution to the strong variations in α. EELS results for CO [15,16] and N_2 [17] adsorption show that there are no dipole allowed vibrational transitions in the 1000 cm^{-1} region. H_2 adsorption does produce an IR allowed vibrational mode in this region [18,19], but it has been previously shown [19] that the maximum saturated-coverage attenuation due to this mode [the W_2–H symmetric stretch (ν_1)] is only $6 \times 10^{-3} \text{ cm}^{-1}$. (This accounts for most of the stronger H_2 adsorption at saturation as compared to D_2.) Oxygen also produces a mode at $\sim 1000 \text{ cm}^{-1}$, but EELS studies [20] show for RT adsorption that exposures greater than those used here are required before this vibration becomes apparent.

Adsorption can also be expected to change $\hat{\epsilon}_d$ by altering the bulk IR parameters near the surface. In general – and especially for H_2 and D_2 – possible α variations resulting from changes in free carrier density and bulk relaxation time are too small to account for the measured changes [6]. The same is also true for changes in high frequency interband structure near the surface [6].

Contributions to $\Delta\hat{\epsilon}_d$ which cannot be ruled out are variations in the IR response due to low frequency (mid-IR) electronic structure of the surface upon adsorption. The dominant low frequency feature on W(100) is a peak in

the surface density of states ~ 0.3 eV below the Fermi level. Both field emission energy distribution (FEED) [21,22] and ultraviolet photoemission spectroscopy studies [23,24] have detected the presence of these states and have shown that they disappear upon chemisorption of each of the molecules studied here. Although 0.3 eV is rather far above 0.125 eV (1000 cm^{-1}) both FEED [22] and surface reflection spectroscopy (SRS) results [25] indicate that these states are rather broad. Further, the SRS data show that final state energies for transitions from surface states on W(100) lie just above the Fermi level. It is therefore reasonable to assume that they contribute to optical absorption in the 1000 cm^{-1} frequency region. Adsorbate induced quenching of these states, and hence their oscillator strength, may account for the negative value of $\Delta\alpha$ at saturation for O_2 and CO, as well as the large dip in $\Delta\alpha$ for H_2 and D_2. In fact, the frequency dependence of the D_2 induced changes in α, which have been measured over the frequency range of the two CO_2 lasers (886 to 1088 cm^{-1}), strongly support this idea [6].

Aside from these intrinsic states it is not clear what contribution other low frequency surface structure has on the SEW attenuation. The lack of calculations on the low frequency optical response of these systems and the rather limited possible frequency range of the present study disallows any answer to this question at present.

4.1.2. Changes in $\hat{\epsilon}_m$

In spite of the uncertainty of the contribution to $\Delta\alpha$ from $\Delta\hat{\epsilon}_d$, variations in the effective bulk dielectric constant $\hat{\epsilon}_m$ caused by changes in diffuse scattering of the bulk free carriers offer an explanation for the size of $\Delta\alpha$ as well as the features in $\alpha(\theta)$.

For W near 10 μm the size of the surface scattering contribution can be estimated using Holstein's phenomenological expression [26]

$$\tau_{ss}^{-1} = (1-p)\frac{3}{8}\left(\frac{v_F}{c}\right)\omega_p \tag{1}$$

for the effective scattering rate due to collisions with the surface along with the Drude model formula [27]

$$\alpha = \left(\omega/\omega_p\right)^2(c\tau)^{-1} \tag{2}$$

for the free carrier contribution to the SEW attenuation coefficient. In these equations ω is the frequency, ω_p the plasma frequency (both in rad/s), v_F the Fermi velocity, c the speed of light, $1/\tau$ the free carrier relaxation rate, and p the Fuchs specularity parameter [1] which characterizes the effective fraction of electrons which are reflected specularly from the surface. The use of the appropriate IR parameters for W [6] and the replacement of $1/\tau$ in eq. (2) by $1/\tau_{ss}$ [eq. (1)] yields the surface scattering contribution to the attenuation: $\alpha = 0.16(1-p)$ cm^{-1}. The largest measured excursion in α, which occurs for H_2 between 2.1 and $\sim 6 \times 10^{14}$ molecules/cm^2, corresponds to a change in

the specularity parameter of -0.4, a value which is well within the maximum variation of $|\Delta p| = 1$.

Diffuse surface scattering is also suggested by the coverage dependence of α for adsorption of the five molecules. The signature of $\Delta\alpha$ versus CO, O_2, and N_2 coverage is similar to adsorbate induced resistivity variations of thin films (either a monotonic increase or a maximum at some intermediate coverage); for a number of the resistivity studies Wissmann [3] has shown that the Fuchs diffuse scattering theory applies. The same signature is also apparent for H_2 and D_2 if the changes before the sharp dip are ignored.

These observations on both the size and coverage dependence of $\Delta\alpha$ lead us to consider this interpretation of the changes, in light of other experimental evidence, for each of the W(100)–adsorbate systems measured here.

4.2. Specific W(100)–adsorbate systems

4.2.1. W(100)-CO

Among the systems studied here W(100)–CO has the possibility of providing the simplest example of adsorbate induced changes in diffuse surface scattering since no ordered superstructures form from RT adsorption. Chemisorption of CO results in approximately sequential filling of the β and then the α states. β-CO is thought to be dissociated [15] (although strong remnant C–O interactions cannot be ruled out [16]) with the C and O atoms occupying separate four-fold hollow sites. α-CO is molecular with the C bonded to the substrate in the on-top position [15].

Initial adsorption of CO (as well as all of the other gases) results in an increase in $\Delta\alpha$ suggesting that initially the C and O atoms adsorb randomly resulting in a disordered surface and hence an increase in the diffuse scattering of the free carriers. Such disorder has also been inferred from low energy electron diffraction (LEED) studies [28] which, upon CO adsorption, initially show an increase in the diffusely scattered background.

With adsorption beyond $\sim 1 \times 10^{14}$ cm^{-2} (henceforth all coverages are molecular unless otherwise stated) $\Delta\alpha$ decreases. There are two apparent possibilities whose relative contributions cannot be distinguished. The first is that adsorption beyond this point results in an overlayer which is more ordered, resulting in a peak in $\Delta\alpha$ at an intermediate coverage [3,29] (similar to a binary alloy $A_x B_{1-x}$ where the resistivity shows a maximum at an intermediate value of x between 0 and 1 [30]). The other possibility is that CO induced quenching of the 0.3 eV intrinsic surface states begins to dominate the IR response at this point. If, however, the magnitude of the quenching is a constant per adsorbed molecule (a reasonable assumption, see ref. [21]) and only these two processes contribute to $\Delta\alpha$, then it can be concluded that adsorption beyond 1×10^{14} cm^{-2} results in less disorder per adsorbed molecule than initially occurs.

41

Because α-CO is top bonded and therefore further away from the W surface it should have less of an effect on electronic surface scattering than β-CO. The fact that $\Delta\alpha$ is constant for coverages $\geq 5 \times 10^{14}$ cm^{-2} lends some support to this idea, although the data of fig. 3 show that α-CO adsorption does induce some change in the SEW attenuation. Desorption of α-CO and recooling to room temperature results in a decrease in $\Delta\alpha$ of $\sim 6.5 \times 10^{-3}$ cm^{-1} as signified by the jump between curves a and b. Readsorption of α-CO, however, causes a further $\Delta\alpha$ decrease, rather than an increase back to the previous saturated coverage value. Another RT–700 K–RT thermal cycle and readsorption (curve c) results in $\Delta\alpha$ values essentially the same as for curve b.

Two conclusions are suggested by these last observations. The first is that thermal annealing of β-CO to ~ 700 K results in an increase in order of this layer. Previous work function measurements [11] have shown that some kind of structural rearrangement takes place within the saturated β-CO layer upon heating to 700 K. That this rearrangement results in more order is not too surprising since it is well known that further annealing (to ~ 1150 K) results in a well ordered c(2×2) superstructure upon desorption of half the β-CO [28]. The second conclusion is that α-CO has no effect on the amount of diffuse surface scattering since initial adsorption into any state should increase the disorder of the surface (assuming that no simultaneous reconstruction of the surface occurs).

Although the effects of CO adsorption are not as simple as might have been expected, they do point to surface assisted absorption caused by diffuse surface scattering as a contribution. The main support comes from the θ dependence of β-CO adsorption and the fact that initial α-CO adsorption decreases the attenuation of the surface wave.

4.2.2. W(100)–O

The similar qualitative changes in $\Delta\alpha$ for O_2 and CO are at first surprising since LEED [31] and EELS [20] indicate that O_2 produces ordered superstructures on W(100). Initially, diffuse LEED streaks are formed along the {10} directions as O_2 is adsorbed. As the coverage approaches 2.5×10^{14} cm^{-2} the diffuse streaks break apart into a p(4×1) pattern. With further coverage a complicated series of LEED patterns is formed which, along with EELS, suggests that the oxygen atoms are serially forming double (at 2.5×10^{14} cm^{-2}), triple (at 3.75×10^{14} cm^{-2}), and quadruple (at 5.0×10^{14} cm^{-2}) rows.

As expected, $\Delta\alpha$ increases as oxygen initially bonds to the surface; this continues until a coverage of 2.5×10^{14} cm^{-2}. Even though a well ordered structure forms at this coverage it is not inconsistent that there exists a peak in $\Delta\alpha$ due to surface scattering. This is because free carrier reflections equivalent to ($[2n + 1]/2$, 0) and ($[2n + 1]/4$, 0) LEED spots are effectively diffuse since such reflections result in nonzero changes in the conduction electron velocity parallel to the metal–vacuum interface [6,26]. The decrease in $\Delta\alpha$ after this

coverage indicates that the effective disorder per adsorbed atom is decreasing up to $\sim 5 \times 10^{14}$ cm^{-2}, probably due to less scattering into these effectively diffuse LEED channels.

A comparison of the CO and O_2 results is interesting. Initially, both molecules are thought to break apart with individual atoms occupying the four-fold hollow sites [15,20]. If this is the case then our results indicate that the carbon atoms interact more strongly with the free carriers than do the oxygen atoms. In addition, the fact that nearly saturated O_2 coverages, which exhibit p(4 × 1)-like structures, have a higher value of $\Delta\alpha$ than comparable CO coverages further implies that the $([2n+1]/2, 0)$ and $([2n+1]/4, 0)$ reflections are effectively diffuse.

So, O_2 adsorption, in spite of the complicated superstructures which form, affects $\Delta\alpha$ in a manner similar to what would be expected for a simpler order–disorder–order type of coverage dependence.

4.2.3. W(100)-H and W(100)-D

Although H_2 and D_2 adsorption result in the most complicated structure in $\alpha(\theta)$, these two W(100)-adsorbate systems provide the best examples of adsorbate induced changes in electronic surface scattering among those studied here. Partly this is due to the fact that a fairly small fractional coverage ($\theta \approx 0.2$) of either adsorbate (as compared to $\sim$ saturated coverages of O_2 and N_2, and $\sim$ half-saturated coverage of CO) is sufficient to remove the 0.3 eV intrinsic surface states [21–25]. Because of this we concentrate on changes in α after the sharp minimum at 2.1×10^{14} cm^{-2} ($\theta = 0.21$).

The coverage dependence of α between $\theta = 0.21$ and 2.0 is again suggestive of changes in diffuse surface scattering as the dominant α-changing mechanism. This is corroborated by other experimental results on this system. At $\theta = 0.21$, where α is a minimum, the surface is reconstructed in what is termed the incommensurate-c(2 × 2)-H (or -D) phase which is characterized by 1/2 order spots split into a quartet along the $\pm(10)$ and $\pm(01)$ directions [9,32]. As more gas is added the spots of the 1/2 order quartet streak along directions perpendicular to their splitting and then eventually disappear, indicating a loss of order in one dimension followed by a loss of order in both dimensions. These LEED changes, signalling the onset of disorder, are accompanied by a sharp rise in the SEW attenuation until the maximum at $\theta = 0.6$. The subsequent fall in α as the surface approaches the well-ordered p(1 × 1)-H state at saturation occurs concurrently with a decrease in the diffuse LEED background. The high degree of order at saturation is also reflected in high energy ion scattering results [7] which show that the top layer is unreconstructed and in IR vibrational spectra [33] which show that the ν_1 and $2\nu_2$ β_1 W$_2$-H vibrational absorption features are their sharpest at $\theta = 1$.

A comparison with O_2 and CO shows that $\Delta\alpha$ for H_2 and D_2 is at least twice as large. This seems strange since it is expected that the larger atoms

should have a higher cross section for electronic scattering and suggests that it is the direct interaction of the free carriers with the reconstructed top W layer by H or D which results in the changes in α for these two adsorbates.

The frequency dependence of $\Delta\alpha$ after $\theta = 0.21$, which has been measured between 886 and 1088 cm^{-1}, also supports the surface scattering thesis. We find that $\Delta\alpha$ between $\theta = 0.21$ and 0.6 and between $\theta = 0.6$ and 2.0 are fit well using the expressions calculated by Dingle [2].

For $\theta < 0.21$ it is not clear what the sharp dip in $\Delta\alpha$ is due to. Contrary to the region for $\theta > 0.21$ the frequency dependence of the α changes for lower coverages does not comform to Dingle's expressions, but instead point to the quenching of the intrinsic surface states as providing some contribution. Surface disorder is largely ruled out by LEED observations [32] which show long range c(2 × 2) order for these coverages. However, unlike the changes in crystal momentum associated with the p(4 × 1)-O structures, the c(2 × 2) 1/2 order LEED reflections connect relatively few states on the W Fermi surface and therefore cannot directly contribute in a large way to changing the character of the free carrier scattering from the surface. An interesting possibility, discussed in detail elsewhere [6], is that a decrease in relaxation of the top layer W atoms as θ approaches 0.2 [9] induces changes in free carrier interband scattering at the surface, thus altering the IR absorption.

So, for W(100)-H (and -D) $\Delta\alpha$ after $\theta = 0.21$ is well explained by the surface assisted absorption process. For $\theta < 0.21$ the removal of the intrinsic surface states seems to play a role although it is not clear that this is the only α-altering mechanism operating in this region.

4.2.4. W(100)-N

The simple behavior of α with N coverage is a bit puzzling in light of the data for the other four adsorbates. At all stages of RT adsorption c(2 × 2) structure is evident in LEED measurements [14,34]. Analysis of the LEED data has resulted in the interpretation that the N atoms are bound in the four-fold hollow sites and that the atoms are grouped into islands [34].

This island formation may be the key to the difference between N$_2$ adsorption and that of the other gases. As shown in figs. 1 and 2 $\Delta\alpha$ is strictly increasing for N$_2$ while all the other gases have regions of negative slope as well as negative $\Delta\alpha$. This difference is somewhat surprising since N$_2$ adsorption is also effective in removing the W intrinsic surface states [21,24]. Since the c(2 × 2) 1/2 order spots should contribute negligibly to effective diffuse scattering, as mentioned above, this suggests that diffuse scattering from the island edges is quite strong – strong enough, in fact, to cancel any negative $\Delta\alpha$ tendencies caused by intrinsic surface state quenching.

A recently proposed model [35] for N$_2$ adsorption onto W(100) offers some explanation for why scattering at the island edges should be so strong. The model involves displacements of the top layer W atoms with the largest

displacements occurring at the edges of the islands. As in the case of H_2 and D_2, the interaction of the free carriers with the reconstructed W atoms is expected to be quite large, and thus could negate the loss of oscillator strength from the surface states.

A possible problem with this explanation is that beyond some coverage $\Delta\alpha$ should still decrease somewhat since the total length of the island boundaries should decrease as the islands begin to coalesce. Although not apparent in the data of figs. 1 and 2 some N_2 runs do seem to show a slight decrease in α beyond $\sim 2 \times 10^{14}$ cm^{-2} before the plateau, but the measured decrease is always less than the long term fluctuations ($\approx 2 \times 10^{-3}$ cm^{-1}) in the detected signal. LEED measurements do indicate, though, that such coalescence is not very pronounced unless the sample is annealed above room temperature. (Although it has not yet been studied, the effect on α of such annealing should provide a good test of this idea of strong scattering from the island edges.) In addition, at the highest coverages there exist 1/5 order features in the $\pm(10)$ and $\pm(01)$ directions around the integral order beams which should contribute to effectively diffuse scattering.

For N_2, then, we propose that strong scattering from the displaced W atoms on the boundaries of the N-induced islands is responsible for the increase in diffuse scattering upon adsorption.

5. Summary

Changes in the SEW attenuation coefficient α upon chemisorption of N_2, O_2, CO, H_2, and D_2 have been presented and discussed. Although the adsorption behavior of each species on the W surface is quite different (N_2, island formation; O_2, row formation; CO, no superstructures; H_2 and D_2, W reconstruction), the changes in α can be fairly well understood, in large part, in terms of changes in the diffuse scattering of the free carriers of the metal.

A useful extension of the present work would involve measuring the adsorbate induced IR changes over a broader frequency range, both higher and lower in energy. Such a study, which would necessitate the use of a more broad-band, albeit less sensitive, technique such as IR absorption spectroscopy, should help in sorting out the importance of the different contributions, such as surface states and surface scattering, to the broad-band IR response of these W(100)–adsorbate systems.

References

[1] K. Fuchs, Proc. Cambridge Phil. Soc. 34 (1938) 100.

[2] R.B. Dingle, Physica 19 (1953) 311; 19 (1953) 729.

[3] P. Wissmann, in: Springer Tracts in Modern Physics, Vol. 77, Ed. G. Höhler (Springer, New York, 1975), and references therein.

[4] J.W. Geus, in: Chemisorption and Reactions on Metallic Films, Vol. 1, Ed. J.R. Anderson (Academic Press, New York, 1971) p. 327, and references therein;
C. Pariset and J.P. Chavineau, Surface Sci. 47 (1975) 543.

[5] J.D. McIntyre and D.E. Aspnes, Surface Sci. 24 (1971) 417.

[6] D.M. Riffe, L.M. Hanssen and A.J. Sievers, Phys. Rev. B34 (1986) 692.

[7] I. Stensgaard, L.C. Feldman and P.J. Silverman, Phys. Rev. Letters 42 (1979) 247.

[8] T.E. Madey, Surface Sci. 36 (1973) 281.

[9] D.A. King and G. Thomas, Surface Sci. 92 (1980) 201.

[10] L.R. Clavenna and L.D. Schmidt, Surface Sci. 33 (1972) 11.

[11] C. Wang and R. Gomer, Surface Sci. 90 (1979) 10.

[12] D.A. King and M.G. Wells, Proc. Roy. Soc. A339 (1974) 245.

[13] T.E. Madey, Surface Sci. 33 (1972) 355.

[14] K. Griffiths and D.A. King, in: Proc. 4th Intern. Conf. on Solid Surfaces, Suppl. No. 201, Le Vide, Les Couches Minces (Société Française du Vide, Paris, 1980) p. 237.

[15] H. Froitzheim, H. Ibach and S. Lehwald, Surface Sci. 63 (1977) 56.

[16] A. Adnot and J.D. Carette, Surface Sci. 74 (1978) 109.

[17] W. Ho, R.F. Willis and E.W. Plummer, Surface Sci. 95 (1980) 171.

[18] Y.J. Chabal, Phys. Rev. Letters 55 (1985) 845.

[19] D.M. Riffe, L.M. Hanssen, A.J. Sievers, Y.J. Chabal and S.B. Christman, Surface Sci. 161 (1985) L559.

[20] H. Froitzheim, H. Ibach and S. Lehwald, Phys. Rev. B14 (1976) 1362.

[21] E.W. Plummer and J.W. Gadzuk, Phys. Rev. Letters 25 (1970) 1493.

[22] E.W. Plummer and A.E. Bell, J. Vacuum Sci. Technol. 9 (1972) 583.

[23] B.J. Waclawski and E.W. Plummer, Phys. Rev. Letters 29 (1972) 783.

[24] B. Feuerbacher and B. Fitton, Phys. Rev. Letters 29 (1972) 786.

[25] J. Anderson, G.W. Rubloff, M.A. Passler and P.J. Stiles, Phys. Rev. B10 (1974) 2401.

[26] T. Holstein, Phys. Rev. 88 (1952) 1427.

[27] See, e.g., G.N. Zhizhin, M.A. Moskalova, E.V. Shomina and V.A. Yakovlev, in: Surface Polaritons, Eds. V.M. Agranovich and D.L. Mills (North-Holland, New York, 1982) p. 93.

[28] J. Anderson and P.J. Estrup, J. Chem. Phys. 46 (1967) 563.

[29] D. Lessie, Phys. Rev. B20 (1979) 2491.

[30] N.F. Mott and H. Jones, The Theory of the Properties of Metals and Alloys (Dover, New York, 1958) p. 297.

[31] C.A. Papageorgopoulos and J.M. Chen, Surface Sci. 39 (1973) 313;
E. Bauer, H. Poppa and Y. Viswanath, Surface Sci. 58 (1976) 517.

[32] R.A. Barker and P.J. Estrup, J. Chem. Phys. 74 (1981) 1442;
A.H. Smith, R.A. Barker and P.J. Estrup, Surface Sci. 136 (1984) 327.

[33] Y.J. Chabal, J. Electron Spectrosc. Related Phenomena 38 (1986) 159.

[34] D.L. Adams and L.H. Germer, Surface Sci. 26 (1971) 109.

[35] K. Griffiths, C. Kendon, D.A. King and J.B. Pendry, Phys. Rev. Letters 46 (1981) 1584.

Intensity-dependent cyclotron resonance in a GaAs/GaAlAs two-dimensional electron gas

G. A. Rodríguez,[a] R. M. Hart,[a] A. J. Sievers,[a] and F. Keilmann

Max–Planck-Institut für Festkörperforschung, 7000 Stuttgart 80, Federal Republic of Germany

Z. Schlesinger, S. L. Wright, and W. I. Wang

IBM Thomas J. Watson Research Center, Yorktown Heights, New York 10598

Cyclotron resonance of a two-dimensional electron gas at a GaAs/GaAlAs interface is measured in the far infrared at intensities of up to 10 kW/cm^2. Both the cyclotron mass and the carrier density are independent of intensity but the relaxation time changes with a dependence which is similar to that observed earlier in high dc field mobility studies.

The high electron mobility in a two-dimensional electron gas (2DEG) system decreases at large dc electric fields because of field induced electron heating above the lattice temperature.[1,2] When a magnetic field is applied perpendicular to the conducting plane, the high mobility translates into a narrow resonance line shape centered at the cyclotron frequency[3] and the nonlinear properties of the 2DEG can be probed in more detail with intense far-infrared (FIR) radiation. For example, with circularly polarized radiation tuned to the resonance condition, the analogue of the dc electric field experiment can be carried out. In addition, by mapping out the complete line shape at different intensities, the electric field dependence of the effective carrier density, the cyclotron mass, and the relaxation time can be measured to provide a more complete picture of the underlying dynamics.

In this letter we report on the intensity dependence of the cyclotron resonance transmissivity profile of a high mobility $(5 \times 10^5$ cm^2/V s) GaAs/Ga$_{0.7}$Al$_{0.3}$As 2DEG at three FIR frequencies: 8.2, 27.8, and 53.4 cm^{-1}. For all samples, the resonant field to zero field transmissivity ratio (termed normalized transmissivity) is observed to increase for laser intensities above 10 W/cm^2 and approach 1 at the highest intensities of 10 kW/cm^2. Off resonance, in the wings of the cyclotron mode, the transmissivity decreases with increasing intensity. Fitting these cyclotron resonance line shapes using the Drude conductivity relation shows that the dramatic change in the transmissivity occurs because of FIR field induced changes in the cyclotron resonance relaxation time.

The experimental arrangement is shown schematically in Fig. 1. A high power pulsed transversely excited atmospheric (TEA) CO$_2$ laser C is used at a repetition rate of 0.2 Hz to pump the superfluorescent FIR transitions in CH$_3$F gas at 27.8 and 53.4 cm^{-1} and in ^{13}CH$_3$F at 8.2 cm^{-1}. The gas is enclosed in an 8-m-long Pyrex tube and the pressure optimized to obtain maximum FIR power at each frequency. FIR pulses of 40 ns with up to 12 mJ of energy are obtained.[4] The output FIR laser pulse polarization is fixed by a metal wire polarizer P. About 10% of the FIR laser output reflected by a Mylar beamsplitter B is focused by a parabolic mirror onto a pyroelectric detector R as a reference signal, and the

remainder is sent through an oversized stainless-steel waveguide W to the polymethylpentene (TPX)[5] cryostat input window Q. Inside the liquid helium cryostat H the radiation is focused through a linear polarizer onto the sample by a TPX lens, recollimated after the sample by a second TPX lens and reflected back to the cryostat output window by a copper mirror. The energy detector D is either a Golay cell or a Ge:Ga bolometer operated at 2 K. The detector signal is digitized and read by a computer. To obtain good statistics 20 shots in which the reference signal does not vary by more than 20% are taken at each magnetic field value and zero field normalizing measurements are made periodically to cancel out slow changes in detector sensitivity. The pulse energy at the sample position, measured with a pyroelectric detector, divided by the area of the aperture and by the pulse
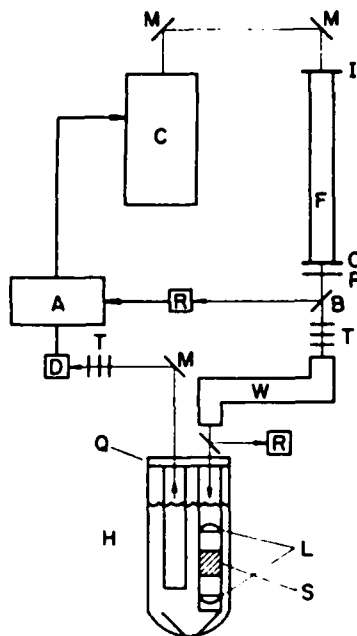

FIG. 1. Experimental arrangement. Legend: M, mirror; C, TEA CO$_2$ laser; I, input NaCl window; F, FIR laser; O, crystal quartz and TPX output window; A, digitizer and microcomputer; R, reference pyrometer detector; P, linear polarizing grid; B, Mylar beamsplitter; T, metal mesh attenuators; D, Ge:Ga bolometer or Golay cell detector; W, oversize waveguide; Q, TPX cryostat window; H, liquid helium cryostat; L, TPX lens; S, superconducting magnet and 2DEG sample.

[a] Permanent address: Laboratory of Atomic and Solid State Physics, Cornell University, Ithaca, NY 14853-2501

47

duration is the average incident intensity quoted here. Although it is difficult to estimate reliably the degree of lattice heating in the 2DEG sample since both the nature of the electron-phonon coupling and the dissipation of heat in heterostructure in a magnetic field are not well understood, for a given power the shorter pulse length the smaller will be such heating. Our FIR pulses are an order of magnitude shorter than those used in the high dc field mobility studies.[1,2]

The 2DEG sample with the GaAs substrate wedged at $2°$ to minimize interference effects is mounted in a 4 T superconducting magnet in the Faraday configuration. Black polyethylene on each side of the sample compartment eliminates room light. The electron density is monitored by Shubnikov–de Haas resistivity measurements and can be increased by activating a light-emitting diode near the sample. Both the magnet and the sample are immersed in liquid helium at 4.2 K. To measure the intensity-dependent transmissivity, calibrated metal mesh attenuators T are placed before and after the waveguide cryostat system so that the detector signal remains about the same throughout the experiment. In this manner the intensity at the sample can be varied over five orders of magnitude without saturating the detector. Two types of experiments have been performed: (1) at fixed FIR laser frequency the normalized transmissivity is measured as a function of incident intensity and (2) at fixed intensity the magnetic field is scanned stepwise to map out the cyclotron resonance line shape.

The intensity dependence of the normalized transmissivity at the cyclotron resonance condition has been studied at three FIR frequencies: 8.2, 27.8, and 53.4 cm^{-1}. The experimental results are shown in Fig. 2. At 8.2 and 53.4 cm^{-1} the density is 2.5×10^{11} electrons/cm^2. At 27.8 cm^{-1} three dif-

ferent densities have been studied: 1.5, 2.5, and 4.5×10^{11} electrons/cm^2. Within the uncertainty of the measurement the transmissivity begins to rise for all curves in Fig. 2 at the same intensity, independent of laser frequency and electron density. When the magnetic field is scanned at a fixed intensity to map out the cyclotron resonance line shape, results like those shown in Fig. 3 are obtained at the three frequencies. The cyclotron mass is essentially independent of laser intensity.

In order to quantify these experimental results the data as typified by Fig. 3 are fitted to the frequency-dependent transmissivity equation for linearly polarized light[6]

$$T(\omega_c) = 2\beta^2 \left[\left| \frac{1}{1 + 4\pi\beta\sigma_+(\omega_c)/c} \right|^2 + \left| \frac{1}{1 + 4\pi\beta\sigma_-(\omega_c)/c} \right|^2 \right]. \quad (1)$$

where $\beta = (1 + n_{GaAs})^{-1}$, n_{GaAs} being the refractive index of the GaAs substrate and c being the speed of light. The 2DEG conductivity $\sigma_\pm(\omega_c)$ is assumed to be of the Drude form, namely,

$$\sigma_\pm(\omega_c) = \frac{n_s e^2 \tau}{m^*} \frac{1}{1 - i(\omega \mp \omega_c)\tau}, \quad (2)$$

where n_s is the 2DEG electron density, e is the electron charge, m^* is the electron effective mass, τ is the electron relaxation time, and $\omega_c = eB/m^*c$ is the cyclotron frequency for the magnetic field B. The values $n_{GaAs} = 3.5$ and $m^* = 0.067m_e$ are used in the calculation.
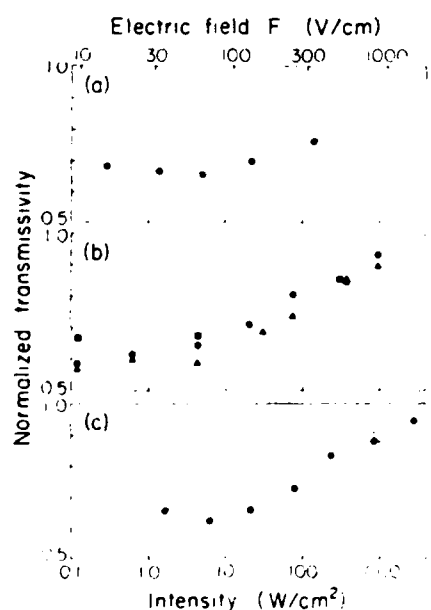

FIG. 2. Normalized transmissivity vs intensity at three different laser frequencies. (a) 53.4 cm^{-1}, 2.5×10^{11} electrons/cm^2. (b) 27.8 cm^{-1} squares, 1.5×10^{11} electrons/cm^2; circles, 2.5×10^{11} electrons/cm^2; triangles, 4.5×10^{11} electrons/cm^2. (c) 8.2 cm^{-1}, 2.5×10^{11} electrons/cm^2. Typical experimental error is represented by the error bar in (c).
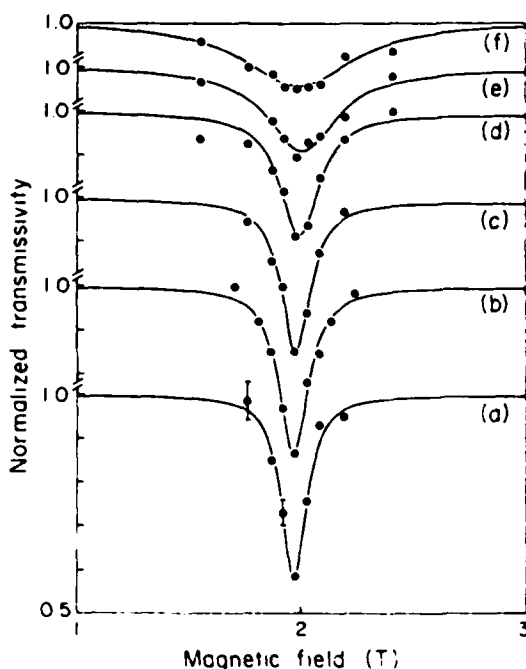

FIG. 3. Variation with FIR intensity of the 2DEG cyclotron resonance transmissivity profile. (a) 0.1 W/cm^2, (b) 0.6 W/cm^2, (c) 4.3 W/cm^2, (d) 20 W/cm^2, (e) 74 W/cm^2, (f) 360 W/cm^2. Laser frequency is 27.8 cm^{-1}, temperature is 4.2 K, density is 2.5×10^{11} electrons/cm^2.
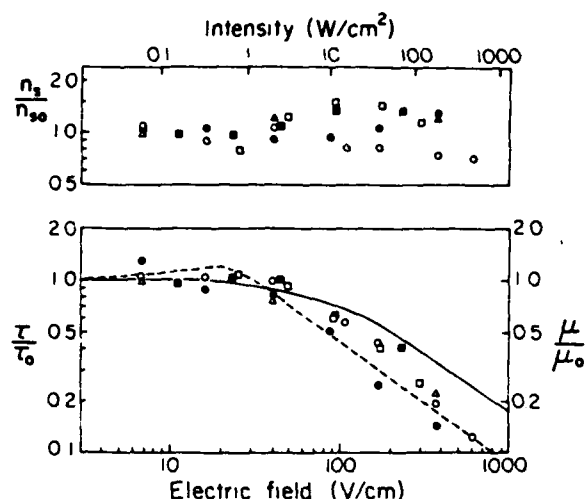
48

FIG. 4. Two-dimensional electron gas density n_s and relaxation time τ vs FIR intensity at the sample. The values are obtained by a least-square fit of the intensity-dependent line shape data, e.g., Fig. 3, to the transmissivity equation [Eq. (1)]. For each set of data n_s and τ are normalized by their values at low intensity. Open squares: $n_{s0} = 2.3 \times 10^{11}$, $\tau_0 = 11$ ps, 8.2 cm^{-1}; filled circles: $n_{s0} = 2.9 \times 10^{11}$ electrons/cm^2, $\tau_0 = 11$ ps, 27.8 cm^{-1}; open circles: $n_{s0} = 3.0 \times 10^{11}$, $\tau_0 = 13$ ps, 27.8 cm^{-1}; triangles: $n_{s0} = 2.2 \times 10^{11}$ electrons/cm^2, $\tau_0 = 9$ ps, 27.8 cm^{-1}; filled squares: $n_{s0} = 2.6 \times 10^{11}$ electrons/cm^2, $\tau_0 = 8$ ps, 53.4 cm^{-1}. Solid and dashed lines: Refs. 1 and 2, respectively.

At each laser intensity the two fit parameters n_s and τ are determined. The solid lines in Fig. 3 show the best fits of this particular set of data to Eq. (1). The low power values for the electron density n_{s0} and relaxation time τ_0 obtained from the fit compare well with the Shubnikov–de Haas derived electron density and with the electron relaxation time derived from the measured dc mobility. Figure 4 shows the behavior of n_s/n_{s0} and τ/τ_0 (or μ/μ_0) as a function of the FIR electric field $[(8\pi/c)(I/2)]^{1/2}$, where I is the measured linearly polarized incident intensity so that $I/2$ is the intensity of the circularly polarized component that causes Landau level transitions. As Fig. 4 shows above 20 V/cm, n_s is roughly constant while τ decreases with increasing electric field.

Since the effective density is independent of intensity, our data do not appear to be consistent with an incoherent saturation mechanism. Our results do not agree with the observation by Helm et al.[7] of partial saturation of a 2DEG with laser intensities of 100 mW/cm^2 in 0.3 ms pulses at a frequency of 84.2 cm^{-1}. Although the pulse times in the two experiments differ by 10^4, a comparison can be made because

both times are much longer than the relaxation time for the 2DEG.

The field dependence of τ obtained from the FIR data appears to show nearly the same behavior as has been found in the earlier dc mobility studies. The lines superimposed on top of our results in Fig. 4 show the electric field dependence of the normalized dc mobility measured by Shah et al. on two different GaAs/GaAlAs multiple quantum well heterostructures.[1,2] Because of the different way in which the two kinds of measurements have been made this agreement is quite surprising. Whereas, at resonance in the FIR, electron heating could proceed in the same way as has been proposed for the dc case; off resonance, this same heating mechanism must become ineffective. Inspection of curves (a) and (f) in Fig. 3 shows that off resonance the absorption is greater at high FIR intensities than it is at low ones, an observation which is not consistent with a resonant process.

We conclude that electron heating does occur when cyclotron resonance is probed at large FIR laser intensities and that the FIR electric field dependence of the relaxation time is the same as that previously found for dc mobility measurements. Since the heating does not follow the resonance shape of the conductivity, the good agreement between these two very different kinds of measurements indicates that a nonresonant process must be important.

[1] J. Shah, A. Pinczuk, H. L. Störmer, A. C. Gossard, and W. Wiegmann, Appl. Phys. Lett. 44, 322 (1984) and references therein.
[2] J. Shah, A. Pinczuk, H. L. Störmer, A. C. Gossard, and W. Wiegmann, Appl. Phys. Lett. 42, 55 (1983).
[3] The scattering times obtained from dc conductivity measurements and cyclotron resonance linewidths are not in general the same. See S. Das Sarma and F. Stern, Phys. Rev. B 32, 8442 (1985) and J. P. Harrang, R. J. Higgins, R. K. Goodall, P. R. Jay, M. Laviron, and P. Delescluse, Phys. Rev. B 32, 8126 (1985).
[4] A. Mayer and F. Keilmann, Phys. Rev. B 33, 6954 (1986).
[5] TPX is a registered trademark of Mitsui Petrochemical Industries, Ltd.
[6] K. W. Chiu, T. K. Lee, and J. J. Quinn, Surf. Sci. 58, 182 (1976).
[7] M. Helm, E. Gornik, A. Black, G. R. Allan, C. R. Pidgeon, K. Mitchell, and G. Weimann, Physica B 134, 323 (1985).

49

Proton Tunneling with Millielectrovolt Energies at the Be-H Acceptor Complex in Silicon

K. Muro[a] and A. J. Sievers

Laboratory of Atomic and Solid State Physics and Materials Science Center, Cornell University, Ithaca, New York 14853

(Received 23 April 1986)

High-resolution temperature-dependent measurements of the infrared spectra associated with the acceptor complexes Be-H and Be-D in Si together with direct far-infrared studies of the low-lying transitions provide an unambiguous identification of motional tunneling at electronic defects in elemental semiconductors. This novel system consists of a proton or deuteron tunneling around the substitutional Be double acceptor.

PACS numbers: 71.55.Fr

A dynamical tunneling model has been proposed to account for the unusual electronic states found for shallow acceptor and donor complexes containing hydrogen in ultrapure germanium.[1-4] Tunneling of the H ion around the substitutional impurity should, in general, alter the multiplicity and symmetry of the electronic ground state so that its behavior is completely different from that found for a monatomic substitutional impurity. Because these special defects have only been observed with the sensitive photothermal ionization spectroscopic technique, a complete experimental determination of the tunneling properties has not been possible; hence the model fits to the available experimental data do not provide a unique explanation.[4] If dynamic tunneling does play an important role in the electronic structure of these defects, then this internal degree of freedom may also appear in the electronic spectra of other complex impurity centers which involve the lightest element. We have searched for such effects in two-component complexes in Si.

In this paper the first observation of proton tunneling at deep-level acceptor complexes in silicon is described. High-resolution temperature-dependent measurements of the infrared (ir) spectra associated with the acceptor complexes Be-H and Be-D together with direct far-infrared (fir) studies of the low-lying transitions are combined with analysis based on the tunneling model[2] to produce an unambiguous picture of a proton or deuteron tunneling around the substitutional Be double acceptor. Large isotope shifts in the electronic and protonic spectra demonstrate that a strong interaction occurs between the hole in its electronic ground state and the proton which tunnels between four $\langle 111 \rangle$ symmetry directions near the acceptor site.

Pure float-zone–refined silicon wafers have been doped with use of diffusion techniques. Procedures for double doping which are somewhat different from those described in earlier works[5,6] are outlined here. Samples for the ir and fir have been treated differently because of the discrepancy in size ($2.5 \times 6 \times 17$ mm^3 vs $5 \times 10 \times 25$ mm^3). Typically, for the ir, a Si sample with about 1 μm of Be evaporated onto two sides is

sealed off in a carbonized quartz ampule together with a 500-Torr-He + 200-Torr-H gas mixture and then heated to 1300 °C for 20 min and air quenched. For the fir, the standard sandwich-sample technique[5] is employed, but the quartz ampule is charged with 1 atm of H$_2$ and maintained at 1300 °C for 1 h to permit diffusion deep into the sample. The optical absorption spectra are measured with fast Fourier-transform Michelson and Lamellar grating interferometers.

Low-temperature ir spectra for three acceptor complexes, $A(\text{Li,Be})$, $A(\text{D,Be})$, and $A(\text{H,Be})$, are shown in Fig. 1. The acceptor $A(\text{Li,Be})$, an example of a nontunneling center,[5] produces eight spectral features[7]; the strongest of these are numbered in the figure. With increasing temperature a second sequence of lines appears shifted to lower frequency by 11.3 cm^{-1} with respect to the trace shown in Fig. 1. These data demonstrate that the Γ_8 ground state is split into two Kramers doublets ($\Delta E \sim 11.3$ cm^{-1}) as a result of symmetry lowering ($T_d \rightarrow C_{3v}$) produced by the nearby interstitial Li$^+$ ion.[5]

The absorption spectra of the $A(\text{D,Be})$ and $A(\text{H,Be})$ centers which are also presented in Fig. 1 display new lines in addition to the main sequence. The ratio of the line strengths of the secondary to the main transitions is observed to be constant for many samples doped with a variety of diffusion procedures. A simple sum of the two absorption spectra has been obtained for a sample heated in a mixture of H$_2$ and D$_2$ gas, demonstrating that the complex contains the hydrogen isotope in the monatomic form. Further analysis of the spectra shows two additional distinguising features:

(1) When D $\rightarrow$ H the eight transitions of the main sequence (some of the strong transitions, labeled I, are recorded in Table I) all display a large isotope shift of 7.8 cm^{-1} to lower frequencies. This isotope effect is an order of magnitude larger than that previously reported for shallow dynamical tunneling centers in germanium.[1]

(2) The low-temperature fine structure is a weak high-frequency replica (labeled I* in Table I) of the main sequence with a shift of 16.2 cm^{-1} for $A(\text{D,Be})$ and 38.7 cm^{-1} for $A(\text{H,Be})$. Note that the complete replica spectrum can be identified for the $A(\text{D,Be})$
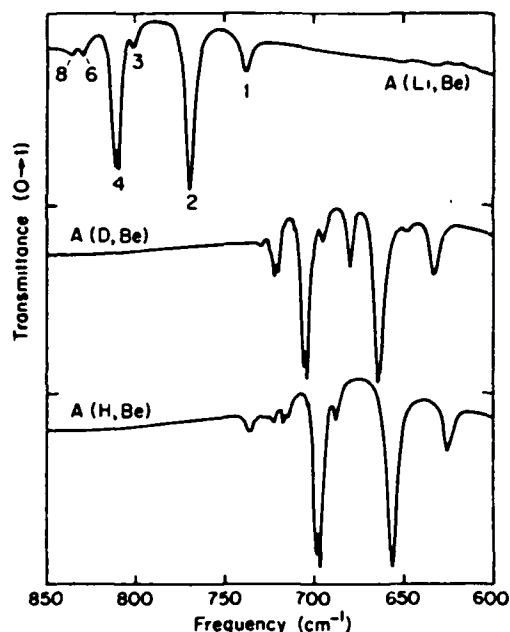
FIG. 1. Infrared transmittance of deep-level acceptor complexes in Si. The spectra measured with the sample at 1.7 K are normalized to 70-K data so that the bulk-Si phonon absorption divides out. In each case the ordinate extends from 0 to 1. Instrumental resolution is 0.5 cm^{-1}.

FIG. 2. Temperature dependence of the ir transmittance for the A(D,Be) center. The temperatures are (a) 1.7 K, (b) 5 K, (c) 8 K, and (d) 15 K. Again the bulk phonon contribution is removed by normalizing to the 70-K spectrum. The main acceptor absorption series at low temperature is identified in (a) by the markers labeled I, while the replica of this series, which also occurs, is labeled I*. With increasing temperature other absorption lines appear which follow the series pattern. These have been labeled II*, III*, and IV* in succession. The absorption series II* is accompanied by a lower-frequency replica II. The instrumental resolution is 0.5 cm^{-1}.

center in Fig. 1, but only one replica line can be clearly observed for the A(H,Be) center because of accidental coincidences with the strong lines of the main sequence. The apparent simplicity of the low-temperature A(H,Be) spectrum makes it clear why earlier workers,[6] who did not investigate the heavy isotope, missed this effect.

The multiplicity of the low-lying energy-level scheme can be seen most easily with temperature-dependent measurements. The spectra for the A(D, Be) center at a number of temperatures are shown in Fig. 2. As the temperature is increased from 1.7 K [2(a)] to 15 K [2(d)] two additional replicas (II* and
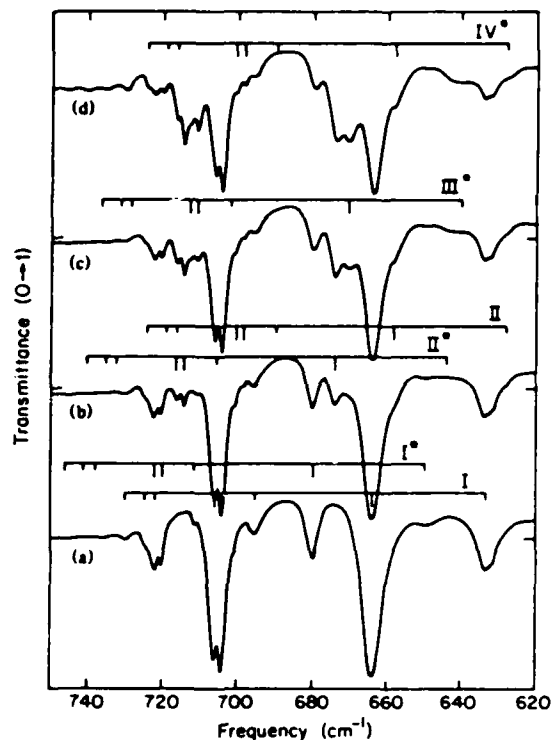
III*) appear on the high-frequency side of the main lines. This blue shift is quite unusual and indicates that splittings in the electronic excited states must oc-

TABLE I. ir acceptor plus tunneling transition frequencies (cm^{-1}) for strong lines 1, 2, and 4 of A(D,Be) and A(H,Be). Since the transition labeled 4 is a doublet ($\Delta E = 1.9 \pm 0.1$ cm^{-1}), the recorded values are for the lower of the two lines unless they are not resolved in which case the center of gravity is given.

Electronic level	I	I*	II	II*	III*
			D		
1 (Γ_8)	633.3	~649	$\cdots$	~642	$\cdots$
2 (Γ_8)	663.9	680.0	658.0	673.9	670.3
4 ($\Gamma_6 + \Gamma_7$)	704.3	720.5	698.3	714.4	710.6
			H		
1 (Γ_8)	625.4	Hidden	$\cdots$	Hidden	$\cdots$
2 (Γ_8)	655.7	Hidden	642.1	680.6	668.3
4 ($\Gamma_6 + \Gamma_7$)	696.5	736.3[a]	Hidden	721.5[a]	710.5[a]

[a]Not resolved.
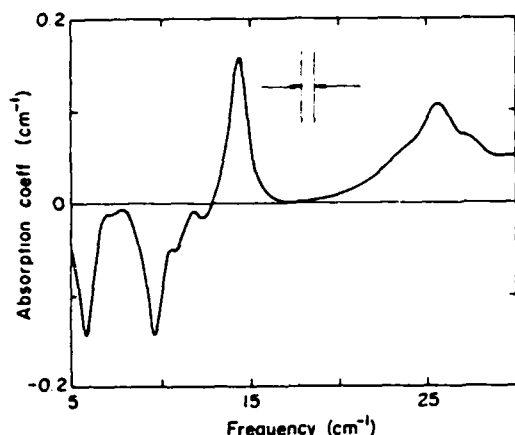
FIG. 3. Far-infrared absorption spectrum of A(H,Be) and A(D,Be). The absorption coefficient difference [A(H,Be) $- A$(D,Be)] is shown vs frequency for a sample temperature of 1.2 K. The instrumental resolution is 0.8 cm^{-1} and the A(D,Be) lines are unresolved.

TABLE II. Far-infrared tunneling transition frequencies A, B, and C in inverse centimeters for A(D,Be) and A(H,Be).

	fir		ir	
	D	H	D	H
C	12.9 (weak)	...	...	...
B	9.75	25.5	9.8	26
A	5.9	14.5	6.0	~ 14

cur. Absorption series II* and II [shown in Fig. 2(b)] have the same thermal activation energy and hence start from the same excited state. Inspection of Table I indicates that the energy difference between II* and II is the same as that between I* and I. At still higher temperatures the series III* appears without its low-frequency partner and series IV*, which overlaps II, also may exist.

Ir spectra for A(H,Be) show quite similar temperature dependences, but the spectral changes occur at somewhat higher temperatures. The corresponding transitions are recorded in Table I.

The fir absorption spectrum produced by direct excitation of the tunneling states is shown in Fig. 3 where the difference in absorption coefficient [A(H,Be) $- A$(D,Be)] is plotted versus frequency. All of the transition frequencies which are given in Table II agree with those obtained from the ir measurements. Note that both ratios of H/D for the transition frequencies A or B give ~ 2.5 which is too large to stem from vibrational or rotational motion of the defect but is consistent with dynamical tunneling. A new observation is the rapid dependence of the tunneling linewidth with frequency. Since both spectral widths for the hydrogen isotope are resolved in this figure, one can determine that the inverse lifetime varies as ω^2, and hence is proportional to the Si phonon density of states. Higher-resolution measurements on the deuterium isotope indicate that the 9.8-cm^{-1} mode linewidth is (FWHM) ~ 0.3 cm^{-1} while the 5.9-cm^{-1} mode has a width < 0.2 cm^{-1}. In a magnetic field of 6.7 T all of these lines show a weak magnetic field dependence, i.e., the field-induced frequency shift is only resolvable for the lowest-frequency deuterium line.

What kind of center can produce both the giant iso-

tope effects and the complex electronic spectra? Because Be in Si acts as an acceptor and belongs to group II, it is considered to be a substitutional double acceptor.[5] Since Li is an interstitial donor then as a result of compensation the complex A(Li,Be) can be pictured[5] as the single acceptor $(Be^{2-} + Li^+ + h^+)$. Although hydrogen usually acts as an acceptor in elemental semiconductors,[8] it is natural when combining H with substitutional Be to view it as a donor, just like the Li case. The resultant defect configuration is $(Be^{2-} + p^+ + h^+)$, which should be contrasted with the previously reported[2] tunneling acceptors $(Si + H^- + h^+)$ and $(C + H^- + h^+)$ in Ge. Of course, the general theoretical formalism for a dynamic tunneling system developed by Haller, Joos, and Falicov[2] is still valid and we now outline its application to the system of interest.

Our data together with the theoretical model of an acceptor with a tunneling proton produces energy level schemes such as the one shown in Fig. 4. This 1s-like electronic ground state of a substitutional acceptor is a fourfold–degenerate Γ_8 state while a p-like excited state has Γ_6, Γ_7, or Γ_8 symmetry.[7] A noninteracting proton tunneling between the four interstitial sites around the Be gives rise to a singlet Γ_1 and a triplet Γ_5 level. Shown on the left-hand side of Fig. 4 is the energy scheme with the proton-hole interaction turned off so that each electronic state (0,1,2,4) has available two proton-tunneling configurations. This weak-coupling limit is expected to describe the p-like excited states since the hole wave function, which vanishes at the defect origin, has a small amplitude in the proton neighborhood; however, for this deep center a strong interaction between the 1s-like electronic ground state (Γ_8) and the tunneling proton should occur. The resultant level structure is pictured on the right-hand side of Fig. 4. According to Haller, Joos, and Falicov[2] the three Γ_8 levels have mixed proton-tunneling configurations while the Γ_6 and Γ_7 states have only Γ_5 tunneling character; hence two sets of optical transitions are possible from a Γ_8 state but only one from Γ_6 or Γ_7.

The assignments for the observed absorption series, designated by I, I*, II, II*, and III*, are shown in Fig. 4. The asterisk identifies the ir transition to the excited state with the higher-energy proton-tunneling con-
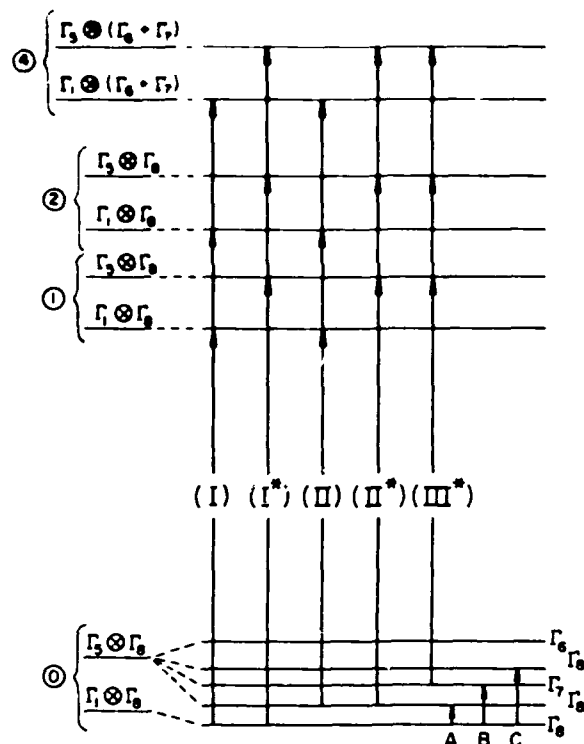
FIG. 4. Energy-level diagram of the ir and fir transitions observed for A(H,Be) and A(D,Be). The numbers on the left-hand side identify a few of the strong acceptor transitions. Next is shown the multiplet arrangement for the acceptor (Γ_8, Γ_8, Γ_8, and $\Gamma_6 + \Gamma_7$) and tunneling proton (Γ_1, Γ_5) with no interaction. A strong coupling between the hole and motional degrees of freedom for the ground-state manifold is shown at the lower right. The vertical transitions are described in the text.

figuration. The deuteron or proton tunnel splitting, called $4t$ in Ref. 2, is found directly from the energy difference between the series I*-I or II*-II to be 16.2 cm^{-1} for A(D,Be) and 38.8 cm^{-1} for A(H,Be). The ground-state splittings calculated from the difference between I and II, I* and II*, etc., are both consistent with the temperature-dependent profile and the fir measurements as shown in Table II.

In conclusion, three new distinguishing features have been found for this novel dynamical tunneling system: (i) The observation of the low-temperature ir replica spectrum makes possible the first direct deter-

mination of the tunneling parameter. (ii) The appearance of other ir replicas at elevated temperatures and the direct observation of fir transitions provide confirmation of the tunnel splittings in the ground-state manifold. (iii) The large ir and fir isotope shifts demonstrate that a strong interaction exists between the electronic ground state of the hole and the tunneling proton for this deep-level defect. Previous photothermal ionization spectroscopic studies[1-4] of shallow dynamical tunneling centers in Ge have been made with very low defect densities ($\sim 10^{11}$ cm^{-2}) so that the small isotope effect (< 0.5 cm^{-1}) can be resolved but no direct determination of the tunneling energy for these delicate centers has been possible. Our discovery that large isotope effects can be observed for a deep-level tunneling center in Si (density $\sim 10^{16}$ cm^{-3}) opens up the experimental possibilities. Now a variety of spectroscopic tools can be employed to probe more completely the dynamical behavior of these unusual yet robust electronic defects.

(a)Permanent address: Osaka University, Faculty of Engineering Science, Toyonaka, Osaka, Japan.

[1]E. E. Haller, Phys. Rev. Lett. **40**, 584 (1978).

[2]E. E. Haller, B. Joos, and L. M. Falicov, Phys. Rev. B **21**, 4729 (1980).

[3]B. Joos, E. E. Haller, and L. M. Falicov, Phys. Rev. B **22**, 832 (1980).

[4]E. E. Haller, W. L. Hansen, and F. S. Goulding, Adv. Phys. **30**, 125 (1981).

[5]R. K. Crouch, J. B. Robertson, and T. E. Cilimer, Phys. Rev. B **5**, 3111 (1972).

[6]R. K. Crouch, J. B. Robertson, H. T. Morgan, T. E. Gilmer, and R. K. Frank, J. Phys. Chem. Solids **35**, 833 (1974).

[7]A. Onton, P. Fisher, and A. K. Ramdas, Phys. Rev. **163**, 686 (1967).

[8]N. M. Johnson, C. Herring, and D. J. Chadi, Phys. Rev. Lett. **56**, 769 (1986).

Reply to "Comment on 'Observation of an index-of-refraction-induced change in the Drude parameters of Ag Films'"

H. Gugger,* M. Jurich, and J. D. Swalen

IBM Research Laboratory, San Jose, California 95193

A. J. Sievers

Max-Planck-Institut für Festkorperforschung, 7000 Stuttgart 1, Federal Republic of Germany

(Received 23 August 1985)

Our experimental attenuated-total-internal-reflection curves for Ag films are reanalyzed to include the thin contamination layer which has been proposed by W. H. Weber to account for the observed differences in the optical constants at the metal-air and metal-liquid interfaces. In contradiction to Weber's claim, the Drude parameters of the Ag film still show the same behavior as when this adlayer is ignored.

It has been proposed[1] that the reported differences in optical constants of Ag films measured at metal-air and metal-liquid interfaces[2] can be attributed to the thin contamination layer that exists on Ag films which have been exposed to air. In this Comment, we describe our test of Weber's hypothesis and show that the inclusion of such an adlayer into the data analysis does not alter our original interpretation of the experimental results.

The values of the complex dielectric function of Ag are calculated by a nonlinear least-squares fit of the exact Fresnel reflection formulas to the experimental attenuated-total-reflection curves. The three-layer model used in the original analysis[2] is now replaced by a four-layer model. The added layer has a thickness of 12 Å and a dielectric constant $\epsilon_0 = 4$, values chosen by Weber to minimize the apparent difference in the real part of the Ag dielectric function for the metal-air and metal-liquid interface. The calculated values of ϵ_1, ϵ_2, and τ_e^{-1} for this four-layer model are given in Table I. The values obtained with the three-layer model are given in Ref. 2.

The change in the Drude parameters are most clearly seen with plots of ϵ_1 versus wavelength squared, and τ_e^{-1} versus frequency squared for each model. Since

$$\epsilon_1 = \epsilon_\infty - \frac{\omega_{p,e}^2}{\omega^2} \tag{1}$$

and

$$\tau_e^{-1} = \tau_0^{-1} + \beta_0 \omega^2 , \tag{2}$$

the slope of the straight-line fits to the data in Fig. 1 is directly related to $\omega_{p,e}^2$ and the slope in Fig. 2 to β_0.

Figure 1 shows our original ϵ_1 values for a three-layer least-squares fit to λ^2, and the new calculated values of a four-layer system with the adlayer parameters assumed by Weber. Inspection of this figure demonstrates that the addition of the layer to the Ag surface does, indeed, alter the relative intercept and change the relative values of the two slopes for air and for liquid. The result overall is approximately the same as Weber's correction equation for ϵ_1 would imply.[1] Note that for the four-layer system, although the two curves cross at some wavelength, the slopes are different with $\omega_{p,e}$ still larger in the metal-liquid interface than for the air-metal interface (9.56 ± 0.03 eV compared to 9.43 ± 0.03 eV). At this point it may appear that the four-layer model, with perhaps slightly different parameters, could make the proposed index-of-refraction-induced effect vanish. We now examine the imaginary part of the metal dielectric function and demonstrate that this is not the case.

By means of Eq. (6) in Ref. 2, the inverse relaxation time is obtained from the values of ϵ_1 and ϵ_2 for the three- and four-layer model. In Fig. 2 the triangles identify the

TABLE I. Experimentally determined dielectric function of Ag and related optical parameters for the four-layer models. The adlayer has a thickness of 12 Å and a dielectric constant of 4.

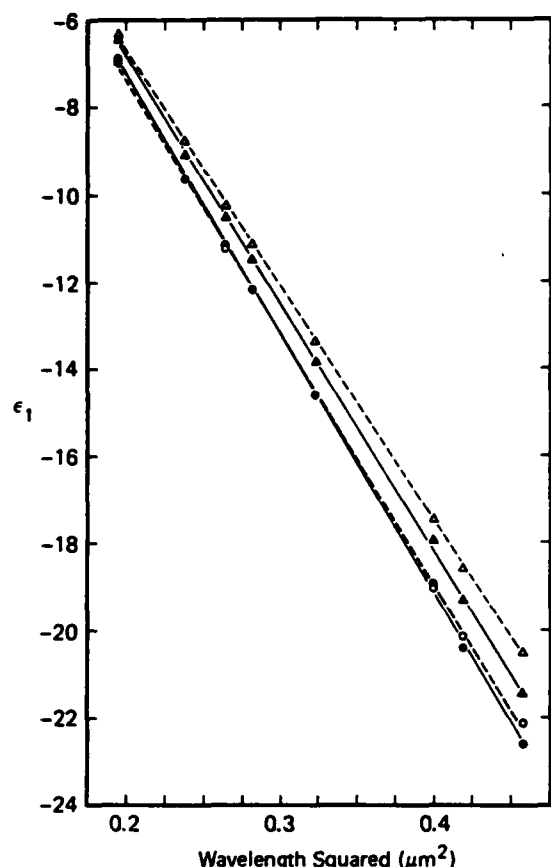| λ (Å)	CCl₄			Air		
	ϵ_1	ϵ_2	τ_e^{-1} (10^{14} sec^{-1})	ϵ_1	ϵ_2	τ_e^{-1} (10^{14} sec^{-1})
4416	−6.881	0.413	1.538	−6.971	0.565	2.171
4880	−9.639	0.533	1.446	−9.626	0.630	1.770
5145	−11.148	0.653	1.520	−11.238	0.721	1.719
5309	−12.153	0.692	1.467	−12.191	0.759	1.650
5682	−14.613	0.843	1.456	−14.587	0.830	1.471
6328	−18.925	1.086	1.375	−19.032	1.148	1.477
6571	−20.385	1.136	1.324	−20.130	1.127	1.353
6764	−22.598	1.292	1.325	−22.107	1.211	1.286

FIG. 1. Measured real part of the dielectric function of silver vs wavelength squared. For air (Δ, dashed line) and CCl_4 ($\blacktriangle$, solid line) half spaces using the three-layer model described in Ref. 2. For air, (O, dashed) and CCl_4 ($\bullet$, solid) with the four-layer model described in the text.

FIG. 2. Measured relaxation frequency vs frequency squared. For air (Δ, dashed line) and CCl_4 ($\blacktriangle$, solid line) half spaces using the three-layer model. For air (O, dashed) and CCl_4 ($\bullet$, solid) with the four-layer model.

three-layer case and the circles the four layer. For each model, the change is identified by the appropriately labeled arrow. In contrast with the result found in Fig. 1, now the presence of the same adlayer increases the difference between the two slopes over that given by the three-layer case. For both models, β_0 is smaller for the metal-liquid interface.

These comparisons in the same figures of the four- and three-layer results demonstrate that both models produce the same qualitative behavior for the Ag-film Drude parameters; namely, $\tau_0^{-1}(\text{liquid}) > \tau_0^{-1}(\text{air})$, $\beta(\text{liquid}) < \beta(\text{air})$, and $\omega_p(\text{liquid}) > \omega_p(\text{air})$. Also note that when the adlayer parameters are chosen in such a way as to minimize the difference between $\omega_p(\text{liquid})$ and $\omega_p(\text{air})$, the difference between $\beta(\text{liquid})$ and $\beta(\text{air})$ is actually increased. The adlayer does not produce the required effect of decreasing the difference for both Drude parameters at the same time.

Our complete data analysis using both the three- and four-layer models shows that the differences in the Ag-film optical constants which occur when the air half space is replaced by the liquid one, are not eliminated when Weber's hypothetical thick adlayer is included. It should be mentioned at this point that electron-spectroscopy for chemical analysis measurements on our Ag films showed
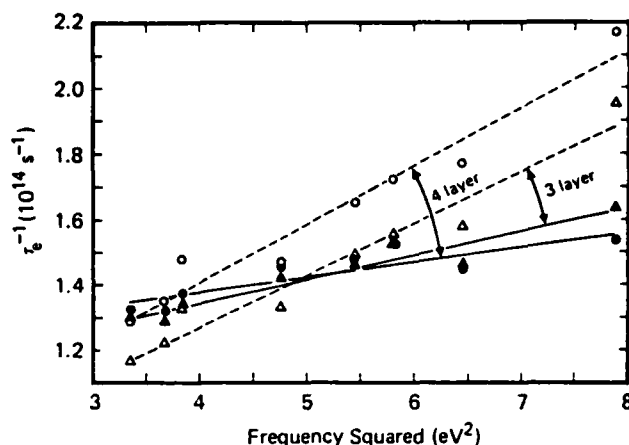
about 3 Å of physisorbed oxygen, less than a monolayer of chemisorbed oxygen, and no sulfur. Whether such a layer should be added to the three-layer model without at the same time treating surface roughness is a moot point since both components are clearly present on the Ag-film surface and they produce corrections of opposite sign for $\text{Re}(\epsilon_{Ag})$ when the index of the neighboring half space is changed.

Weber has argued qualitatively that an absorbing adlayer can account for the systematic changes which we have found for $\text{Im}(\epsilon_{Ag})$ between the air and liquid interface. The argument seems reasonable until one acknowledges the restrictions imposed on the optical properties of this adlayer. First, at frequencies below the interband transitions the optical constants of noble metals obey the frequency dependencies described by Eqs. (1) and (2) both in vacuum and in air.[2] Second, irrespective of the mechanism, the parameters must obey Kramers-Kronig (KK) relations. In this Comment we have shown that the transparent adlayer, which automatically satisfies KK relations, preserves the known frequency-dependent properties of Ag, i.e., a plasma frequency which is constant and a relaxation rate which varies quadratically with frequency (see Figs. 1 and 2). Forcing the adlayer to absorb strongly in the visible region causes its index of refraction to be frequency dependent as well. To account for our experimental results on Ag, these frequency dependences must conspire in such a way to give the same frequency-dependent properties, as found for the nonabsorbing adlayer described above. This line of reasoning leads us away from the absorbing adlayer concept.

The recent attenuated-total-reflection measurements on silver films at 5145 Å by Kurosawa, Pierce, Ushioda, and Hemminger[3] provide additional experimental information on the index-of-refraction-induced change. From their measurements they conclude that the polar liquid-induced changes in the Ag optical constants can be explained by assuming a 10-Å-thick nonabsorbing adlayer on the silver surface with dielectric constant 3; however, the changes in optical constants were not measured as a function of fre-

quency. In this Comment we have shown that frequency-dependent measurements are required to demonstrate that an adlayer alone cannot account for the index-of-refraction-induced changes in both optical constants.

In Weber's conclusions, it is argued that Table I in the earlier work by Eagen and Weber[4] shows that an index-of-refraction-induced change in the optical constants does not occur. This table presents values of ϵ_1 and ϵ with estimated uncertainties at a number of wavelengths for one Ag film measured at a metal-vacuum interface and for another film measured at a metal-substrate interface. Our least-squares fits to these data give Drude plasma frequencies which differ by more than the uncertainties of the measurement. These Drude parameters are listed in Table II. Although these differences are comparable in magnitude, but opposite in sign, to the differences reported in our measurements on a single dirty film,[2] the variations in the optical properties from sample to sample are large enough so that the differences evident in Table II are not deemed significant[1,4] by the authors. We conclude that because of these sample-to-sample limitations, a comparison of the optical properties of the two films listed in Table I of Ref. 4 cannot be used to argue for or against the

TABLE II. Drude parameters for the two Ag films described in Ref. 4.

	Metal-vacuum	Metal-substrate
$\omega_{p,e}$ (eV)	9.77 ± 0.03	9.39 ± 0.03
β_0 ($10^{12}\,\mathrm{sec}^{-1}\mathrm{eV}^{-2}$)	8.2 ± 1.4	3.40 ± 0.5

index-of-refraction-induced changes which we have described.

In conclusion, our analysis demonstrates that the presence of a thin contamination layer on Ag films does not qualitatively alter our original interpretation of the experimental results. An index-of-refraction-induced change still is observed in the Drude parameters of Ag films.

*Permanent address: Ciba-Geigy AG, K. A. Forschungs-zentrum, CH-1701 Fribourg, Switzerland.

[1]W. H. Weber, preceding Comment, Phys. Rev. B 34, 1319 (1986).

[2]H. Gugger, M. Jurich, J. D. Swalen, and A. J. Sievers, Phys. Rev. B 30, 4189 (1984).

[3]K. Kurosawa, R. M. Pierce, S. Ushioda, and J. C. Hemminger, Phys. Rev. B 33, 789 (1986).

[4]C. F. Eagen and W. H. Weber, Phys. Rev. B 19, 5068 (1979).

Infrared surface-wave interferometry on W(100)

L. M. Hanssen, D. M. Riffe, and A. J. Sievers

Laboratory of Atomic and Solid State Physics and Materials Science Center, Cornell University, Ithaca, New York 14853-2501

An IR grating on a clean W(100) surface is shown to generate both homogeneous and inhomogeneous surface electromagnetic waves. An observed interference between these two components, which can be described in terms of a two-beam interferometer with variable arm amplitude and fixed optical path, is used to measure the plasma frequency accurately in the IR.

The attenuation of surface electromagnetic waves (SEW's) propagating on a clean W(100) surface has been used to monitor adsorbate vibrational modes,[1] surface reconstruction,[2] and chemisorption-induced[3] changes in the free-carrier behavior of the metal in the room-temperature regime. We report on the measured properties of SEW's at elevated temperatures. At temperatures greater than 1000 K the SEW signal is attenuated to such a large extent that low-intensity surface skimming plane electromagnetic waves (PEW's), which are also generated at the grating coupler, can be detected. Since both kinds of wave are generated coherently at the input but travel across the surface with different velocities, interferometry is possible. This interferometer has been used to measure the plasma frequency of W in the 10-μm wavelength region.

A description of the experimental apparatus and procedures for making SEW attenuation measurements in ultrahigh-vacuum UHV conditions has been given in Ref. 2. Because the SEW wave vector is greater than that of light, gratings etched into the surface are used to couple CO_2 laser radiation into and out of the SEW spectrum.

To identify the interference signature between SEW's and PEW's, the temperature dependence of the signal from the output coupler is measured at many laser frequencies across the ranges of the $^{12}CO_2$ and $^{13}CO_2$ laser gases. Each of the eight data traces shown in Fig. 1 represents an intensity-versus-temperature run at a fixed frequency. Note the strong minimum in log (intensity) that occurs near $T = 400°C$ and $\bar{\nu} = 1000$ cm^{-1}. For all frequencies the temperature dependence at low temperatures agrees with that calculated for SEW's from the temperature dependence of the dc resistivity $\rho(T)$, namely,

$$I_S(T) = I_{0S} \exp[-\omega^2 L \rho(T)/4\pi c], \quad (1)$$

where ω is the angular frequency, L the propagation distance, and c the velocity of light. For high temperatures an additional component, which tracks the SEW intensity when the laser's beam angle, input power, or polarization is changed, comes from PEW's generated at the input grating.

Next it is shown that the phase difference between SEW's and PEW's in the IR is large enough over the

sample length to account for the interference effect. The difference in phase between the two beams can be written as

$$\theta = q_S L - q_P L + \phi, \quad (2)$$

where q_S is the SEW wave vector, q_P the PEW wave vector, and ϕ the phase shift between the two waves, which is assumed to be a constant over the frequency region of interest. For a Drude metal in the 10-μm-wavelength region

$$q_S \approx (\omega/c)[1 + \omega^2/2\omega_p^2 + (\epsilon_0 + {}^3\!/_4)(1 - 1/\omega^2\tau^2)\omega^4/2\omega_p^4], \quad (3)$$

where ω_p is the plasma frequency in the IR and ϵ_0 the low-frequency contribution to the dielectric constant from the interband transitions. Since the most effective PEW's are those within a wavelength of the surface at the output coupler, $q_P = \omega/c$; hence the phase difference between the two arms for a Drude metal is

$$\theta \approx (\omega L/c)(\omega^2/2\omega_p^2) + \phi. \quad (4)$$

The resultant intensity at the detector now takes on a familiar form, namely,

$$I = I_S + I_P + 2(I_S I_P)^{1/2} \cos\theta. \quad (5)$$

Destructive interference occurs when $\theta = (2n + 1)\pi$, with n a nonnegative integer, and the largest effect appears when the two arms of the optical bridge are balanced. A temperature sweep at a fixed laser frequency (the data shown in Fig. 1) corresponds to varying the relative amplitudes for the two components of Eq. (5) while keeping θ fixed.

To obtain accurate values for $\theta(\omega)$ each data set must be fitted to Eq. (5), so knowledge of the expected temperature and frequency dependences of I_S and I_P is required. The SEW intensity dependence is given in Eq. (1). Although an accurate expression for the PEW intensity dependence requires the solution of a deep grating diffraction problem, we show here that the appropriate temperature-dependent form can be constructed from a simple phenomenological model.

We assume that the near fields at the source that evolve into interfering PEW's and SEW's extend a distance δ_0 above the grating and that the mean SEW amplitude height is a measure of this range. Now
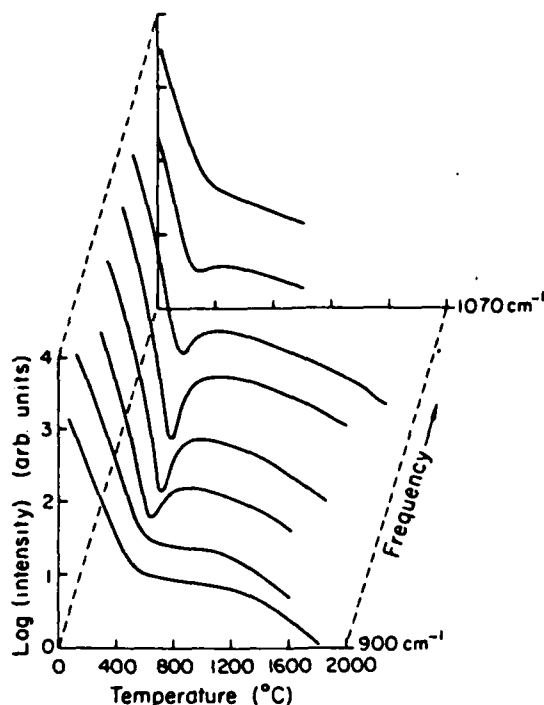
Fig. 1. Transmitted IR intensity as a function of temperature and frequency. Eight SEW signal-versus-temperature scans are shown at approximately equal frequency intervals across the CO_2 laser spectrum.

consider a PEW traveling along the sample surface. In analogy with a parallel-plate transmission line geometry for fixed plate separation δ_0, the transmitted intensity would be

$$I_P = I_{0P} \exp(-2ry/\delta_0), \qquad (6)$$

where r is the normalized real part of the surface impedance of the metal[2] and y the distance along the surface.

Because of diffraction the height of the PEW actually changes with distance from the source; hence from the geometry

$$\delta(y) = \delta_0 + y \tan(\alpha), \qquad (7)$$

where δ_0 is the height at $y = 0$ and $\alpha = \sin^{-1}(\lambda/\delta_0)$, the angle to the first minimum in a single-slit diffraction pattern. The appropriate generalization of Eq. (6) is

$$I_P = I_{0P} \exp\left\{-\int dy[2r/\delta(y)]\right\}. \qquad (8)$$

Another loss mechanism for this component occurs at the output coupler, $y = L$, since only the fraction $[\delta_0/\delta(L)]$ of the PEW will be coupled out to the detector. The resultant expression is

$$I_P = I_{0P}(1 + fL/\delta_0)^{-(1+2r/f)}, \qquad (9)$$

where

$$f = \lambda/(\delta_0^2 - \lambda^2)^{1/2}. \qquad (10)$$

Three adjustable parameters θ, I_{0S}, and I_{0P} in Eqs. (1), (5), and (9) are used to fit the temperature-dependent data with the data near $I_S \approx I_P$ weighted most heavily. Figure 2 shows three data sets with the corre-

sponding best fit given by this model. The destructive interference between the SEW's and the PEW's increases in strength as the laser frequency is decreased from 1072 cm^{-1} [Fig. 2(a)] to 995 cm^{-1} [Fig. 2(c)]. Sample movement produces the high-temperature difference between the data and the model shown in Figs. 3(b) and 3(c). The fits show that the PEW intensity at room temperature is ~1% of the SEW value. Even here the PEW component cannot be neglected since at frequencies where a π phase shift occurs the resultant intensity is ~20% smaller than for the SEW component alone.

In order to compare the results with relation (3) the measured phase angle θ is plotted against the frequency cubed as shown in Fig. 3. A linear dependence is observed over the measured range covering nearly π rad. A least-squares fit to these data gives $L/(2c\omega_p^2)$ = $1.04(\pm0.04) \times 10^{25}$ sec^{-3} and $\phi = -0.51(\pm0.05)\pi$.

Our measurements show that the output coupling of both the SEW's and the PEW's takes place over the full extent of the 3.8-mm-wide output grating, so half of this distance is added to the separation between gratings to obtain the total propagation distance.
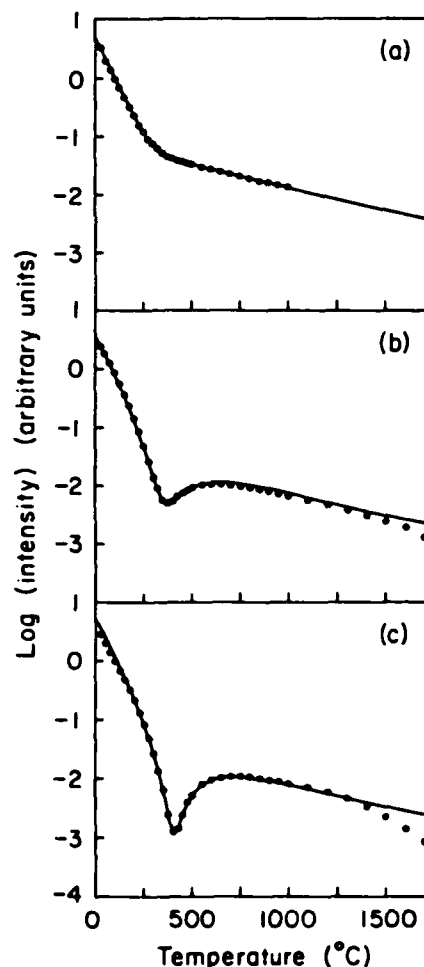

Fig. 2. Comparison of three sets of data with the two-beam interferometer model. The open circles represent the data and the solid line the model fit. The three frequencies are (a) 1072 cm^{-1}, (b) 1027 cm^{-1}, and (c) 995 cm^{-1}.
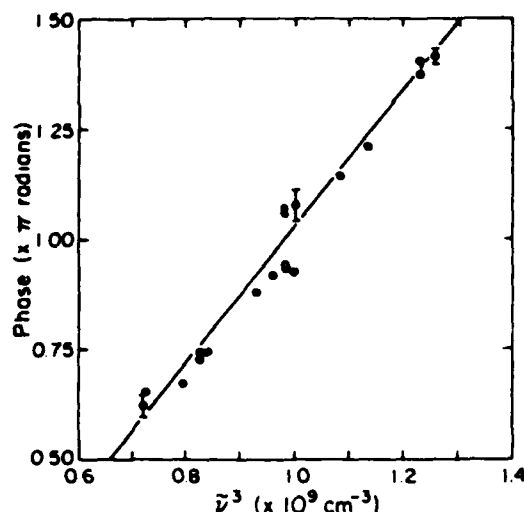
Fig. 3. Frequency dependence of the phase difference between the two arms of the interferometer. The filled circles represent the data; the open circles are alternative values for the data points directly above them [since $\cos(\pi + x) = \cos(\pi - x)$]. The solid line shows a linear least-squares fit.

Substitution of $L = 4.94$ cm gives $\hbar\omega_p = 7.0(\pm 0.3)$ eV for the plasma frequency in the IR.

By measuring the transmitted intensity as a function of placement of the input beam on the input grating, it has been possible to show that the PEW's occur not because of the impedance change at the grating–smooth-metal boundary[4] but instead because of the finite number of grating lines intercepted by the input beam (about 20 in the actual experiment). For a plane wave incident upon an infinite grating at the angle for maximum SEW generation the first-order PEW beam is forbidden, but when the grating consists of a small number of lines this selection rule against the first-order beam is weakened, so some PEW's do appear. The end result is that a narrow grating coupler or a small spot size automatically sends PEW's along with the desired SEW's across the surface.

Another feature of our data that needs examination is the finite intensity at the destructive interference condition. At a frequency near 1000 cm^{-1}, where $\theta = \pi$, the resultant intensity should dip down to the background-noise level when $I_S = I_P$; however, the smallest measured value is ~4% of the SEW (or PEW) value at that temperature. [This is for the data at 995 cm^{-1} shown in 2(c).] There are two contributions to this 4% minimum. The first is that the SEW beam is attenuated more strongly than the PEW beam along the deep grating couplers. This leads to less than complete destructive interference since the two components' intensities cannot be matched across the entire length of the output coupler (and hence across all the detector). The second contribution comes from the difference in SEW and PEW wave vectors. This difference in wave vector (which causes the whole interference effect in the first place) also leads to less than complete destructive interference since the phase angle θ is not a constant across the whole output coupler. From measured values of the difference in attenuation and wave vector of the two components we calculate minimum $I/$

I_S (or I/I_P) $\approx 2.5\%$, in reasonable agreement with the measured value of 4%.

The experimentally determined value of the constant phase factor $\phi = -\pi/2$ cannot be explained within the framework of this simple phenomenological picture. A rigorous diffraction calculation may be required for the relative phases of the two components at the input and output coupler to be explored.

Our direct determination of the real part of the inverse dielectric function of a clean W(100) surface that we have characterized with an effective plasma frequency ($\hbar\omega_p = 7.0$ eV) in the Drude model approximation can be compared with the value deduced for the same frequency region from reflectivity[5] and ellipsometric[6] measurements ($\hbar\omega_p = 6.4$ eV).[7] The errors in these earlier measurements are large enough that the two values are within the uncertainties.

This new measurement technique is not limited to W. From relation (4) the criterion for destructive interference (assuming that $\phi = -\pi/2$) can be rewritten in terms of the SEW attenuation coefficient in Eq. (1) to give

$$\omega^2 L \rho(T)/4\pi c = 3\pi/\omega\tau. \qquad (11)$$

Inspection of the right-hand side of this expression shows that the IR frequency should be chosen to ensure that $\omega\tau > 1$ for a particular metal so that the attenuation of the SEW will not obscure the interference effect.

The analysis given here, which uses the interference between SEW's and PEW's to determine the plasma frequency of the metal, should have general applicability in the IR. Moreover, to produce such an effect gratings are not required, since the interference has already been detected with an aperture-excitation technique[8] on a smooth metal surface.

References

1. D. M. Riffe, L. M. Hanssen, A. J. Sievers, Y. J. Chabal, and S. B. Christman, Surf. Sci. 161, L559 (1985).
2. D. M. Riffe, L. M. Hanssen, and A. J. Sievers, Phys. Rev. B 34, 692 (1986).
3. D. M. Riffe, L. M. Hanssen, and A. J. Sievers, "Infrared observation of adsorbate induced changes in free carrier surface scattering," Surf. Sci. (to be published).
4. Z. Schlesinger and A. J. Sievers, Appl. Phys. Lett. 36, 409 (1980).
5. J. H. Weaver, C. G. Olson, and D. W. Lynch, Phys. Rev. B 12, 1293 (1975).
6. L. V. Nomerovanaya, M. M. Kirillova, and M. M. Noskov, Sov. Phys. JETP 33, 405 (1971).
7. M. A. Ordal, R. J. Bell, R. W. Alexander, L. L. Long, and M. R. Querry, Appl. Opt. 24, 4493 (1985).
8. M. A. Chesters, S. F. Parker, and V. A. Yakovlev, Opt. Commun. 55, 17 (1985).

INCOHERENT SATURATION STUDY OF THE SELENIUM DONOR IN AlSb

R.E. Peale, K. Muro, J.T. McWhirter and A.J. Sievers

Laboratory of Atomic and Solid State Physics and Materials Science Center, Cornell University, Ithaca,
NY 14850-2501, USA

The technique of incoherent laser saturation has been used to probe the
$1s(A_1) \to 1s(T_1)$ transition of the Se donor in AlSb at liquid helium
temperatures. The intensity dependence of the absorptivity is described by
a cascade excitation process in which at high flux two photons promote
the electron into the conduction band. The $1s(T_1)$ lifetime is determined
to be between 1 and 5 psec which is about three orders of magnitude
smaller than found for shallow levels in three-five compounds.

ALTHOUGH HIGH POWER LASER saturation studies
of shallow levels in semiconductors show that impurity
lifetimes in the range 1 nsec to 1 μsec can be obtained at
low temperatures [1–4], no similar measurements on
deep levels have been reported. Yet incoherent saturation
measurements on such transitions should be quite
informative since the data would provide some evidence
as to how the increase in electron–phonon coupling
constant for these localized states is balanced against the
highly forbidden multiphonon decay required to relax
them.

In this paper the technique of incoherent saturation
[5] has been used to investigate the dynamics of the
$1s(A_1) \to 1s(T_1)$ transition of the Se donor in AlSb.
This transition was chosen because linear spectroscopy
[6] shows that it is coincident with both the 10P(18)
and 10P(20) CO_2 gas laser lines. At a sample temperature
of 1.7 K the saturation of the absorptivity com-
mences at a beam intensity of a few hundred kWcm^{-2}.
Although the rate of change of absorptivity with incident
intensity is much faster than can be explained by a
homogeneously or inhomogeneously broadened two
level system, the data can be understood with a three
level cascade excitation model. The measured excited
state lifetime is ~1–5 psec which is about 10^3 times
smaller than the values observed for shallow defects
[1–4].

The sample of Se doped AlSb is from the batch
described in [6]. Our spectroscopically determined
values of the linewidth and center frequency of the
$1s(A_1) \to 1s(T_1)$ transition as a function of tempera-
ture are shown in Fig. 1. At low temperature the tran-
sition which occurs at 944.71 cm^{-1} is straddled by two
CO_2 laser lines, 10P(18) at 945.98 cm^{-1} and 10P(20)
at 944.19 cm^{-1}. The temperature independence of the
linewidth at low temperatures can be interpreted in one

of two ways; either the line is homogeneously broadened
and the low temperature linewidth is a measure of the
intrinsic multiphonon decay lifetime or the line is
inhomogeneously broadened due to crystal strains so the
low temperature line width obtained from linear spectro-
scopy provides no intrinsic information about the
lifetime. For the former case one can readily estimate
the laser intensity where saturation should commence
[5] since

$$I_s = \frac{\hbar\omega}{2\sigma}(\Delta\omega), \qquad (1)$$

where ω is the center frequency, $\Delta\omega$ is the linewidth
(FWHM) and σ is the absorption cross section. For this
transition the linewidth is 5.6 cm^{-1} and $\sigma = 2.7 \times$
10^{-15} cm^{-2} so $I_s = 3.7$ MWcm^{-2}. Since the saturation
parameter will be smaller for the case of inhomogeneous
broadening [5], the I_s calculated above represents the
maximum possible value for this 2 level system.

The incoherent saturation measurements have been
made with the experimental setup shown in Fig. 2. A
line tunable CO_2 laser Q-switched at a frequency of
170 Hz produces 200 nsec pulses with peak power of
1.5 kW. The beam is focused to a spot size of 9 $\times$
10^{-4} cm^2 on the sample which is immersed in pumped
He at 1.7 K in an optical access cryostat. Sample trans-
mission as a function of incident laser intensity is
obtained by moving the CaF_2 calibrated attenuators
(labeled A in Fig. 2) one by one from one side of the
cryostat to the other so that errors associated with
nonlinear detector response are minimized. The laser
output is monitored with a pyroelectric detector which
is also used to normalize the transmission by means of
a two channel box car integrator.

The experimental incoherent saturation results are
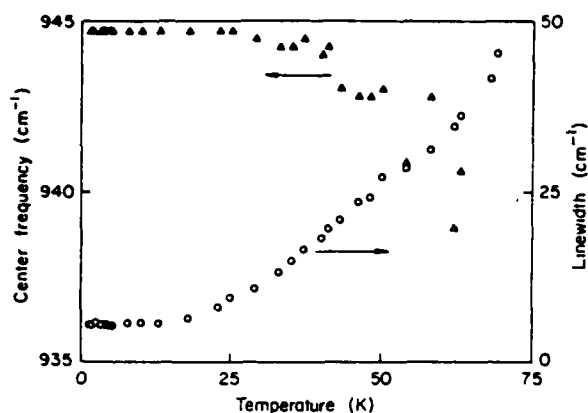shown in Fig. 3. The data in the top picture are for

Fig. 1. Temperature dependence of the line width and center frequency of the $1s(A_1) \rightarrow 1s(T_1)$ transition in AlSb:Se. The value of the low intensity absorption coefficient, α_0, at line center is $4.2\,\text{cm}^{-1}$.
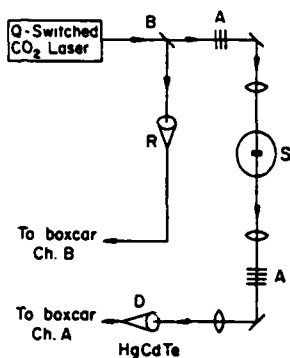

Fig. 2. Experimental arrangement for incoherent saturation measurement. Legend: B, beamsplitter; A, CaF_2 calibrated attenuators; D, HgCdTe detector; R, pyroelectric reference detector; and S, sample cryostat.
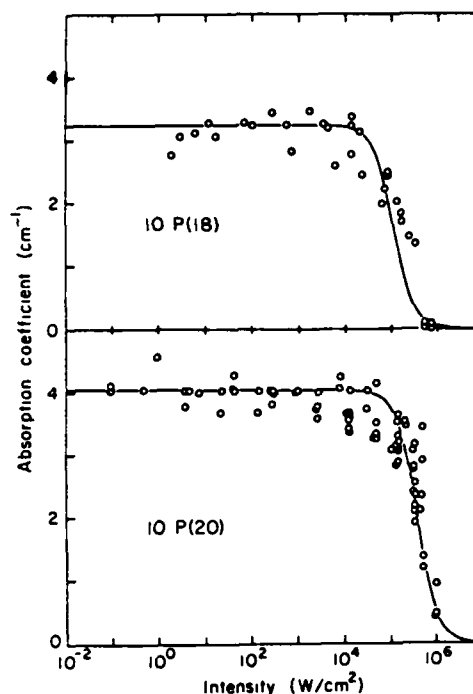

Fig. 3. Absorption coefficient vs laser intensity. Top: 10P(18) laser line on the high frequency side of the $1s(A_1) \rightarrow 1s(T_1)$ donor line. Bottom: 10P(20) on the low frequency side of the donor line. The sample temperature is 1.7 K.
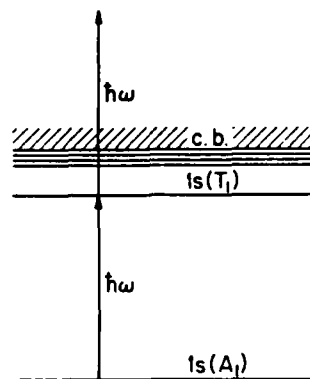

Fig. 4. Schematic diagram of the cascade excitation model.

10P(18) and the bottom picture are for 10P(20). Inspection of these data show that they are qualitatively similar but quantitatively different. The saturation intensity, I_s, taken here to be equal to the incident intensity value at which the absorption coefficient is equal to one half of its low intensity value, is 120 kW cm^{-2} for 10P(18) and 400 kWcm^{-2} for 10P(20). The fact that the two curves do not look identical may be an indication of heating since with increasing temperature the absorption line center frequency in Fig. 1 moves to lower frequencies hence away from the 10P(18) line and towards the 10P(20) line. Such an effect does occur in the data shown in Fig. 3; however, the experiment described next indicates that it is electron heating and not sample heating that is important. By running the laser in a CW-chopped mode, the energy per pulse at the sample can be increased by an order of magnitude over

that in the Q-switched mode. No change in sample transmission occurs in this configuration indicating that sample heating is not important. Another unusual features of the data in Fig. 3 is that the rate of decrease in absorptivity with increasing incident laser intensity is much faster than can be explained by either the homogeneous or inhomogeneous two level system [5]. Because of the electron heating contribution to the intensity dependent transmission only the 10P(20) data which is closest to line center will be analyzed below.

Both the rapid intensity dependence of the absorptivity shown in Fig. 3 and the electron heating result can be understood in terms of a three level cascade excitation model which promotes carriers into the conduction band. This idea is illustrated in Fig. 4. At high laser intensity the first $\hbar\omega$ takes the carrier from the $1s(A_1)$ to $1s(T_1)$ and the second $\hbar\omega$ takes it from $1s(T_1)$ to the conduction band. If the relaxation time from the conduction band back to the bound states is long enough then the $1s(A_1) \rightarrow 1s(T_1)$ transition will appear to saturate at high intensities but the saturation intensity will not be related to the homogeneous line width obtained from linear spectroscopy.

To estimate the functional dependence of this effect with intensity the problem is simplified to three levels. If the saturation intensity between the first two states is called I_{s_1} and the parameter for the next two states, I_{s_2}. then the steady state solution of the rate equations for the three level model gives for the absorption coefficient

$$\alpha = \alpha_0/[1 + (I/I_{s_1}) + (I/\bar{I})^2], \qquad (2)$$

where

$$\bar{I} = [4I_{s_1}I_{s_2}]^{1/2}. \qquad (3)$$

The effective saturation intensity in the high intensity limit is the geometric mean of the saturation intensity for each of the transitions. In this derivation it has been assumed that rapid relaxation occurs within the conduction band and also that the time for relaxation from the conduction band directly to the ground state is much larger than any of the other times in the problem. The solid curve for 10P(20) in Fig. 3 is obtained with $I_{s_1} = 3.7\,\mathrm{MWcm^{-2}}$ and $\bar{I} = 420\,\mathrm{kWcm^{-2}}$. The reasonable fit to the data demonstrates that the cascade excitation process completely masks the saturation behavior of the $1s(A_1) \rightarrow 1s(T_1)$ transition so it is not possible from this incoherent saturation measurement to determine conclusively whether or not the transition is homogeneously broadened; however, the absorption linewidth and the large intensity range for which saturation is not observed to occur provide definite bounds on the $1s(T_1)$ excited state lifetime. The value is between 1 and 5 psec.

The measured saturation intensity $\bar{I}$ together with I_{s_1} determined from the linewidth can be used in equation (3) to estimate the relaxation time for the

electron to go from the conduction band to the $1s(T_1)$ excited state. The $1s(T_1)$ level ionization energy [6] of 29.4 meV ($237\,\mathrm{cm^{-1}}$) is close to the effective mass theory (EMT) ground state binding energy for AlSb of 40 meV ($323\,\mathrm{cm^{-1}}$) so the EMT value [7] of the photoionization cross section, $\sigma_2 \approx 5 \times 10^{-17}\,\mathrm{cm^{-2}}$. is used in the I_{s_2} expression, the excited state analogue of equation (1). Although a rather long relaxation time of 4 to 20 nsec is obtained, inspection of the phonon density-of-states of AlSb indicates that the phonon gap between the optic and acoustic phonon branches occurs for these transition energies [8].

In conclusion, incoherent saturation measurements on the $1s(A_1) \rightarrow 1s(T_1)$ transition show that the saturation intensity is orders of magnitude larger than previously measured for shallow states. The step function turn off of the absorptivity with increasing laser intensity is ascribed to a two step excitation process which promotes the electron into the conduction band coupled with a slow relaxation time back to the $1s(T_1)$ level. This process masks a precise determination of the $1s(T_1)$ excited state lifetime from the saturation profile; however, the value is between 1 and 5 psec, about three orders of magnitude smaller than found for shallow states in three-five compounds [4].

REFERENCES

1. T. Murotani & Y. Nisida, J. Phys. Soc. Japan 32, 986 (1972).

2. E. Gornik, T.Y. Chang, T.J. Bridges, V.T. Nguyen, I.D. McGee & W. Muller, Phys. Rev. Lett. 40, 1151 (1978).

3. K. Muro, N. Yutani & S. Narita, J. Phys. Soc. Japan 49, Suppl. A. 593 (1980).

4. G.R. Allan, A. Black, C.R. Pidgeon, E. Gornik, W. Seidenbusch & P. Cotter, Phys. Rev. B31, 3560 (1985).

5. W.E. Moerner, A.R. Chraplyvy & A.J. Sievers, Phys. Rev. B29, 6694 (1984).

6. B.T. Ahlburn & A.K. Ramdas, Phys. Rev. 167, 717 (1968).

7. G. Lucovsky, Solid State Commun. 3, 299 (1965).

8. H. Bilz & W. Kress. Phonon Dispersion Relations in Insulators, p. 102. Springer Verlag. New York (1979).

VI. Publications and Degrees Awarded (1985-1986)

A. Publications

"Possibility of Observing Quantum Size Effects in the Electromagnetic Absorption Spectrum of Small Metal Particles," R. P. Devaty and A. J. Sievers, Physical Review B **32**, 1951-1954 (1985)

"Two-Dimensional Electron Gas in $In_{0.53}Ga_{0.47}As/InP$ Heterojunctions Grown by Atmospheric Pressure Metalorganic Chemical-Vapor Deposition," L. D. Zhu, P. E. Sulewski, K. T. Chan, K. Muro, J. M. Ballantyne, and A. J. Sievers, J. Appl. Phys. **58**, 3145-3149 (1985)

"Dipole-Dipole-Interaction-Induced Line Narrowing in Thin Film Vibrational-Mode Spectra," Z. Schlesinger, L. H. Greene, and A. J. Sievers, Physical Review B **32**, 1721-1723 (1985)

"Persistent Infrared Hole-burning Spectroscopy of Matrix-isolated CN^- Molecules," R. C. Spitzer, W. P. Ambrose and A. J. Sievers, Optics Letters **11**, 428 (1986)

"Surface Reconstruction Induced Changes in Free Carrier Scattering from the W(100) Surface: An Infrared Surface Electromagnetic Wave Study," D. M. Riffe, L. M. Hanssen and A. J. Sievers, Physical Review B **34**, 692-703 (1986)

"Infrared Observation of Adsorbate Induced Changes in Free Carrier Surface Scattering," D. M. Riffe, L. M. Hanssen and A. J. Sievers, Surface Science **176**, 679-690 (1986)

"Intensity-dependent Cyclotron Resonance in a GaAs/GaAlAs Two-dimensional Electron Gas," G. A. Rodriguez, R. M. Hart, A. J. Sievers, F. Keilmann, Z. Schlesinger, S. Wright, and W. I. Wang, Applied Physics Letters **49**, 458-460 (1986)

"Proton Tunneling with meV Energies at the Be:H Acceptor Complex in Silicon," K. Muro and A. J. Sievers, Physical Review Letters **57**, 897-900 (1986)

" Reply to "Comment on 'Observation of an index-of-refraction-induced change in the Drude parameters of Ag films', " H. Gugger, M. Jurich, J. D. Swalen, and A. J. Sievers, Phys. Rev. B **34**, 1322-1324 (1986)

"Observation of an Energy and Temperature Dependent Carrier Mass for Mixed Valence CePd$_3$," B. C. Webb, A. J. Sievers, and T. Mihalisin, Physical Review Letters **57**, 1951-1954 (1986)

" Infrared Surface Wave Interferometry on W(100)," L. M. Hanssen, D. M. Riffe, and A. J. Sievers, Optics Letters **11**, 782-784 (1986)

" Observation of Persistent IR Hole Burning in the Vibrational Spectrum of CN$^-$ in KBr," R. C. Spitzer, W. P. Ambrose, and A. J. Sievers, Physical Review B **34**, 7307-7317 (1986)

" Incoherent Saturation Study of the Selenium Donor in AlSb," R. E. Peale, K. Muro, J. T. McWhirter, and A. J. Sievers, Solid State Communications **60**, 753-755 (1986)

B. Degrees Awarded and Thesis Abstracts

Leonard M. Hanssen, Ph. D. 1985 Cornell University

Dr. Hanssen is now a Staff Scietist at the Naval Research Laboratory, Washington, D. C.

END

8-87

DTIC